Structure and Dynamics of Thin Anchored Hydrogel Layers by Fluorescence Correlation and Photon Correlation Spectroscopy

Maria Gianneli

Dissertation

University of Crete
Department of Materials Science and Technology

Heraklion, July 2008

Στη μητέρα μου

To my mother

TABLE OF CONTENTS

List of Abbreviations

Γ	Relaxation Rate
η	Viscosity
ξ	Mesh Size
τ_D	Diffusion Time
ϕ	Polymer Volume Fraction
$\chi(\phi,T)$	Interaction Parameter
A_2	Second-order Virial Coefficient
AAc	Acrylic Acid
AIBN	2,2′-Azobis(isobutyronitrile)
BIS	Methylene-bis-acrylamide
BSA	Bovine Serum Albumin
cBSA	Cationized Bovine Serum Albumin
D	Diffusion Coefficient
D_{coop}	Cooperative Diffusion Coefficient
D_s	Self-diffusion Coefficient
DLS	Dynamic Light Scattering
DSC	Differential Scanning Calorimetry
ECM	Extracellular Cellular Matrix
FCS	Fluorescence Correlation Spectroscopy
$g^{(1)}(\tau,q)$	Field Autocorrelation Function
$g^{(2)}(\tau,q)$	Intensity Autocorrelation Function
q	wavevector
QELS	Quasi Elastic Light Scattering
LCST	Lower Critical Solution Temperature
LLS	Laser Light Scattering
M	Tracer Molar Mass
M_m	Matrix Molecular Weight
M_w	Weight-average Molecular Weight

MaBP	4-Methacryloyloxy-benzophenone
MAA	Methacrylic Acid
MSD	Mean Square Displacement
N_{eff}	Number of Repetition Units Between Crosslinks
OWFS	Optical Wavequide Fluorescence Spectroscopy
P	Partition Coefficient
PAAc	Poly(Acrylic Acid)
PAAm	Poly(acrylamide)
PBS	Phosphate Buffer Saline
PCS	Photon Correlation Spectroscopy
PEG	Poly(ethyleneglycol)
pNIPAAm	Poly(N-isopropylacrylamide)
R_g	Radius of Gyration
R_h	Hydrodynamic Radius
Rh6G	Rhodamine 6G
SEM	Scanning Electron Microscopy
Silane**1**	4-(3'-chlorodimethylsilyl)propyloxybenzophenone
Silane2	4-(3-triethoxysilyl)propoxybenzophenone
SLS	Static Light Scattering
SPFS	Surface Plasmon Fluorescence Spectroscopy
T_g	Glass Transition Temperature
T_{UV}	UV exposure time

- ***Keywords***: *hydrogels, thermoresponsive gels, polymer dynamics, self diffusion, cooperative diffusion, fluorescence correlation spectroscopy, photon correlation spectroscopy*

SUMMARY

This thesis reports on the structure and dynamics investigation of hydrogel layers. Photocross-linked thin films of a thermo-responsive polymer anchored onto solid substrates were prepared from copolymers of N-isopropylacrylamide (NIPAAm, 94%), methacrylic acid (MAA, 5%) and 4-methacryloyloxy-benzophenone (MaBP, 1%).

FCS measurements were performed on these gel films swollen in two different solvents, ethanol and water, and several different fluorescent probes of various sizes and charges were used. In water, positively charged tracers (e.g. Rh6G, and a positively charged perylene derivative) were strongly attracted into the gel and suffered a hindered diffusion due to attractive electrostatic interactions with the negatively charged polymer. However, in the case of negatively charged tracers (e.g. fluorescein and a negatively charged perylene derivative), the presence of repulsive electrostatic forces prevented their diffusion into the like-charged gels.

Different cross-linking densities (corresponding to different irradiation times in the cross-linking process) were examined and the FCS results indicate that the probe molecules are slowed down and the swelling ratio of the gels decreases with increasing cross-linking density.

An attempt to extend the FCS diffusion study from rigid small molecules to flexible macromolecules was not successful since the negative charge of the fluorescently labelled macromolecule utilized (labelled PEG) prevented the diffusion inside the gel layer due to repulsive electrostatic interactions.

Measurements on the diffusion process of proteins have shown that a positively charged protein (cBSA) was immobilized inside the hydrogel layer, whereas a neutral one (native BSA) diffuses into the hydrogel layer. Increase of the characteristic diffusion time of the protein was observed with increasing cross-linking density.

The translational motion of a molecular (Rh6G) and macromolecular (pNIPAAm) tracer in transient pNIPAAm-MAA-MaBP networks (semi-dilute polymer solutions) in ethanol at varying polymer concentrations (up to c ~ 20 vol %) at ambient conditions were found by FCS to exhibit a Brownian diffusion in the absence of specific interactions

with the polymer matrix, which is explained by the lack of ion dissociation in ethanol as a solvent.

The dynamics of surface anchored and crosslinked pNIPAAm-MAA-MaBP layers with different crosslinking densities swollen in the good solvent ethanol were probed by the newly developed micro-photon correlation spectroscopy in the time range 1 x 10^{-6} s to 1 s. The cooperative diffusion coefficient describes the fast motion associated with the effective mesh size of the network in analogy to the transient physical network of uncrosslinked pNIPAAm chains. Assuming one dimensional swelling vertical to the surface for an estimate of the polymer volume fraction, the cooperative diffusion was found to increase faster with increasing volume fraction in the swollen gel layers than in the uncrosslinked pNIPAAm semidilute solutions. The present tethered pNIPAAm gel layers also revealed a second, slow diffusive process for the relaxation of the concentration fluctuations which in contrast to the physical network of the linear pNIPAAm chains, is virtually insensitive to the concentration i.e. crosslinking density. Also, unexpected for common unconfined gels, this slow diffusive mode was fully relaxed at times less than 0.1 s at wavevectors larger than 0.008 nm^{-1}. This mode was related to long wavelength dynamic heterogeneities but its nature is still unknown.

Finally, the effect of added salt and varying temperature on the dynamics of the surface anchored pNIPAAm crosslinked layers swollen in water was investigated. An initial small increase of the ionic strength (addition of NaCl up to 0.02 mol / L) resulted in an increase of the cooperative diffusion coefficient D_{coop} possibly due to the electrostatic screening of the anionic carboxylate groups in the polymer gel. Further increase of the ionic strength resulted in a decrease of D_{coop} with increasing NaCl concentration, which may be related to a salting-out effect by decreasing the solvent quality. Very high ionic strengths (>1M) completely erased the dynamic behavior due to the collapse of the gel. Similarly, when the temperature was increased towards the transition temperature (LCST), the collective diffusion coefficient D_{coop} exhibited a critical slow down upon the swollen gel approaching the collapse.

In conclusion, FCS and PCS have proven to be complementary and powerful optical techniques to investigate the structure and dynamics of thin anchored gel layers.

Chapter 1: Introduction

1.1 Overview

Hydrogels are crosslinked network polymeric materials that are not soluble but can absorb large quantities of water. These materials are soft and rubbery in nature, resembling living tissues in their physical properties.[1] In view of their biocompatibility and non-toxicity, they are excellent choices as biomaterials in several applications, like actuators, controlled release systems and biosensors. Recently, hydrogels have been used as an alternative substrate or platform for protein microarray applications[2,3,4] for a number of reasons:

• Hydrogels provide suitable three-dimensional environments for molecular-level biological interactions[5,6,7]

• Many hydrogels provide inert surfaces that prevent nonspecific adsorption of proteins, a property known as antifouling;

• Biological molecules can be covalently incorporated into hydrogel structures using a range of chemistries;[7]

• Hydrogel mechanical properties are highly tunable, for example elasticity can be tailored by modifying cross-link densities; and

• Hydrogels can be designed to change properties (e.g. swelling/ collapse or solution-to-gel transitions) in response to externally applied stimuli, such as temperature, ionic strength, solvent polarity, electric/magnetic field, light, or small (bio)molecules.[8,9,10]

Specifically in biosensing applications, it is convenient that many hydrogels can be readily micro- or nanopatterned to allow the development of lab-on-a-chip devices.
The realization of such devices often necessitates a thorough understanding of the structural properties and the dynamics of the constituent polymer gels in thin films. The latter are essentially unexplored due to the paucity of experimental techniques to address spatio-temporal fluctuations resulting from molecular motions in thin samples.

Tanaka and coworkers[11] first suggested the existence of responsive hydrogels in the late seventies while studying the water absorption properties of gels. When the temperature of a clear polyacrylamide gel decreases, the gel clouds up and eventually

becomes opaque, and any small change in solvent concentration or temperature could then cause the gel to swell abruptly to many times its original size or collapse into a compact mass. Since that time this phenomenon has opened up new and exciting routes for responsive polymeric hydrogels.

Hydrogels that can reversibly change shape or properties depending on external physicochemical factors are usually called ‘‘smart’’ or ‘‘stimuli-responsive’’ polymers. In such systems, the polymer conformation in solution is governed by both the polymer–solvent and polymer– polymer interactions. In a good solvent, it is the polymer–solvent interactions that dominate and the polymer chains are relaxed. In a poor solvent however, the polymer will aggregate due to a restricted chain movement because of increased polymer–polymer interaction. Such a phase transition leads to varying physical properties of the polymer solution. It is possible to alter the polymer–solvent interaction by imposing an external stimulus, such as changing the pH, temperature, and ionic strength of the solution. Among the many polymeric systems studied in the literature, poly(N-isopropylacrylamide) (pNIPAAm) has been widely exploited, mostly because of its well-defined lower critical solution temperature (LCST) in water (around 32^0C), which is close to the body temperature.

But, while macroscopic gels have been hindered by slow response times, the collective diffusion of the network is the rate-limiting step; therefore, reducing their dimensions to the microscale should significantly enhance performance.

A critical issue for understanding the properties of surface-attached polymer networks is the impact of confinement on their swelling behavior.[12] Chemical linkage of the network to a substrate prevents swelling parallel to the substrate, and confines the volume change to one dimension, normal to the surface. Such an effect may have a significant impact on properties such as the structure, mechanical properties, dynamics, and permeability of the network.

1.2 Aim of the Thesis

From one side, there has been great interest in studying particle transport and diffusion of solutes within hydrogels, since this problem is important in a wide variety of biotechnological fields from cell encapsulation to controlled drug delivery. While pNIPAAm-based gels have commonly been studied[13] as model systems for drug delivery applications, there are still many factors affecting the solute diffusion within these systems, which are poorly understood. There is an extensive body of previous research on probe diffusion in nondilute polymer solutions[14,15,16] but the area can hardly be considered mature because of the involved parameters as well as the presence of interactions. While Fluorescence Correlation Spectroscopy (FCS) has been successfully utilized to study transport properties in various biological environments,[17,18] its applications in other soft systems are rare and only recently reported.[19,20,21,22,23] On the basis of the very small detection volume (approximately femtoliters) and its high sensitivity, FCS is perfectly suited to study the single tracer diffusion in thin, supported gels.

On the other hand, the thermo-responsive properties and microscopic structural features of poly(N-isopropylacrylamide) (pNIPAAm) layers grafted onto solid substrates have been extensively studied using techniques such as dynamic light scattering,[24,25] surface plasmon resonance,[26,27] neutron reflectivity,[28,29] quartz crystal microbalance[30] and others. However the dynamics of these confined charged cross-linked networks have been much less studied and the effects of parameters like temperature and pH,[31] are not yet understood.

Dynamic light scattering[32,33] and fluorescence spectroscopic techniques[34] are among the main experimental tools which can be applied to study polymer dynamics in submicron thick films. The present study focuses on the optical structure and dynamics investigation of supported hydrogel films and polymers in solutions.

Motivation of the present work was to relate the diffusion retardation of a probe to the properties of the pNIPAAm network. To produce responsive hydrogels that can be spin-coated as photocross-linkable thin films and to investigate their dynamic behavior, terpolymers of N-isopropylacrylamide (NIPAAm), methacrylic acid (MAA) and 4-

methacryloyloxy-benzophenone (MaBP) were synthesized. The tracer diffusion in pNIPAAm gels and pNIPAAm semi-dilute solutions was monitored by means of FCS and, at the same time, the utility of micro-photon correlation spectroscopy was exploited to study the collective dynamics of pNIPAAm layers.

The thesis is structure as follows:

- Chapter 2 provides the historical background and state of the art concerning gels and the manifestation of their unique properties, with emphasis placed on the dynamical aspects of these materials. Also, provided in this section, the theoretical background of the two main techniques used for the investigation of the grafted pNIPAAm layers, FCS and Laser Light Scattering (LLS).
- Chapter 3 explains the synthesis of the chemical compounds and the experimental set-ups and procedures used in our measurements.
- Chapter 4 reports the results obtained with FCS on the diffusion of probe molecules in pNIPAAm semi-dilute solutions and pNIPAAm gels swollen in ethanol. The role of the cross-linking density, size of the diffusant and electrostatic interactions between polymer matrix and tracers is explained in detailed.
- Chapter 5 investigates the dynamics of pNIPAAm gels with respect to the solvent quality, temperature and ionic strength effect.
- Chapter 6 consists of the conclusive remarks and the outlook of this work.

Chapter 2: Theoretical Background

2.1 The Sensor Concept

Protein microarray-based technologies have rapidly transformed biotechnology and biological research by providing a highly parallel interrogation method for measuring protein–protein interactions. These microarray platforms offer the capability of generating and assessing a variety of bio-information using a systematic approach towards understanding many of the post-translational cellular mechanisms from such protein–ligand interactions. As a result of these new platforms, advances have been made in drug design, therapeutics and diagnostics.[35,36]

At the basis of each protein microarray exists a unique architecture of chemical constructs that assemble to form the ligand networks. The fabrication of these hierarchical networks has been achieved through a number of chemical modification strategies that range in diversity and complexity. Traditionally, self-assembled thin films of these nanostructured materials deposited on solid supports are used for the design and the development of microarrays or microchips.

One of the future research goals is the development of a multi-array hydrogel biosensor based on poly(N-isopropylacrylamide) (pNIPAAm), which is one of the best studied environmentally responsive polymers.

Figure 2.1 schematically depicts the concept of the hydrogel based multi-analyte sensor. The sensor can be composed of several sensor pads (here only two are shown). Each sensor pad consists of a dry hydrogel layer that has been previously modified with a receptor that can bind selectively to a specific analyte. Due to the multiplicity of sensor pads per biological chip, a large range of analyte molecules can be detected in parallel. The addition of the analyte solution under examination will cause the swelling of the layer and will result to the specific analyte binding by diffusion of the analyte into the gel. An external stimulus (for example, temperature increase over the Lower Critical Solution Temperature (LCST)) can cause the collapse of the gel, and subsequently, the solvent is ejected from the gel together with all of the unbound analytes. The analyte of interest is entrapped now in the layer and by the drastically reduced volume of the gel, its

effective concentration close to the substrate will increase significantly. This increase can be read-out by surface-sensitive detection techniques, such as Surface Plasmon Fluorescence Spectroscopy (SPFS) and Optical Waveguide Fluorescence Spectroscopy (OWFS).

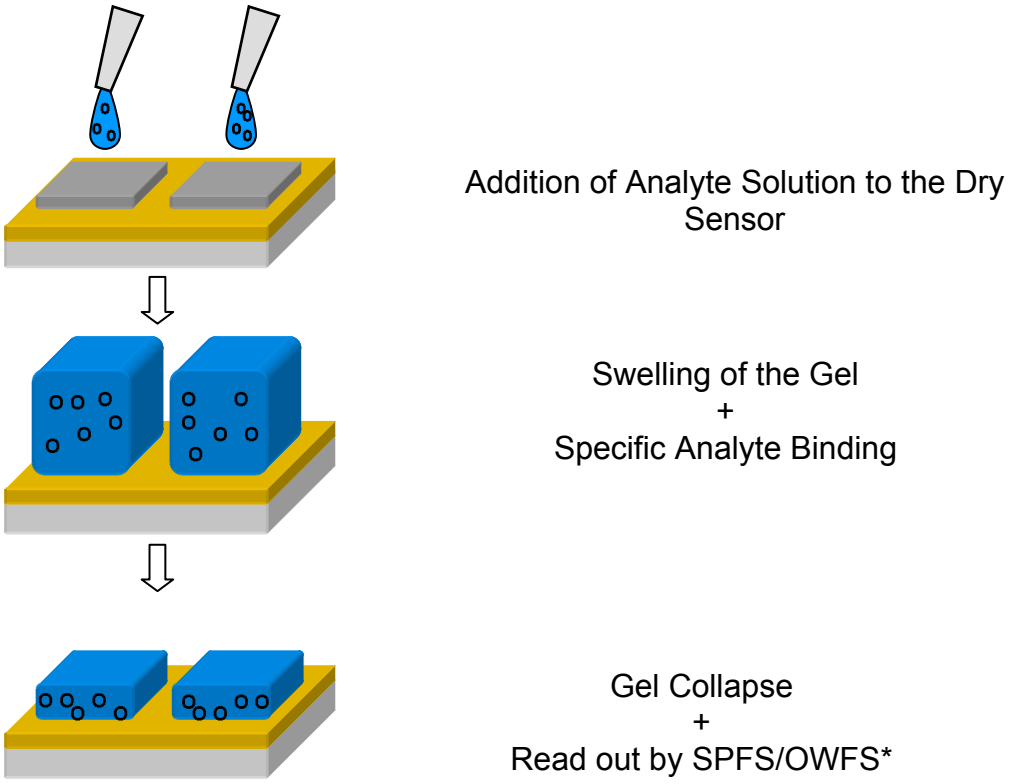

Figure 2.1: Concept of the hydrogel-based multi-analyte sensor (schematics courtesy of Patrick Beines)

2.2 Gels

2.2.1 From *Historical Background* …

"It was very puzzling," says Toyoichi Tanaka, referring to a discovery he made shortly after joining the physics faculty at Massachusetts Institute of Technology in 1975. He and his coworkers were studying gels, cross-linked polymer networks that can absorb enough solvent to swell. They discovered that by cooling a clear polyacrylamide gel, they could make it cloud up and eventually become opaque. Warming the gel restored its clarity. That was not the kind of behavior Tanaka had been expecting. What he had stumbled upon was a phase transition in a polymer network-a phenomenon akin to the interconversion of the liquid and vapor phases of water at the critical point. Some of Tanaka's colleagues, however, were skeptical of his explanation because the gel transition occurred at about -20°C. They thought his observations might be due to the formation of tiny ice crystals in the gel. To prove them wrong, Tanaka embarked on another experiment, one involving ionized gels immersed in water-acetone solutions. He was hoping to quell the doubts by pushing the phase transition into the room-temperature range. But he ended up making an even more dramatic discovery that opened up a new field of research. In essence, Tanaka discovered that a small change in solvent concentration or temperature could cause a gel to abruptly swell to many times its original size--or collapse into a compact mass.

Such a definitive phase transition had not been seen before in synthetic polymers, although it had been predicted in 1968. Certainly, gels that swell or contract gradually over time had been known for more than 25 years before Tanaka began his experiments. But his gels were different--they reacted to an external stimulus in a manner more reminiscent of living organisms than inanimate matter. The unique properties of these gels soon attracted other investigators, including chemists and chemical engineers, who were intrigued by the materials' potential uses in fields as far-flung as medicine and robotics.

Today, two decades after Tanaka's demonstration of the first "smart" or "intelligent" gels, these materials are just beginning to trickle into the marketplace. Behind the commercialization effort is a much larger effort--most visible in academic labs--that is aimed at gaining a better understanding of these fascinating materials and improving their properties and performance.

2.2.2 … to *State of the Art*

Polymer gels had long been a subject of polymer chemistry or polymer physical chemistry before Tanaka proposed the collective diffusion theory of polymer gels in 1973.[37] Since then, gel science became a field of physics as well. Tanaka found a volume phase transition in aged poly(acrlyamide) (PAAm) hydrogel in 1979.[11] He observed a discrete transition in the size of the gel by a slight composition change of the water/acetone mixture.

The volume phase transition is defined as a discrete (or a continuous) transition in volume by a small change of environmental parameters, such as temperature, pH, ionic strength, etc.[38] Although this concept was proposed by Dusek and Patterson in 1969,[39] this discovery triggered rapid developments in gel science, such as functional materials including, drug delivery systems, micro-actuators, sensors, lab-on-a-chip technology, and tissue engineering.[40,41] The presence of multiphases, in addition to swollen and shrunken phases, was observed by Annaka and Tanaka in 1990s.[42] It is needless to say that, in order to use gels as functional materials, the structures of gels have to be well elucidated. For example, the optical properties of soft-contact lenses, which is a gel swollen in a saline solution, are strongly affected by inhomogeneities and mesoscopic structures in the lens. However, structure investigations on polymer gels have been interesting problems due to the complexity of gels, such as the presence of cross-links, hierarchical structures, and inhomogeneities. Particularly, inhomogeneities, which are rather unique properties of gels, are introduced during the cross-linking process. Due to cross-linking, polymer chains in a polymer gel are allowed to have a limited motion in the phase space, i.e., a restricted Brownian motion. This notion led to the concept of nonergodicity in 1989, which is discussed further below.

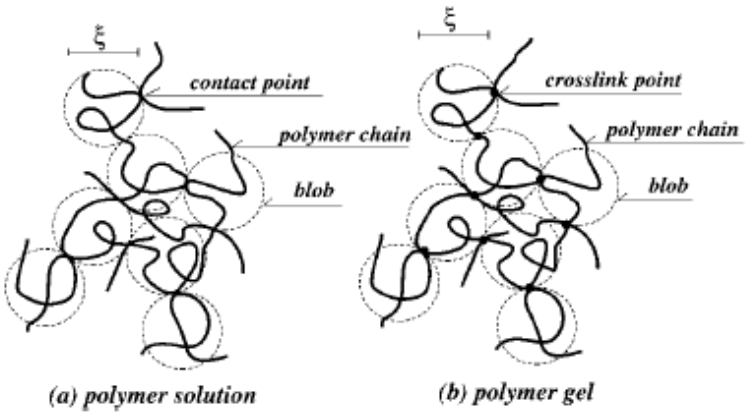

Figure 2.2: Comparison of a) a semi-dilute polymer solution and b) a polymer gel. The difference is the presence of the cross-links in the second case (adapted from Shibayama, Bull. Chem. Soc. Jpn. Vol. 79, No. 12, 1799–1819 (2006))

The Fig. 2.2 above schematically illustrates the essential difference between a semi-dilute polymer solution and a polymer gel. As can be seen, the structure of gels is essentially the same as that of polymer solutions, and the only difference is the absence/existence of permanent cross-links. However, in reality, cross-links play a major role in the unique properties of gels, such as shape, swelling capability, solvent absorbency, elasticity, molecular recognition, etc. In addition to these properties, which can be observed macroscopically, structural inhomogeneities are not visible in most cases, but strongly influence the physical properties of gels.

2.2.3 Characteristic Features of Gels

I. Structure Inhomogeneities in Gels

Dynamic light scattering (DLS) technique is among the most powerful tools in characterizing concentration fluctuations, therefore the discussion that follows is directly related to the concept of light scattering, which will be discussed in detailed in Section 2.5 Experimental Techniques.

There are two types of concentration fluctuations in a gel: (a) the fluctuating component (dynamic thermal fluctuations) that originates from Brownian motion of the solvent and/or the solute, (b) the frozen concentration inhomogeneities introduced by cross-linking, or, (c) the superposition of (a) and (b). In the case of polymer solutions, only thermal fluctuations exist. In the case of polymer gels, on the other hand, the concentration fluctuations, δc, consist of dynamic fluctuations, δc_F, and the frozen (constant) inhomogeneities δc_C,

$$\delta c(r) = \delta c_F(r) + \delta c_C(r)$$

where r is the position vector. Statistically, there are two averages, time average $\langle\ \rangle_T$, and ensemble average $\langle\ \rangle_E$. Since the frozen inhomogeneites do not change with time, a time average of the concentration fluctuations of a gel at a given position is not zero, i.e., $\langle \delta c \rangle_T \neq 0$, while that of the dynamic fluctuations is zero, i.e., $\langle \delta c_F \rangle_T = 0$. On the other hand, the ensemble average of the frozen inhomogeneities is zero, i.e., $\langle \delta c_C \rangle_E = 0$ by definition. This is why polymer gels have to be treated as nonergodic media.[43] The term ‘‘nonergodicity’’ has been used to describe glasses,[44] and gels.[43,45] It means that the ensemble average and the time average are not equal, i.e.,

$\langle A \rangle_E \neq \langle A \rangle_T$,

where A is a variable describing a property of the sample.

In order to characterize these two types of concentration fluctuations, it is more convenient for light scattering to use the Fourier transform of the concentration fluctuations,

$\delta c(q) = \delta c_F(q) + \delta c_C(q)$,

q is the magnitude of the scattering vector defined by $q = \left|\vec{q}\right| = (4\pi n/\lambda)\sin(\theta/2)$, n is the refractive index of the scattering medium, and λ is the wavelength of the light in vacuum and θ is the scattering angle. These concentration fluctuations are observed as scattering intensity.

II. Collective Diffusion of Gels and Gel Mode

An important feature of the gels that one has to keep in mind when discussing about the dynamics of gels is that polymer chains in a gel do not ‘‘diffuse’’ or, in other words, do not undergo translational diffusion due to constraints by the crosslink points. The polymer chains in a gel, however, move locally around their average position due to thermal motion, which is called collective diffusion of gels. In 1973, Tanaka, Hocker, and Benedek (THB) realized that a gel has to be treated as a continuum and proposed a theory of collective diffusion of polymer network.[37] This became a standard theory to describe the dynamics of gels. This theory predicts that $g^{(2)}(q,\tau)$, the intensity autocorrelation function, is given by a single-exponential function even if cross-links are randomly introduced to a polymer solution. According to the theory of elasticity, a small deformation of a unit volume of a gel having the mass density, ρ, follows the equation,

$$\rho\frac{\partial^2}{\partial t^2}\mathbf{u} = \mu\nabla^2\mathbf{u} + \left(K + \frac{1}{3}\mu\right)\nabla(\nabla\cdot\mathbf{u}) - \zeta\frac{\partial}{\partial t}\mathbf{u},$$

where $\mathbf{u}(\mathbf{r},t)$ is the displacement vector, representing the displacement of a point *r* on the network from its average position at time *t*. *K* and μ are the bulk modulus and the shear modulus, respectively, and ζ is the friction coefficient between the polymer chains and the solvent.

This is the fundamental equation to describe not only the dynamics of polymer networks but also the kinetics of gel swelling/shrinking.[46]

The collective diffusion coefficient is given by[47,48]

$$D = \frac{1}{3N}\int_0^\infty g(r)\frac{kT}{6\pi\eta r}dr,$$

where *N* is the degree of polymerization of the polymer chains, *k* is the Boltzmann constant, η the solvent viscosity and T the absolute temperature. Since the spatial correlation function for semi-dilute polymer solutions is given by[48]

$$g(r) \approx \frac{\xi}{r}\exp(-\frac{r}{\xi}),$$

one obtains

$D \approx \frac{kT}{6\pi\eta\xi}$, where ξ is a measure of the distance of concentration correlation (correlation length).

III. Factors Affecting the Swelling of Ionic Hydrogels

Hydrogels can be neutral or ionic in nature. In neutral hydrogels, the driving force for swelling arises from the water-polymer thermodynamic mixing contribution to the overall free energy, which is coupled with an elastic polymer contribution. In ionic hydrogels, the swelling process is due to the previous two contributions as well as the ionic interactions between charged polymer and free ions.

Therefore, the degree of ionization, the concentration of ionizable groups inside the polymer network, pH and ionic strength of the swelling medium, valence and nature of the counterion, and the composition of the swelling medium influence the dynamic and equilibrium swelling behavior. Other material properties of the polymer, e.g. degree of crosslinking, hydrophilic/hydrophobic balance, tacticity, size distribution, and polymer architecture (like branching, or in the case of copolymers the comonomer sequence) may also control the swelling behavior.

Effect of ionic content

An increase in ionic content in the polymer network increases the hydrophilicity, as well as the osmotic pressure, and therefore leads to a faster and higher equilibrium swelling ratio. In the case of weak polyelectrolytes, the charge density of the polymer network can also affect the pH sensitivity of the gel. Anionic–hydrogels, for example containing carboxylic acid groups, swell at a pH higher than the gel pK_a due to ionization. On the other hand, the gel is in a nonionized state at a pH below the gel pK_a and therefore swells only to a lower extent. Opposite behavior is observed in the case of basic or cationic gels containing amine groups and the transitional pH depends here on the gel pK_b. In the case of an ampholyte, i.e. a gel containing both acidic and basic groups, an isoelectric pH where the polymer is essentially uncharged is the deciding factor. Below the isoelectric pH the gel is negatively charged while at higher pH the gel is positively charged. Proteins and polyaminoacids are examples of polyampholytes. Strongly acidic

or basic gels show only a very small pH-dependent swelling due to very low or high gel pK_a.[49]

Electrostatic attraction

The counterion may be localized near the fixed ionic groups by the electrostatic attraction between the two opposite charges, while thermal motion (Brownian motion, driven by kT) tends to diffuse the free ion randomly in the solution. The strength of this ionic interaction depends upon the ionic charge, the dielectric constant of the medium, and the distance between the counterion and the fixed ionic group. The counterions with higher valence are more strongly held because the electrostatic attraction is proportional to the ionic charge and inversely proportional to the square of the distance between the charges.[50]

Effect of temperature

Some ionic and non-ionic hydrogels undergo volume-phase transition with temperature. This volume change depends on the chemical nature, the degree of ionization, and the stiffness of the components of the polymer chains, and is reversible. This behavior is associated with polymer phase separation as the temperature is raised to a critical value, known as the 'lower critical miscibility or solution temperature (LCST). Networks that show lower critical miscibility temperature usually shrink, as the temperature is increased above the LCST. Lowering the temperature below LCST results in the swelling of the gels.

2.3 Poly(N-isopropylacrylamide)

Among the many polymeric systems studied in the literature, poly(N-isopropylacrylamide) (pNIPAAm, chemical structure shown in Figure 2.3) has been widely exploited since it is sensitive to temperature.

The polymer exhibits a sharp LCST transition in water at around 32°C. The reason for this sharp transition is a good balance between the hydrophilic and hydrophobic interactions in the polymer.[51] Raising the temperature of an aqueous pNIPAAm solution above this LCST causes a coil to globule transition, followed by a phase separation. This phase transition is accompanied by a release of water bound to the polymer chains, which is an endothermic process.

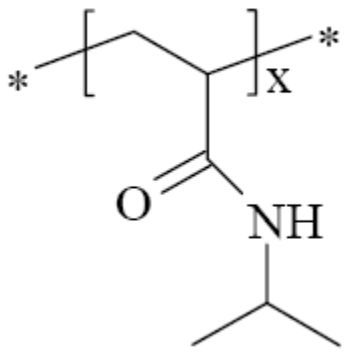

Figure 2.3: Poly(N-isopropylacrylamide)

The mechanism of phase transition of thermosensitive polymers like pNIPAAm was first proposed by Heskins and Guillet[52] and was supported by other authors.[53] The phase transition can be explained using the thermodynamic model:[38]

$\Delta G_{mix} = \Delta H_{mix} - T\Delta S_{mix}$,

where ΔG_{mix} = free mixing energy of polymer solution

ΔH_{mix} = mixing enthalpy

T = temperature

ΔS_{mix} = mixing entropy

The solubility of pNIPAAm in water is controlled by a well-balanced equilibrium between the favourable water interactions with the hydrophilic amide groups (CONH) and the unfavourable water interactions with the hydrophobic isopropyl- and polymer backbone methylene groups. Below the LCST, the hydrophilic interactions dominate, making the polymer soluble.

Negative entropy of mixing exists due to the special structure of water and polymer i.e. the formation of solvation layers of highly organized water molecules around the polymer. By raising the temperature above the LCST, the entropy term dominates over the exothermic enthalpy (ΔH_{mix}) of the hydrogen bonds between the polar groups in the polymer and the water molecules. Therefore, the free energy change becomes positive and two phases exist above the LCST.[38] In the literature some methods for the detection of the phase transition temperature (T_c) have been reported.[54] For example, light scattering was used to detect the coil to globule transition,[55] turbidimetric measurements to observe phase separation[56] and Differential Scanning Calorimetry (DSC) to measure the heat of transition.[57]

The T_c of pNIPAAm copolymers is strongly influenced by the nature of the comonomers. Hydrophilic comonomers like acrylamide increase the LCST, while hydrophobic comonomers tend to decrease the LCST.[58] The pNIPAAm polymers exhibit limited physical features and weak mechanical properties[59] but copolymerization helps to circumvent these problems. The use of copolymers of pNIPAAm containing ionic moieties will also be helpful in designing delivery systems that exhibit both pH and temperature-sensitive characteristics.

2.4 Probe Diffusion in Hydrogels

Transport phenomena in and through gels have attracted much experimental and theoretical attention, especially in the last years, due to the significance of such phenomena in a wide variety of applications, like biosensoring, controlled drug delivery and separation technologies. One of the physical quantities that characterize the transport properties of gels is the diffusion coefficient of probe molecules in the gel. The probe molecule when is dissolved in a simple fluid thermally fluctuates in time and space. The fluctuation and the friction ζ between the probe molecule and the fluid determine the diffusion coefficient of the probe in the solution

$$D = k_B T / \zeta \qquad (2.1),$$

where k_B and T are Boltzmann's constant and the absolute temperature, respectively. The hydrodynamic friction of the fluid of the viscosity η that is experienced by a probe molecule of hydrodynamic radius R_h is given by the following equation:

$$\zeta = 6\pi\eta R_h \qquad (2.2)$$

The equations (1) and (2) yield the Stokes-Einstein equation. However, when the probe molecules are introduced into the gel, they experience additional friction by the polymer network of the gel and their diffusion slows down. To formulate theories of molecule transport through macroporous water-swollen hydrogels necessitates understanding of their structure. Swollen gels are typically characterized by a mesh-like structure, with aqueous domains filling the spaces between the chains. Solute transport occurs primarily in the water-filled regions in the space between the polymer chains. Any factor that reduces the size of these spaces (increasing cross-linking density, for example) will have an effect on the movement of the solute. In general, the diffusivity of a solute through a hydrogel decreases as cross-linking density increases, or the size of the solute increases, and as the volume fraction of water within the gel decrease (e.g. by collapse or by a decreased swelling ratio due to increase of the cross-linking density).[60]

2.5 Experimental Techniques

2.5.1 Fluorescence Correlation Spectroscopy (FCS)

I. The concept

Applications of Fluorescence

Fluorescence is a highly specific property of certain dye molecules. Its principles are used in many aspects of daily life, popular examples of which are neon tubes as well as brilliant fluorescent dyes for traffic signs and signaling. There are also many applications in the life sciences that exploit the properties of fluorescent dyes. They are commonly used as probes for visualization in microscopy. Furthermore, dye lasers exploit fluorescent dyes as the active laser medium.

All the applications are based on the property of the dyes to absorb and eventually emit light. The fluorescent dye always causes a shift in light wavelength between the absorbed and the emitted light. In fluorescence microscopy, the observable spectral shift enables the experimenter to block the omnipresent excitation light by filtering and to detect only the fluorescent light emitted by an object, which might be a ligand labeled with a dye, attached to specific locations of cells or tissues, the so-called binding regions. An image looks as if the cell or the tissue were luminescent on their own.

The Fluorescent Process

Fluorescence is the result of a three-stage process that is found with certain molecules called fluorophores or fluorescent dyes. It is best described by a model of electronic energy levels of a molecule as illustrated by the so-called Jablonski diagram, an electronic state diagram.

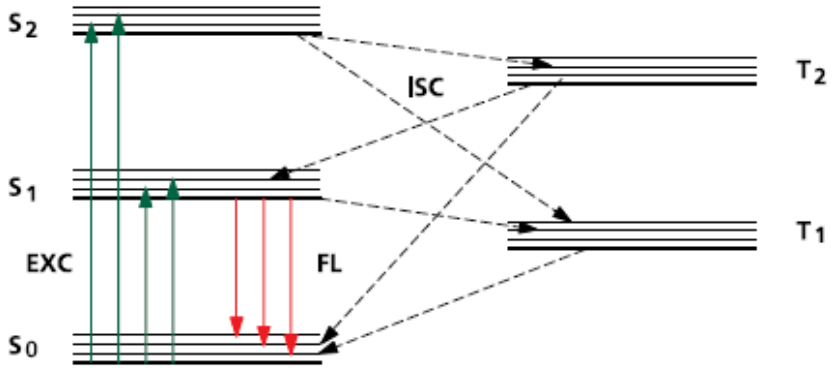

Figure 2.4: Jablonski diagram summarizing the typical photophysical processes. It illustrates the processes involved in the creation of an excited electronic singlet state by optical absorption and subsequent emission of fluorescence. The broken lines represent intersystem crossings (ISC), solid lines either excitation (EXC) or fluorescence emission (FL). S_0 represents the singlet ground state, whereas S_1 and S_2 represent the first and the second excited singlet state. T_1 and T_2 are the triplet states, which have slightly less energy than their corresponding singlet states. Transitions between singlet and triplet states are spin-forbidden and therefore comparatively slow. The lines above the electronic states are vibronic levels.

In the first stage (excitation), a photon supplied by an external source, such as a laser, is absorbed by the molecule in the ground state S_0 generating an excited electronic singlet state S_2 of the molecule with a higher energy level. In the second stage (excited-state lifetime) this level is quickly converted to the relaxed singlet excited state S_1. Depending on the molecule studied and its chemical environment, the excited state is usually populated for an averaged time of 0.1 to 10 ns (fluorescence lifetime τ_T). After this delay, in the third step (fluorescent emission), the molecule emits a photon spontaneously from the relaxed singlet excited state S_1 and returns in the ground state.
The triplet excited state is created from the singlet state S_1 via an excited-state process called intersystem crossing. If a triplet state of a molecule is occupied, no fluorescence light can be recorded from this molecule. The higher the laser intensity is, the higher is the occupation number of the triplet state. The triplet lifetime (typically between 0.5 and 10 µs in water) is short compared to the diffusion time of a labeled molecule through the

confocal volume element. Due to energy losses, the fluorescence photon emitted always carries less energy than the absorbed photon. The corresponding red shift in photon wavelength, the so-called Stokes shift, can be used to separate the emission from the excitation light.

Fluorescence Fluctuations Analysis

A very elegant way to improve sensitivity is to record fluctuations of the fluorescence intensity instead of just averaging the signal. Fluctuations of a signal are usually associated with the noise that is expected to bear no information at all. Under specific circumstances, however, the fluctuations carry a wealth of information, even more than the average intensity. This information can be exploited, the information content being extractable by means of sophisticated signal processing techniques. Such fluctuation analysis was introduced by D. Magde, E. Elson and W. Webb in 1972,[61] as described further in the text. They called it Fluorescence Correlation Spectroscopy (FCS). The enthusiasm for FCS was somewhat dampened in those early days when it was realized that the full potentials of FCS could not be obtained without extremely stable light sources, powerful computers for signal processing and better optical equipment than was available at that time.

Optimization of the Method

In 1992, R. Rigler and co-workers introduced the major prerequisite for the improved analysis of fluorescence fluctuations- the ultra small detection volume of 1 femtoliter. Together with stable laser light sources, sufficient computer power and precision optics, a real renaissance was opened up for FCS, demonstrated by a series of papers describing applications of this method.[62,63,64,65]

"Light Cavity"

Why is the small measuring volume so important? Within 1ml of a nanomolar fluorophore solution, about $6x10^{11}$ fluorophore molecules are present. By contrast, 1

femtoliter, corresponding to 1 cubic micron (μm^3), contains only 0.6 fluorophore molecules on average. The diffusion of molecules in solution is subjected to Browian motion. As a consequence, at any given point in time, the measurement volume may be 'empty' or occupied by molecules. Thus, in turn, large fluctuations in fluorescence intensity occur, which are associated with the diffusion process of the molecules, whereas the background signal is relatively constant over time.
Thus, fluctuations can be interpreted as diffusion statistics of the fluorescent molecules. It is obvious that a measurement process samples single molecular diffusion events; however, a complete measurement relies on statistics from a multitude of such events.

II. The Principle of the Technique; Theoretical Basis

Fluorescence correlation spectroscopy (FCS) is an analysis method that can measure the dynamics of molecular processes from observations of spontaneous microscopic fluctuations in molecular concentration. These measurements are commonly performed in thermal equilibrium where spontaneous fluctuations of molecules result from Brownian motion. In order to derive phenomenological parameters, e.g., diffusion coefficients and chemical rate constants, it is necessary to perform a statistical analysis on these fluctuations. In FCS, this statistical analysis is performed by a correlation function, which directly gives information about the diffusion time, bound/free ratio of molecules, triplet time and triplet fraction, indirectly yielding information about concentration, binding constants and on/off constants. Single-molecule detection sensitivity is enabled by a small open volume element generated by a Gaussian laser beam. A high signal-to-noise ratio (SNR) is guaranteed, because a pinhole is inserted into the image plane of the objective, rejecting the out of focus laser light. In the early 1970s, Elson et al [61, 66-68] as well as Ehrenberg and Rigler[69] derived the principle theory behind FCS. Thereafter, the confocal volume element was introduced[64] and FCS has evolved in different disciplines depending on its application.

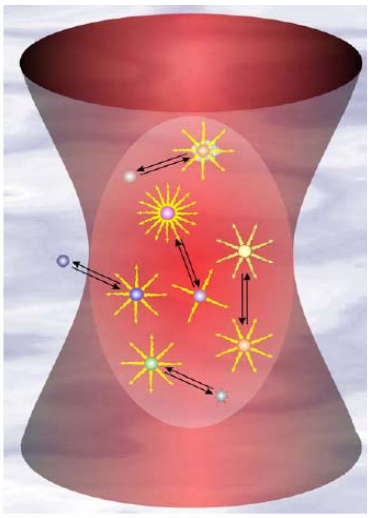

Figure 2.5: Molecular mechanisms that might give rise to florescence fluctuations in the confocal volume (red double cone) comprise particle movements, conformational changes, chemical or photophysical reactions (adapted from "Fluorescence Correlation Spectroscopy'' by Petra Schwille and Elke Haustein, previously published in Biophysics Textbook Online (BTOL))

.

III. Practical Realization – Aspects of the Standard Equipment

In order to realize the FCS experiment, a small illuminated volume must be created from which the fluorescent light is collected and recorded. A typical FCS spectrometer is based on a confocal fluorescence microscope. In contrast to confocal scanning, the confocal pinhole in FCS does not primarily serve to enhance the spatial resolution but its purpose is to reject the out-of-focus emission. A typical range of diameters of the pinhole used in FCS is 30 to 100 μm. A laser is used as the light source for excitation. The main reason for using a laser is the possibility of focusing its well-collimated beam into a very small spot of about 0.5 μm in diameter. Additionally, the small spectral width of the laser light facilitates the spectral separation of the fluorescence emission from the excitation. The filter in front of the detector is usually a bandpass interference filter. At shorter wavelengths, it blocks the scattered laser light, and at longer wavelengths, it blocks the strongest band of Raman scattering from water.

A typical sample is a dilute water-based solution of fluorescently labeled molecules. However, there is a relatively large flexibility in the choice of measurement environment.

What is important is that the molecules are able to move in and out of the illuminated volume.[70, 71] This exchange of molecules is necessary for two purposes: (1) exchanging the photobleached molecules with the fresh ones or (2) measuring the kinetic parameters of the motion. The experimental measurement of the fluorescence intensity *I(t)* is accomplished by counting the number of photons, *n*, during time intervals of a predetermined width Δt.

$$I(t) = I(i\Delta t) = \frac{n_i}{\Delta t} \tag{2.3}$$

The time-dependent experimental correlation function is calculated as

$$G_{\exp}(\tau) = G_{\exp}(k\Delta t) = \frac{\frac{1}{M-k}\sum_{i=1}^{M-k} n_i n_{i+k}}{\left[\frac{1}{M-k}\sum_{i=1}^{M-k} n_i\right]} \tag{2.4}$$

where *M* is the total number of counting intervals, so that the total duration of the measurement is $M\,\Delta t$.

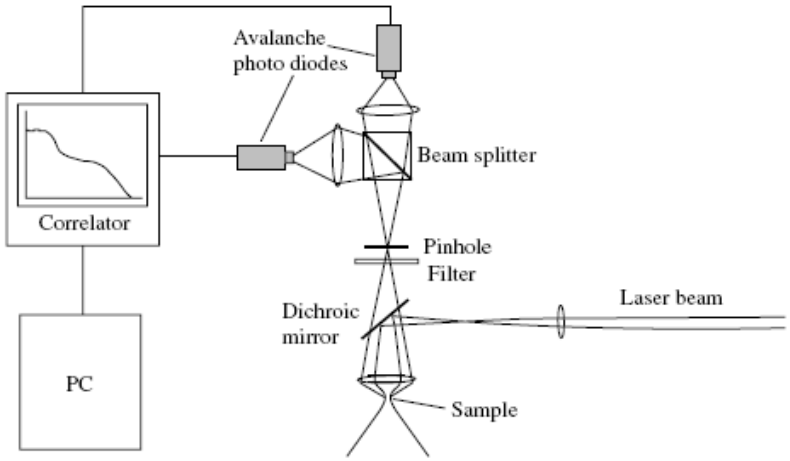

Figure 2.6: Typical instrumentation for FCS experiments. A laser beam is directed via a dichroic mirror into a confocal microscope and focused by the objective into the sample. Emitted fluorescence is collected by the same objective, passes through the beam splitter, and is focused onto the image plane where the pinhole is located. The light passing the pinhole is spectrally filtered by highly selective bandpass emission filters and is focused onto the sensitive areas of the avalanche photodiodes. Standard pulses from the diodes are fed to the PC-based correlator (adapted from "Fluorescence Correlation

Spectroscopy'' by Petra Schwille and Elke Haustein., previously published in Biophysics Textbook Online (BTOL))

IV. Theoretical Aspects

Autocorrelation Analysis

The primary data obtained in an FCS measurement is the time-dependent fluorescence intensity F(t), which is proportional to the number of particles in the observation volume at time t. The autocorrelation function of *F(t)* contains all relevant information relating to the diffusion of the fluorophores. The normalized autocorrelation function *G(t)* is computed as

$$G(\tau) = \frac{\langle F(t)F(t+\tau)\rangle}{\langle F(t)\rangle^2} \tag{2.5}$$

For obtaining quantities such as diffusion coefficients, concentrations or reaction rate constants, one has to fit a theoretical correlation function to the measured *G(t)* which is based on a model that contains these quantities as free parameters. For a solution of a single fluorescent species with diffusion coefficient *D* and molar concentration *c* and for Gaussian profiles for the excitation intensity and detection efficiency, *G(t)* evaluates to:[64]

$$G(t) = \frac{1}{cV_{eff}}\left(1+\frac{4D\tau}{\omega_0^{\,2}}\right)^{-1}\left(1+\frac{4D\tau}{z_0^{\,2}}\right)^{-1/2}+1 \tag{2.6}$$

Here V_{eff} is the effective observation volume that depends on the geometry of the focus for excitation and emission, w_0 and z_0 are the half-widths of the focus in the x-y plane (the observation plane of the lens) and in the z-direction, respectively. *Veff*, w_0 and z_0 can be measured independently by calibration with a solution of a fluorophore of known concentration and diffusion coefficient. If only relative changes are of interest, one can use the average particle number $N = cVeff$ and an effective diffusion time $t_{diff}=w_0^{\,2}/4D$ as parameters:

$$G(\tau) = \frac{1}{N}(1+\frac{\tau}{\tau_{diff}})^{-1}(1+\frac{\tau}{\tau_{dif} f \kappa^2})^{-1/2} + 1 \qquad (2.7)$$

κ (also called the structure factor) is the axial ratio of the observation volume, z_0/w_0. For a high aperture lens (NA = 1.2) at optimal alignment κ typically ranges between 4 and 6. In a typical FCS experiment one would therefore determine κ on a monodisperse solution of a known fluorophore and keep its value fixed for the measurements of the unknown sample.

The intercept of the FCS autocorrelation function *G(t)* is inversely proportional to the number of particles in the focal volume, and thus to their concentration. In practice, deviations from this ideal behavior are found at very high and very low concentrations. At low concentrations these deviations are due to the background which becomes comparable to the fluorescence signal, and which is caused by incomplete suppression of the excitation light, detector dark counts and background fluorescence. At a particle concentration c the measured particle number *N* in the presence of background is then

$$N = cV_{eff}(1+\frac{\nu}{c})^2 \qquad (2.8)$$

where $\nu = U\ f\ F$ is the ratio of the background signal to the normalized fluorescence intensity of the fluorophore.

2.5.2 Laser Light Scattering Technique

I. The concept

The field of light scattering is a well-studied, detailed scientific discipline on which a lot of information has been published. Lord Rayleigh first described the science of light scattering at the end of the 19th century; experiments in the field have proceeded thereafter within the limitations of the technology. When monochromatic, polarized lasers became available in the early 1970s, laser light scattering (LLS) technology began to be applied to practical instruments for research and industrial use. In contrast to the well known analytical tools such as fluorescence, phosphorescence and Raman

spectroscopy, the fundamentals of LLS is based on the elastic light scattering where the frequency of the scattering light is the same as the incident light.

In a light scattering experiment, when a laser passes through a sample containing scatterers, it introduces a phase shift that results from a path length difference in the scattered light. The scattered light from different regions in the scattering volume interferes to form a scattering pattern that consists of both constructive and destructive interference of the scattered light. The regions of constructive interference show up as a bright spots and are called speckles. In general the scatterers are able to undergo random motion around their mean positions, which causes the phase shifts to fluctuate with time, which results in the speckles to change intensity over time. The average intensity of these speckles over time as a function of the scattering vector, $I(q)$, provides information regarding the shape and spatial orientation of the scatterers, and is known as static light scattering. On the other hand, measuring the fluctuations in the intensity of the speckles provides information regarding the dynamics of the scatterers, and is known as dynamic light scattering.[72,73] Assuming that the particles are at rest in the solution, there will be no discrimination of the scattered light intensity in each direction and the value of scattering light intensity should be independent of time. In fact, however, all the particles or scatterers in solution are undergoing constant Brownian motion. This Brownian motion leads to a fluctuation of the scattered intensity pattern. The fluctuation rate can be related to different kinds of relaxation processes such as diffusion (transition and rotation) and internal motions of the macromolecules. Faster relaxation process may lead to the faster intensity fluctuation.

In dynamic light scattering, the measured quantity in is the fluctuation of the scattered intensity with time t, caused by the particle Brownian motion. The motion of the particles includes transitional, rotational or internal motion.

The particle's translational diffusion coefficient (D), relaxation rate (Γ) and hydrodynamic radius (R_h) can be determined by DLS. In contrast, the static light scattering SLS is used to measure the time-average scattered intensity at different angles and concentrations, with which we may calculate other physical parameters of macromolecules: the weight-average molecular weight (Mw), the z-average root-mean-

square radius of gyration $<Rg^2>^{1/2}$, (simply R_g), and the second-order virial coefficient (A_2).

II. Dynamic Light Scattering (DLS)

As mentioned above, the measured subject of dynamic light scattering DLS (also known as Quasi Elastic Light Scattering (QELS)) is the intensity fluctuation, which is essentially caused by the Doppler effect. When an incident light beam is scattered by a moving macromolecule or particle, the frequency of the scattered light will be slightly higher or lower than that of the incident light, depending on the relative velocity between the detected particle and the detector. As a result, the frequency distribution of the scattered light will be slightly broader than that of the incident light.

Compared with the incident light frequency (10^{15} Hz), the scattered light frequency broadening (10^5-10^7 Hz) is very small and very hard to be detected in the frequency domain. Nonetheless, it can be accurately recorded in the time domain through a time correlation function. For this reason, dynamic light scattering is sometimes referred to as photon correlation spectroscopy (PCS).

However, in the time domain, the fluctuation of the scattered intensity is closely related to the frequency broadening and can be sensed by a highly sensitive and fast response photodiode detector. It is equally efficient to have either the fluctuation of the scattered intensity or the frequency broadening because the two effects are related to each other. But how do these fluctuations in the intensity of scattered light arise? Imagine if a laser illuminates a cuvette, containing particles that are stationary, and a frosted glass screen is used to view the sample cell. A classical speckle pattern can be seen in Fig. 2.8.

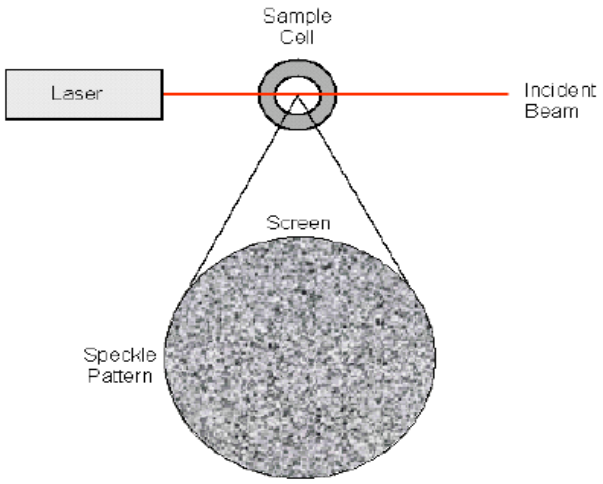

Figure 2.8: Schematic depiction of a speckle pattern (adapted from DLS technical notes; Malvern Instruments)

The speckle pattern will be stationary both in speckle size and position because the whole system is stationary. The dark spaces are where the phase additions of the scattered light are mutually destructive and cancel each other out (figure 2.9A). The bright blobs of light in the speckle pattern are where the light scattered from the particles arrives with the same phase, and interfere constructively to form a bright patch (figure 2.9B)

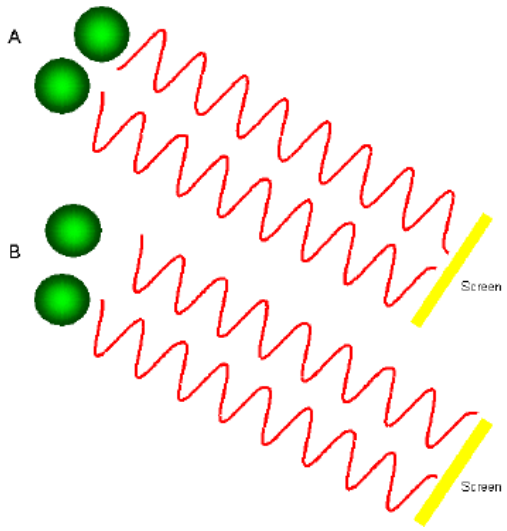

Figure 2.9: The observed signal depends on the phase addition of the scattered light falling on the detector. In example A, two beams interfere, 'canceling each other' resulting in a decreased intensity. In example B, two beams interfere and 'enhance each

other' resulting in an increased intensity (adapted from DLS technical notes; Malvern Instruments)

As mentioned in Paragraph 2.2.3, the scatterers in a polymer gel are localized near fixed average positions and are able only to execute limited Brownian motion about these positions. By virtue of this localization of the scatterers, one sample of such a system will be trapped in a restricted region of phase space, whose location and extent are determined, respectively, by the average position of the scatterers and the magnitude of their displacements. Such a system, that cannot explore enough of phase space so that the time average is the same as its ensemble average, is called non-ergodic. One approach to treat the complications caused by non-ergodicity of such systems is the heterodyne optical mixing approach; therefore, a short introduction to the basic optical mixing methods will follow.

There are two basic forms of the optical mixing heterodyne and homodyne. Heterodyne mixing is the mixture of the scattered light with a reference beam (local oscillator), which has a constant frequency same as the incident light beam.

In the homodyne model, however, the scattering light is not mixed with a reference signal but directly being detected. The DLS theory illustrated in the following paragraphs is based on the homodyne intensity-intensity time correction spectroscopy.
In dynamic light scattering information about the dynamics of the scatterers can be obtained by measuring the normalized intensity autocorrelation function $g^{(2)}(\tau,q)$[72] given by

$$g^{(2)}(\tau,q)=\frac{\langle I(t,q)I(t+\tau,q)\rangle}{\langle I(t,q)\rangle^2}$$

where the intensity at a particular time is correlated with the intensity measured at a later delay time for any scattering wave vector, q and the angular brackets denote time average.

For ergodic samples where the time averaged intensity is equal to the ensemble averaged intensity, the measured intensity autocorrelation function is converted into field autocorrelation function $g^{(1)}(\tau,q)$ by the Siegert relation[72, 73] given below

$$g^{(2)}(\tau,q)=1+\beta\left|g^{(1)}(\tau,q)\right|^2$$

where β is the coherence factor that depends on the experimental set-up and for fiber based optical detection systems it is very close to 1.

For non-ergodic systems, the Pusey method[43, 74] is used to calculate the true ensemble averaged correlation function. For these type of systems, the Siegert relation is no longer valid and the ensemble averaged field correlation function, $g^{(1)}$ (τ ,q), is given by[43, 74]

$$g_1^E(\tau,q) = \frac{Y-1}{Y} + \frac{(g_2^T(\tau,q)-\sigma^2)^{1/2}}{Y}$$

where $g_2(\tau,q)$ is the measured time averaged intensity correlation function, $\sigma^2 = \langle I^2(0)\rangle_T / \langle I(0)\rangle_T^2 - 1$, $Y = \langle I\rangle_E / \langle I\rangle_T$ is the non-ergodic parameter, where $\langle I\rangle_T$ is the time averaged intensity and $\langle I\rangle_E$ is the ergodic averaged intensity which is measured while the sample is rotated so that different ensembles of the sample are illuminated and a proper ensemble averaged measurement can be obtained.

Further, the transitional diffusion coefficient D may be related to the molecular friction factor f through the Stokes-Einstein relation:

$$D = k_B T / f$$

where k_B and T are the Boltzmann constant and the absolute temperature, respectively.

For a hard sphere with a radius of R, the friction factor f is given by the equation:

$f = 6\pi\eta R$, where η is the viscosity of the solvent.

For a polymer coil, R is replaced by its hydrodynamic radius R_h, so that

$$R_h = \frac{k_B T}{6\pi\eta D}$$

In order to obtain good statistics for the light scattering measurements the experiments are typically run for long durations. Typically the measurement time should be many orders of magnitude greater than the slowest relaxation time. There are two ways in which the signal to noise ratio can be improved, one way is by increasing the intensity of the scattered light by increasing the intensity of the incident light and the other is by increasing the duration of the experiment. The output signal from the amplifier discriminator is typically in the range of few hundred kilohertz. The photons that enter the detector follow Poisson statistics and hence the statistical error in the

measurement is given by $\frac{\sqrt{N}}{N} = \frac{1}{\sqrt{N}}$ where N is the number of photons entering the detector.

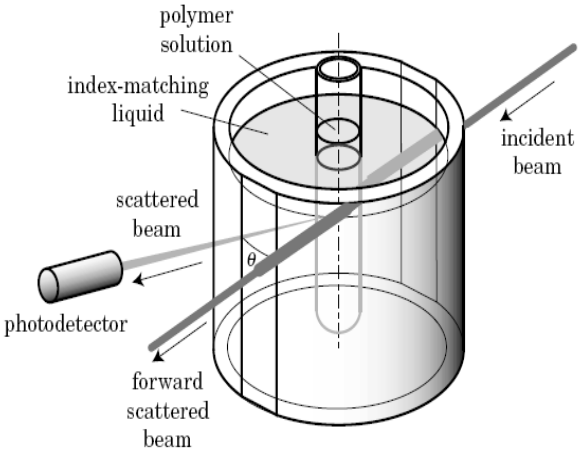

Figure 2.10: Schematic diagram of a typical dynamic light scattering set-up (figure courtesy of N. Gomopoulos)

Chapter 3: Experimental Procedures

3.1 Introduction

This chapter describes the experimental procedures employed for the dynamic characterization of thin hydrogel layers grafted onto solid substrates. In the beginning of this section, the synthesis of the photo-crossslinker, adhesion promoters, and polymer is explained. Patrick Beines and Robert F. Roskamp from the Max Planck Institute for Polymer Research, in Mainz, Germany, performed the synthesis and kindly provided the polymer and the adhesion promoters used in this work. After a brief description of the process of film formation and the intoduction of crosslinks via UV irradiation, emphasis will be given on the experimental set-ups and procedures used for the dynamic study of the gel layers by means of fluorescence correlation spectroscopy (FCS) and light scattering technique.

3.2 Materials

N-Isopropylacrylamide (NIPAAm, Aldrich) was purified by recrystallization from a mixture of toluene/hexane (1:4) and dried in vacuum. Methacrylic acid (MAA, Aldrich) was distilled prior to use. 2,2′-Azobis(isobutyronitrile) (AIBN) was recrystallized from methanol. Dioxane used for the polymerization was distilled over calcium hydride. Tetramethylrhodamine cadaverine (Biotium) and all other reagents of analytical grade were used as received. The synthesis of 4-methacryloyloxybenzophenone (MaBP) monomer, 4-allyloxybenzophenone, 4-(3'-chlorodimethylsilyl)propyloxybenzophenone (silane1), and trifluoroacetyl *N*-succinimidylester is described elsewhere.[75]

Shortly, the MaBP monomer was synthesized from 4-hydroxybenzophenone and methacryloyl chloride via a typical esterification reaction in dichloromethane solvent and triethylamine as the acid scavenger.

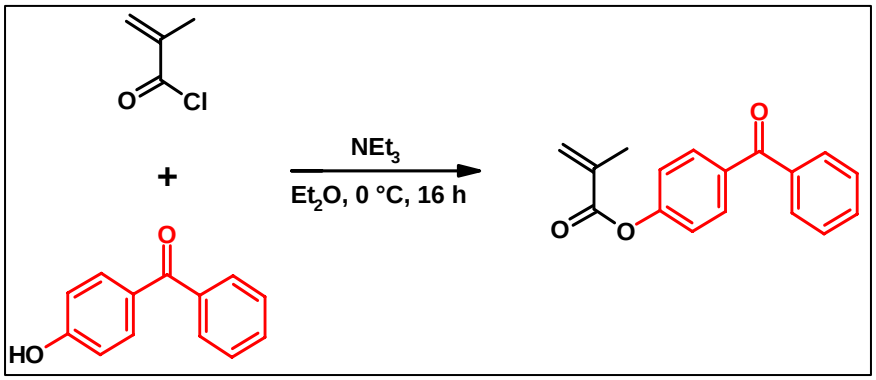

Figure 3.1: Synthesis of 4-Methacryloyloxybenzophenone

3.3 Synthesis of the Terpolymer [27]

The pNIPAAm terpolymer was obtained by free radical polymerization of NIPAAm, MAA, and MaBP, initiated by AIBN. The polymerization solvent was dioxane. The reaction was carried out at 60 °C under argon for 24 h. A scheme of the polymerization reaction is shown in Figure 3.2. The polymer was precipitated directly from the reaction mixture in ice cold diethyl ether, purified by reprecipitation from methanol into ice cold diethyl ether, and freeze-dried from *tert*-butanol.

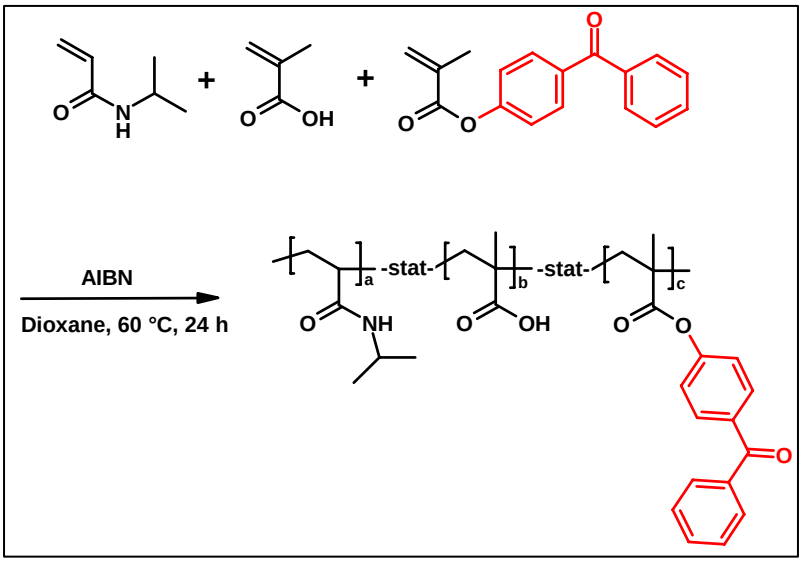

Figure 3.2: Free radical copolymerization

3.4 Synthesis of the Adhesion Promoters

It has been observed that physisorbed hydrogel layers detach from the surface upon exposure to solvents.-To avoid the delamination two adhesion promoters were synthesized for the covalent attachment of thin hydrogel layer to glass substrates, a chlorodimethylsilane (silane1) and a triethoxysilane (silane2). The reactive silane anchor group of these adhesion promoters is responsible for the chemisorption on the substrate and the surface reactions in this case leads to covalent Si-O bonds between the silanes and the silanol functions at the substrate surface.

3.4.1 Synthesis of 4-(3'-Chlorodimethylsilyl)propyloxybenzophenone (silane1)

Standard hydrosilation procedures[76] were employed for the synthesis of this compound. Typically, 2 g of 4-allyloxybenzophenone was suspended in ca. 20 mL of freshly distilled dimethylchlorosilane. Pt-C (10 mg, 10%Pt) was added and the mixture was refluxed for 5 h. The excess dimethylchlorosilane was removed in vacuum, yielding the desired product in quantitative yields as oil. The catalyst was removed by filtration of

a solution of 4-allyloxybenzophenone in toluene. This solution was then directly used for the surface modification. The silane1 can be immobilized on SiO2 surfaces by immersing an appropriate substrate into a dilute (typically 1 mM) solution of silane1 in toluene. A few drops of dry NEt_3 are added to bind the formed HCl and to act as a catalyst.[77] This procedure yields monolayers of the benzophenone silane (BPML) of a typical thickness of ca. 1 nm. More details about the procedure can be found in the literatute.[78]

3.4.2 Synthesis of 4-(3-triethoxysilyl)propoxybenzophenone (silane2)

The detailed synthesis is described elsewhere.[79] Briefly, 4-allyloxybenzophenone (1g, 4.2 mmol) was dissolved in triethoxysilan (10 mL, 44.4 mmol) at room temperature under argon. After addition of platinum on activated charcoal (10mg, 10%) the solution was stirred at room temperature until TLC shows complete conversion of the 4-allyloxybenzophenone, which was achieved after 2 days. The catalyst was filtered off and the excess of triethoxysilane was removed in high vacuum. The product was obtained in quantitative yield as brownish-white solid and used without further purification. Functionalisation of the glass surface was achieved by immersion into a 1 mM ethanolic solution over night. The triethoxysilane anchor group has the advantage of lower reactivity and no autocatalytic activity compared to chlorosilanes, and it is stable in ethanolic solution (no self-condensation), which makes convenient handling under standard laboratory conditions possible.

3.5 Fluorescent Probe Molecules

For the FCS measurements on semi-dilute pNIPAAm solutions in ethanol, two different fluorescent tracers were used: rhodamine 6G (Rh6G, Sigma-Aldrich) with R_h = 0.8 nm in ethanol and tetramethylrhodamine labeled pNIPAAm with R_h = 19 ± 1 nm (synthetic details further below). Various probes were used for the FCS measurements on pNIPAAm gel layers swollen in ethanol and water. In an attempt to elucidate the role of electrostatic interactions between the polymer gels and the tracer on the diffusion process, fluorescent probes with different charges have been tested. In this work,

experimental results are reported that were obtained with the probes listed on the table 3.1. The corresponding laser lines used, wavelengths and sizes (R_h) are presented as well.

Table 3.1: Summary of fluorescent probes used in the FCS experiments

Fluorescent Probe	II. III. IV. Laser Line	**Excitation Wavelength / Emission Filter**	R_h	**Molecular Structure**
Rh6G (Sigma-Aldrich, Germany)	HeNe	543/ LP560	~0.8 nm (in ethanol)	Fig. 3.3b
Tetramethylrhodamine labeled pNIPAAm	HeNe	543/ LP560	~19 nm (in ethanol)	
AlexaFluor647	HeNe	633	~1.4 nm (in water)	Fig. 3.3a
FluoSpheres [a)]	HeNe	543/ LP560	~10 nm (in water)	
PEG_Alexa488 [b)]	Argon	488/LP505	~3.5 nm (in water)	
Fluorescently labeled silica particles [c)]	HeNe	543/LP560	~ 42nm / 50 nm (in ethanol)	
Fluorescein (Sigma-Aldrich, Germany)	Argon	488/LP530	~ 1nm (in water)	Fig. 3.3c
Perylene dye [d)]	Argon / HeNe	488/LP530 543/LP560	~ 2.3 nm (in water)	Fig. 3.3d, e
Protein BSA (1) [e)]	HeNe	543/LP560	~ 6nm (in water)	

Protein BSA (2) [e]	HeNe	543/LP560	~ 4.2 nm (in water)	

a) Nile red fluorescent Fluospheres beads (Molecular Probe, Germany): Carboxylate-modified polystyrene microspheres maximally excited at 535nm, with broad excitation and emission bandwidth.

b) Commercial PEG, labeled with Alexa488 by Georgi Mihov - Prof. Muellen's group, at Max-Planck Institute for Polymer Research (MPIP), Mainz, Germany.

c) Commercial fluorescent silica particles (Kisker, Germany), labeled with a dye (absorption: 528 nm/emission: 596 nm)

d) Synthesized at MPIP by Kalina Peneva - Prof. Muellen's group.
Negative perylene: 1,6,7,12-Tetra[4-sulfophenoxy]-N,N'-(2,6 diisopropylphenyl)-pery lene-3,4,9,10-tetracarboxidiimide
Positive perylene: 1,6,7,12-Tetra[4-(2-trimethylammonio-ethyl)-phenoxy]-N,N' (2,6-diisopropylphenyl)-perylene-3,4,9,10-tetracarboxidiimide tetraiodide

e) Commercially obtained BSAs, labeled with tetramethylrhodamine by Georgi Mihov (Tanja Weil) at MPIP. BSA (1) stands for cBSA (cationized) and BSA (2) is the native one (as purchased).

a

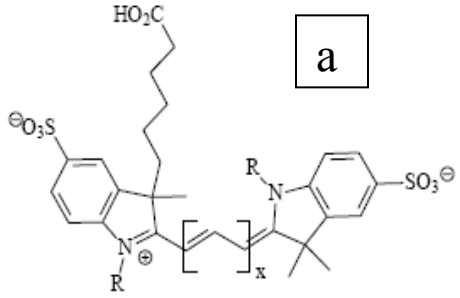

x = 1,2,3...

b

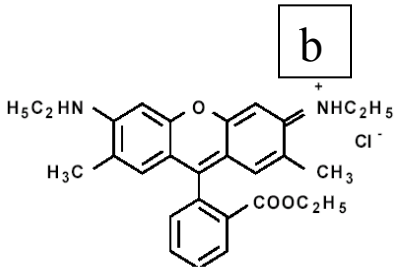

c

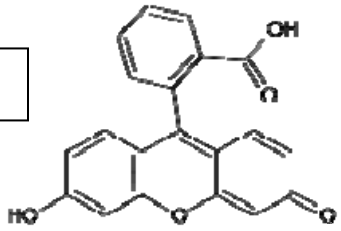

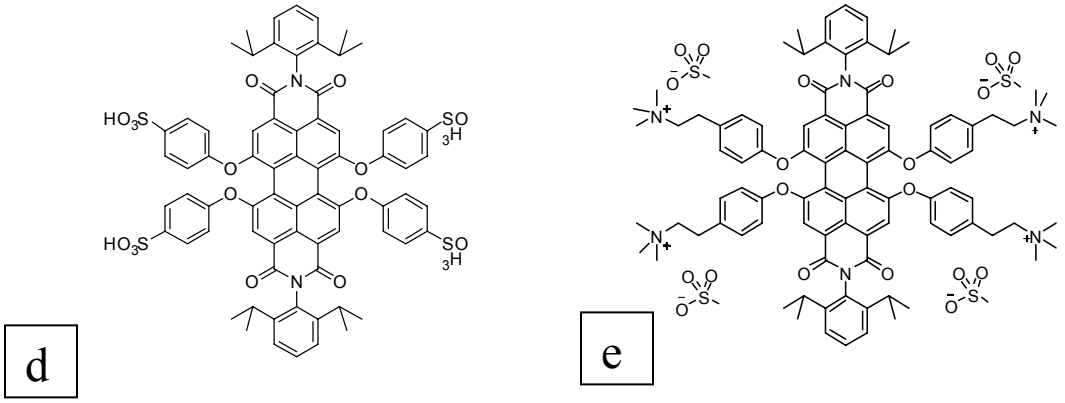

Figure 3.3: Molecular structures of a) Alexa647-cadaverine, b) Rh6G, c) Fluorescein, d) negative Perylene and e) positive Perylene

In the case of the attached tetramethylrhodamine dye, a pNIPAAm sample was first activated with trifluoroacetyl-*N*-succinimidyl ester and then labeled with tetramethylrhodamine cadaverine. The activation was performed in dichloromethane at room temperature for 3 h in the presence of triethylamine. Purification was achieved by precipitation in diethylether twice. For the labeling of the pNIPAAm polymer, addition of the tetramethylrhodamine cadaverine to the activated polymer was achieved by stirring in ethanol at 50 °C for 20 h. In order to remove nonbound dye molecules, the polymer solution was subjected to dialysis in ethanol (MWCO of 3500 g/mol for the utilized tube) for 2 weeks.

3.6 PNIPAAm Gel Film Formation

For the FCS studies, pNIPAAm gels were prepared on round glass microscope cover slides (Menzel-Glaser, Germany). The solution with the glass substrates was left to stand overnight. Then, the samples were cleaned by successively rinsing with dichloromethane, methanol, toluene, and again dichloromethane. After each rinsing step, the sample was blown dry with nitrogen.

pNIPAAm films of about 1 μm thickness were prepared by spin-coating from 10%w/w ethanol solutions onto the silanized microscope slides at 4000 rpm for 1 min. Spin coating provides very precise control over film thickness and, with a suitable solvent

and spin speed, results in uniform films. The samples were then dried over night at 55 °C and under vacuum conditions. Cross-linking of the pNIPAAm films was performed by UV irradiation at wavelength λ = 365nm for different times (from 10 to 240 min).

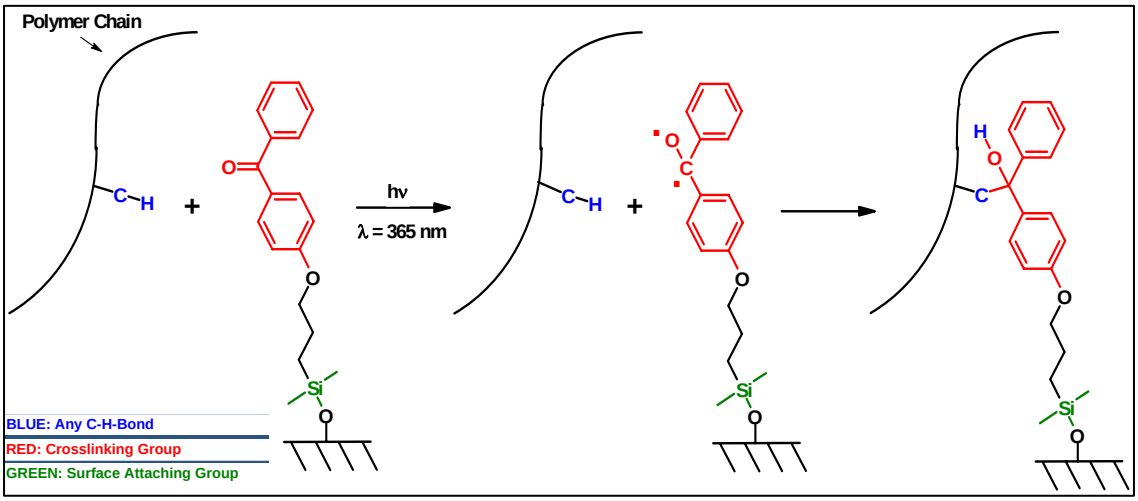

Figure 3.4: Simultaneous photo-crosslinking and surface attachment of thin hydrogel layer to the substrate (figure courtesy of Patrick Beines)

3.7 FCS Experimental Measuring Procedure

The FCS measurements were performed with a commercial FCS setup (Carl Zeiss, Jena, Germany) consisting of the module ConfoCor 2 and an inverted microscope model Axiovert 200. For all experiments, a 40x-C-Apochromat water immersion objective with a numerical aperture of 1.2 and a working distance of 0.29mm was employed.The fluorescent tracers Rh6G and rhodamine labeled PNIPAAm were excited with a He-Ne laser at λ = 543 nm and the fluorescence emission was collected after filtering with a LP560 long pass filter. The excitation laser lines, wavelengths and filters corresponding to all of the fluorescent probes are summarized in table 3.1.

These arrangements result in a Gaussian confocal observation volume: with r_0 =0.2 μm and z_0 =0.8 μm being the distances from the center of the beam focus. The fluorescence intensity fluctuations caused by the tracer diffusion through V_{obs} were detected with an avalanche photodiode enabling single-photon counting. Eightwell, polystyrene chambered cover-glass modules (Lab-Tek, Nalge Nunc International) were

used as sample cells for the ethanol solutions of the pNIPAAm polymer. These cells had bottom slides with a high optical quality surface and a thickness of 0.17 mm. The tracer (Rh6G or rhodamine labeled pNIPAAm) concentrations were in the order of 10^{-8} M in these experiments. An Attofluor steel cell was used for the studies of the hydrogels.

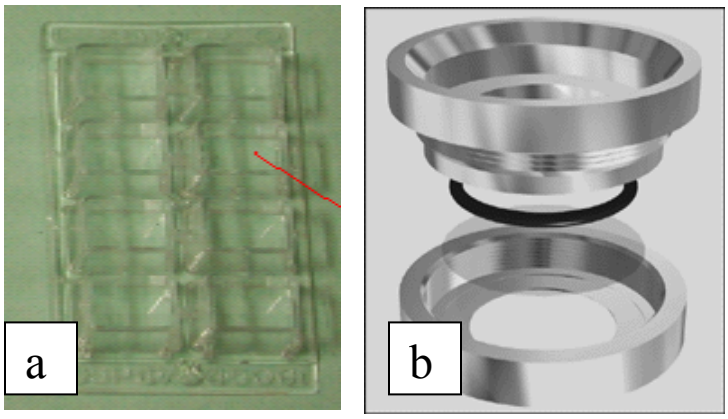

Figure 3.5: (a) Polystyrene chambered cover-glass modules and (b) the steel cell holder used for the FCS study of pNIPAAm solutions in ethanol and swollen pNIPAAm gels, respectively.

Before starting the FCS measurements, the anchored gels were rinsed with ethanol in order to remove all the unbound material and possible impurities from the preparation procedure that could lead, as discussed later, to autofluorescence of the gel. Then, the quantity of 1 mL of ethanol (or water) was added in the cell, and the gel was allowed to swell until it reached an equilibrium state. The tracers were then added to a final concentration of about 10^{-8} M. The FCS measurements were initiated 30 to 60min later in order for the probe to reach the equilibrium concentration in the sample.

Multiple measurements made at different positions in the gel have shown very similar results. At each position, a series of 10 measurements with a total duration of 5 min were performed. From the measured fluctuations of the fluorescence intensity an experimental autocorrelation function $G(t)$ was obtained. For an ensemble of M different types of freely diffusing tracers, $G(t)$ has the following analytical form[17,18] :

$$G(t) = \frac{1 + \frac{T}{1-T} e^{-t/\tau_T}}{N} \left(\sum_{i=1}^{M} \frac{1}{(1 + t/\tau_i)\sqrt{1 + t/(S^2\tau_i)}} \right) + 1 \qquad (3.1)$$

where M is the number of fluorescent components, N is the average number of fluorescent molecules in the detection volume, T and τ_T are respectively the fractional population and the decay time (in the range of 0.5-10 μs) of the triplet state, $\tau_i = r_0^{\,2}/4Di$ is the characteristic diffusion time of the ith fluorescent component with self-diffusion coefficient Di and $S = r_0/z_0$ is the structural parameter of the instrumental set-up.

Precise calibration of the confocal observation volume was performed using a reference dye with known diffusion coefficient, here Rh6G in water.

3.8 Laser Light Scattering Experimental Measuring Procedure

3.8.1 PCS Experimental Measuring Procedure

The structure and dynamics of dilute and nondilute pNIPAAm/ethanol solutions were examined by PCS using an ALV-5000 digital correlator as described in the literature.[80] The relaxation function $C(q,t) = \{[G(q,t) - 1]/f^*\}^{1/2}$ for the concentration fluctuations at a scattering wavevector q was computed from the experimental intensity autocorrelation function $G(q,t) = \langle I(q,t)I(q,0)\rangle / \left|\langle I(q)\rangle\right|^2$. $f^* < 1$ is an instrumental coherence factor and the scattering vector $q = (4\pi n/\lambda)\sin(\theta/2)$ is computed from the scattering angle θ, the refractive index n of the solution, and the wavelength λ of the laser beam.

For dilute solutions of ideally monodisperse polymers, the exponential decay relaxation function

$$C(q,t) = \alpha \exp(-D_0 q^2 t) \tag{3.2}$$

yields the chain translational diffusion:

$D_0 = k_B T/(6\pi\eta R_h)$ and the net intensity $\alpha I(q)$ associated with the solute polymer; k_B is the Boltzmann constant, T the absolute temperature, Rh is the hydrodynamic radius, and η is the solvent shear viscosity. The absolute light scattering intensity Rvv = $\alpha I(q = 0)(n/nt)^2 R_t/I_t$ with n_t the refractive index, I_t the intensity, and R_t = 2.7 x 10^{-5} cm^{-1} the absolute Rayleigh ratio of the standard toluene, yields the weight average molar mass M_w = Rvv/(Kc) for sufficiently dilute solutions of pNIPAAm in ethanol.

In order to obtain the optical constant $K = 2\pi n\,(\mathrm{d}n/\mathrm{d}c)^2/(\lambda^4 N_A)$ where c is the polymer concentration (in grams per milliliter) and N_A is the Avogadro number, the refractive index increment $\mathrm{d}n/\mathrm{d}c$ = 0.152 mL/g was measured at wavelength λ=633 nm using a scanning Michelson interferometer. The molar mass M_w (= Rvv/(Kc)) amounts then to 305 ± 20 kg/mol using the experimental absolute intensity Rvv and the optical constant K. The molecular weight (M_w) of the polymer that was determined by gel permeation chromatography (GPC)* was found equal to 404 kg/mol. This value compares reasonably well to the light scattering-measured M_w, despite the fact they are two completely different techniques with GPC relying on an external standard (PMMA in this case). The polydispersity obtained by GPC amounts to M_w/M_n = 2.2.

3.8.2 Micro-Photon Correlation Spectroscopy (μPCS)

For the laser light scattering measurements on pNIPAAm gels swollen in ethanol and water, the experimental set-up shown in Fig. 3.8 was developed. As excitation light source, a Nd: YAG laser at a wavelength of λ = 532nm with 150mW power and a beam diameter of 0.32mm was used. The scattered light was collected under different scattering angles θ by an optical fiber and detected by a photomultilier tube connected to an ALV-5000 digital fast photon correlator. The output of the correlator is the time average autocorrelation function, $G(q,t) = \langle I(q,t)\, I(q,0)\rangle / \langle I(q,0\rangle^2$, of the scattered light intensity I(q,t), with wave vector $q = (4\pi n/\lambda)\sin(\theta/2)$ where n is the refractive index of the medium and λ the laser wavelength. The immobile inhomogeneities provide a static scattering background, which in addition to the strong elastic light scattering from the laser spot in the film act as local oscillators. Hence the experimental G(q,t) recorded under heterodyne conditions directly relates to the desired relaxation function of the fast concentration fluctuations in the sample.

* For the GPC a Waters instrument equipped with UV and RI detectors and PSS GRAM columns were used. The samples were measured at 60 °C in DMF with a flow rate of 1.0 mL/min.

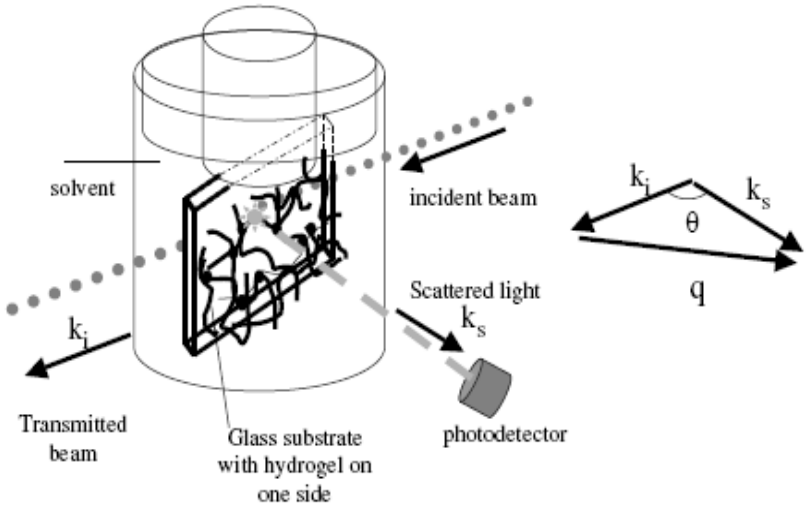

Figure 3.6: Experimental geometry of the sample cell used for the light scattering measurements along with the scattering wavevector $q=k_s-k_i$ and the wavevectors k_i of the incident and k_s scattered light.

3.8.2.1 Salt Concentration and Temperature Dependence

The pNIPAAm gels were immersed in aqueous solutions of NaCl at different concentrations in succession at 22^0C, starting with deionized and distilled (Milli Q) water and going gradually to higher concentrated salt solutions. Reversibility was checked by bringing the gels back into Milli Q water after each measurement, to verify that there is no persistent alteration of the gel structure due to the salt exposure.

For the temperature-dependent measurements in water, the temperature of the samples in the sample cell was regulated by 2 home-built tape heaters (Fig.3.7) and was controlled by a Shimaden SR91 digital temperature controller, via a K-type thermocouple, with an accuracy of 1^0C. When temperature was varied, the sample was allowed to equilibrate before the measurement for 10-30 minutes.

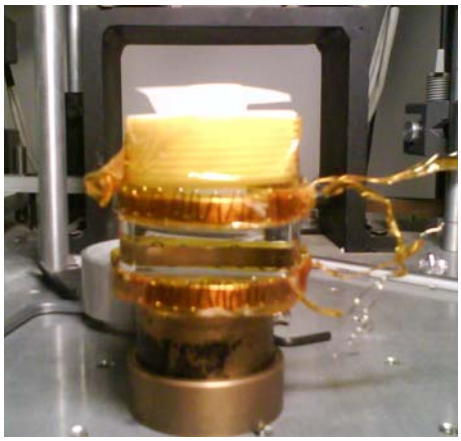

Figure 3.7: A photograph of the sample cell used for the temperature-dependent light scattering measurements surrounded by the two home-built tape heaters.

Chapter 4: Fluorescence Correlation Spectroscopy (FCS) - Results and Discussion

4.1 Overview

The diffusion of solutes within macroporous hydrogels is a very important component in many biotechnological applications and is governed mainly by three parameters, in terms of properties of both the polymer matrix and the structure of the diffusing probe:[81]

1) the size of the diffusing species relative to the mesh size (or screening length) ξ,

2) the fractal dimension of the diffusing species, and,

3) the time for the matrix polymer mesh to rearrange relative to the time that the probe needs to move over the length ξ.

Especially in charged gels, that is gels containing polyelectrolyte moieties that serve as hydrophilic regions allowing the water to diffuse out of the hydrogel upon collapse, the diffusion can be significantly affected by the presence of specific or nonspecific interactions of the probe with the gel matrix.

In an attempt to elucidate the role of the above-mentioned parameters onto the diffusion process, hydrogel pNIPAAm films on glass substrate were prepared and the diffusion of probe particles was investigated by means of fluorescence correlation spectroscopy (FCS). Different cross-linking densities (corresponding to different irradiation times used for the cross-linking process) were examined and the FCS results indicate that the probe particles are slowed down and the swelling ratio of the gels decreases with increasing cross-linking density.

In these gels, the methacrylic acid (MAA) provides the polyelectrolyte character; therefore, it was of great importance to prove that the diffusive behavior of the fluorescent probe inside the gel depends strongly on its nature (electrostatic or other interactions of the fluophore with the matrix). Experiments were performed with a variety of probes with different kind of charges (e.g. fluorescein, positively and negatively charged perylene dye, labelled PS nanospheres etc.) and in two different solvents, ethanol and water. In the case of water, the electrostatic interactions of the probe (Rh6G dye) with the gel were more pronounced, due to the dissociation of the ion pairs (in the dye

and the polymer, respectively). This ion dissociation was mostly absent in ethanol, so no electrostatic interactions are observed. Probing the diffusion in gels in water was achieved by using an AlexaFluor647 dye, which seems not to interact electrostatically with the hydrogel matrix. Also FCS on ethanolic pNIPAAm polymer solutions was able to detect differences in the diffusion times with increasing polymer concentration. The results presented here suggest that the solute diffusion within hydrogels and nondilute polymer solutions is hindered in comparison to its diffusion in an unrestricted medium and that the FCS is a well-suited technique for quantifying the diffusive properties of small molecule probes in thin pNIPAAm hydrogels and polymer solutions.

4.2 FCS Results on pNIPAAm gels

The experimental measuring procedure is described in "Chapter 3: Experimental Procedures" section. Briefly, the polymer was dissolved in ethanol (10% w/w) and then spin-coated on round microscope slides at 4000 RPM for 60 sec providing thin hydrogel films of ~ 1μm of dry thickness. To avoid delamination of the gel layer, gel adhesion was promoted by prior substrate treatment with an adhesion promoter silane. The slides were dried over night at 55^0 C and in vacuum. Cross-linking was performed by UV radiation for 60 min. The slides were then placed in an Attofluor steel cell and on top of the inverted microscope. Measurements were performed in two different solvents, ethanol and water, after rinsing the gel layers with ethanol in order to remove impurities and possible unbound material.

Free Probes in Pure Solvents

Two small dyes of about the same size (R_h in water ~ 1 nm) were employed for the first FCS measurements; Rh6G dye which carries a positive net charge, and AlexaFluor647, which behaves like an overall neutral molecule. The two dyes were initially tested in two different solvents, water and ethanol, in the absence of the gel matrix.

The net fluorescence intensity autocorrelation functions that correspond to the free diffusion of AlexaFluor647 dye in the pure solvents, ethanol and water, are presented in Fig.4.1a. The diffusion times of the dye were slightly different for the two solvents, being faster in water, due to its lower solvent viscosity (by 20%) and probably due to solvation effects. In Fig.4.1b the intensity autocorrelation functions for free Rh6G in both solvents is presented, which resembles essentially the diffusion of AlexaFluor647 in the pure solvents. Again, there was a small difference between the diffusion times in water and in ethanol, with Rh6G displaying a slower diffusion time in ethanol. As for the case of AlexaFluor647, this fact was attributed to viscosity and solvation effects.*

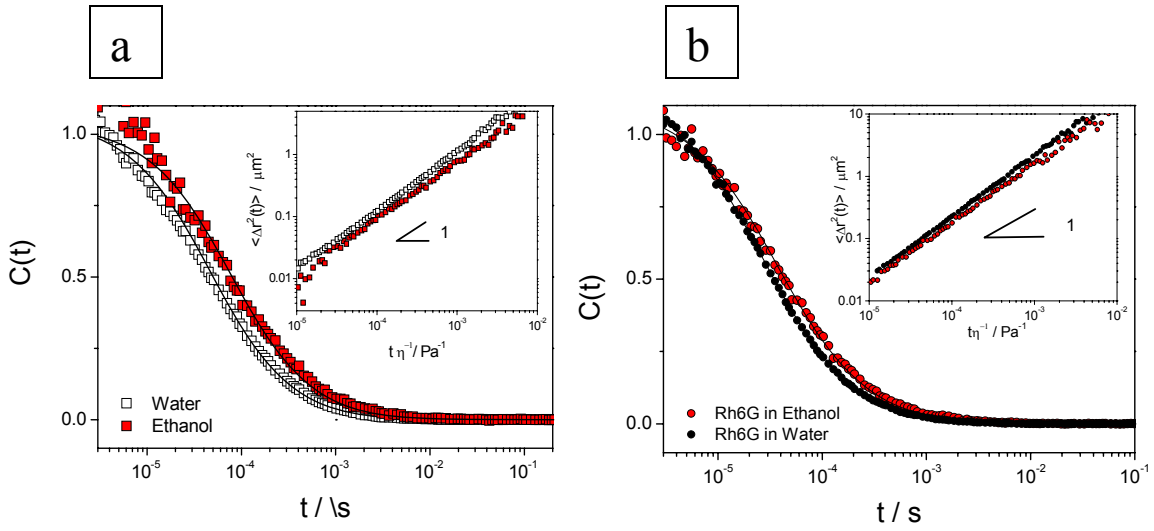

Figure 4.1: Normalized fluorescence intensity autocorrelation functions C(t)= G(t) – 1 corresponding to the diffusion of a) AlexaFluor647 dye, and b)Rh6G dye, in pure solvents (ethanol and water). The insets show the mean square displacement MSD as a function of time, corrected by the viscosity of the two solvents.

The diffusion exponent, which is represented by the slope of the mean square displacement versus time curves in the insets, was derived with the equation that directly relates the G(t) with the dye mean square displacement (MSD) $\langle r^2(t) \rangle$: for N

* In water the AlexaFluor647 and Rh6G ions are fully solvated and dissociated from the counterions, whereas in the less polar ethanol they stay together as a close ion pair, giving rise to a bigger R_h, thus a slightly higher diffusion time.

independent randomly moving dyes in a Gaussian beam, the decay of G(t) due to 3D diffusion is

$$G(t)=N^{-1}[1+(2/3)<r^2(t)>/x^2_0]^{-1}[1+(2/3)<r^2(t)>/z^2_0]^{-1/2} \quad (4.1)$$

where x_o and z_o the dimensions of the sampling volume in lateral and transversal dimensions respectively.[17, 18] A diffusion exponent equal to 1 implies free (unrestricted) diffusive behavior of the probe, whereas smaller than 1 suggests an anomalous (hindered) probe diffusion. This can be caused for a probe diffusing in a heterogeneous medium, like a gel, by a) a fractal gel matrix or b) nonelastic interactions between the network and the diffusing probe.

For the FCS measurements on swollen gels, the quantity of 1 ml of ethanol (or water) was added in the steel cell holder (presented in Fig. 3.5b) carrying the sample gel, and the gel was allowed to swell for some time until it reaches an equilibrium state. With the procedure of the so-called 'Z-scan', discussed in detail below, the swelling ratio of the gels in the two different solvents, as a function of the irradiation dose used at the cross-linking process could be determined.* The swelling ratio k, in this case, is defined as the ratio of the swollen state thickness to the dry state thickness.

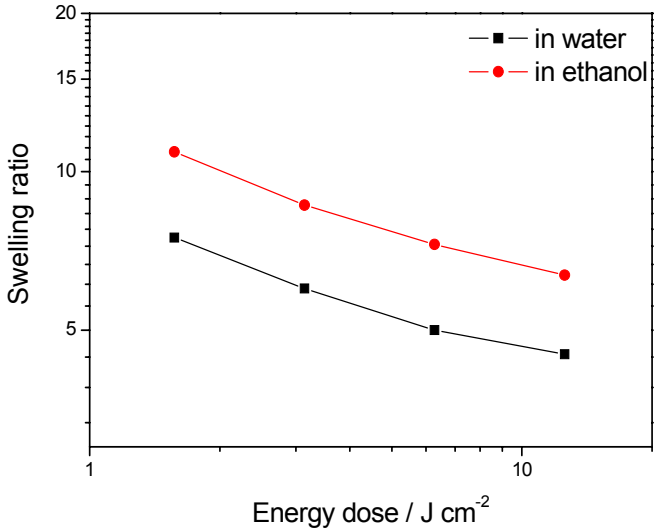

Figure 4.2: Swelling ratio for four different cross-linking densities, corresponding to four different irradiation doses of 1.6, 3.2, 6.3 and 12.6 J cm^{-2}, in ethanol and in water.

* It is the irradiation dose (or corresponding irradiation time) that controls the cross-linking density.

From the double logarithmic plot of Fig 4.2, a higher swelling ratio was observed for the gels in ethanol than in water, for identical irradiation doses (ethanol being a better solvent than water for the specific system). The cross-linking density increased with increasing the irradiation dose, in both solvents, as evidenced from the reduced swelling ratio. This is to be expected since high irradiation doses promote the cross-linking density, increasing the resistivity of the network to the elongation of the chains caused by the swelling and giving rise to a reduced swelling ratio.

Probe Diffusion in the Absence of Specific Interactions

As mentioned previously, in charged gels, the diffusion can be significantly affected by the presence of specific interactions of the probe with the gel matrix. In this section, the simplest case will be presented, that is, diffusion of probes that show no specific interaction with the gel matrix.

First, the case of Rh6G in gels swollen in ethanol was examined. After equilibration of the gel upon addition of ethanol, Rh6G was added in the cell holder upon a final concentration of 10^{-8}M. The dye diffused very fast into the gel, seconds after the addition of the Rh6G solution in the cell, a fact that can be seen by the immediate increase of the fluorescence intensity in the gel.

Fig. 4.3 shows normalized correlation functions for the diffusion of Rh6G in UV cross-linked grafted pNIPAAm gels swollen in ethanol (good solvent), displaying swelling ratios of k = 10.9 and k = 4.5 respectively for irradiation dose of 1.6 and 25.2 J cm^{-2} (corresponding irradiation times T_{UV} of 15min and 4h, respectively). Note the systematic shift of the curves to the right with increasing cross-linking density, resulting in higher diffusion times. The solid lines are the fits of the expression (3.1) to the data, indicating that each of the gels could be satisfactorily described by a single characteristic time, τ_D. Interestingly enough, the short and long T_{UV} times did not affect, however, the purely diffusive random translation of the probe as indicated by the slope in the inset to Fig. 4.3. This is a pertinent finding given the, in general, inhomogeneous structure of gels[82, 83]

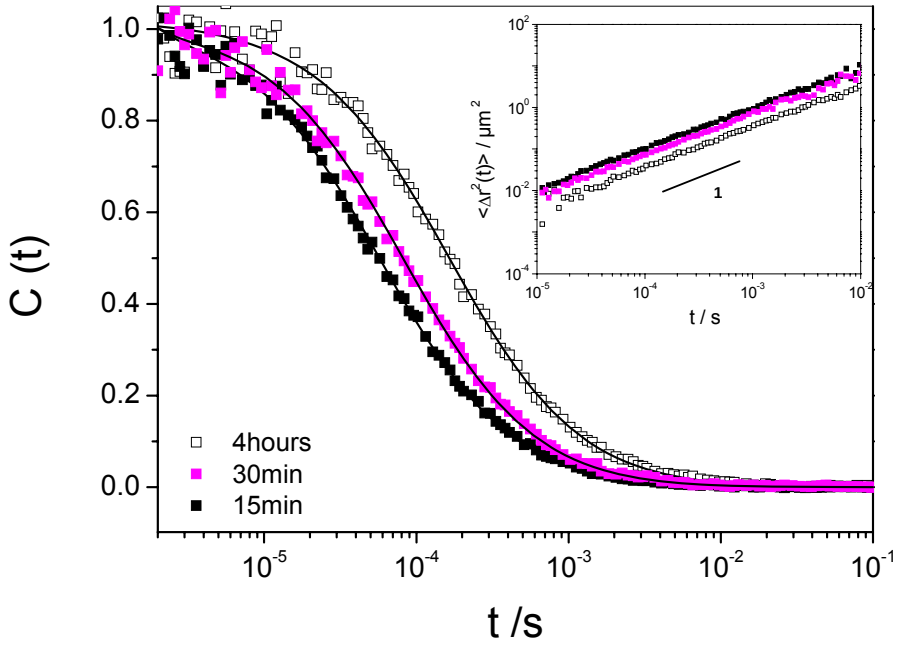

Figure 4.3: Normalized fluorescence intensity autocorrelation function C(t)= G(t) - 1 for Rh6G in cross-linked pNIPAAm films prepared under three different UV exposure times, 15 min, 30 min and 4 h (corresponding to irradiation doses of 1.6, 3.2 and 25.2 J cm^{-2}, respectively) and subsequent swelling in ethanol. The diffusive (slope one) mean square displacement of the single R6Gh is shown in the double log plot in the inset.

It is also interesting to note that, when comparing the diffusion time of Rh6G in pure ethanol and in a gel cross-linked for 60 min (irradiation dose of 6.3 J cm^{-2}) swollen in the same solvent, the mere presence of the gel acted as means of retarding the diffusion of the dye by a factor of three (from 40 μsec in the pure ethanol to 140 μsec in the gel). Fig. 4.4 depicts the effect of irradiation time (cross-linking density) on the diffusion time. Apparently, the prolonged UV exposure time T_{UV} promotes the slow down of the small probe diffusion, from 60 μsec (T_{UV} =15min) to 150 μsec (T_{UV} =240min).

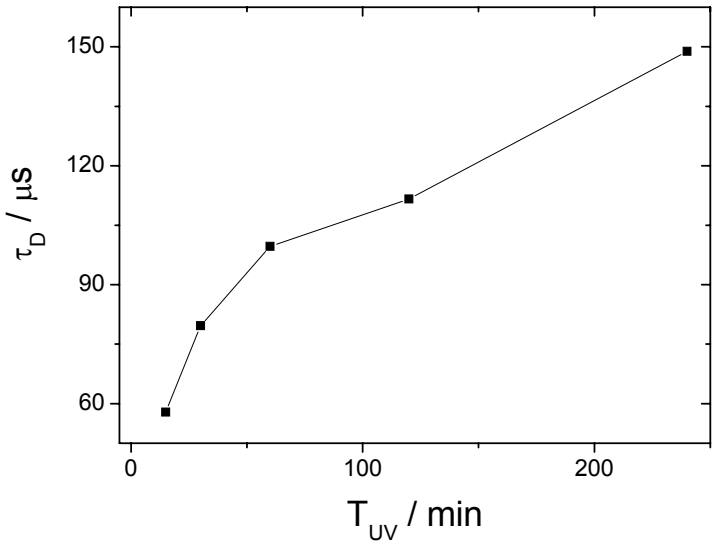

Figure 4.4: The characteristic diffusion time of Rh6G in pNIPAAm gels swollen in ethanol plotted as a function of the cross-linking time.

The diffusion of Rh6G in gel swollen in water displayed a more complex behavior and will be discussed in the section where the role of the electrostatic interactions of the probe and the gel in the diffusion process is explained.

For the diffusion of Alexa Fluore647 in a gel crosslinked for 60min (corresponding to 6.3 J cm^{-2} energy dose) shown in Fig.4.5 one can observe that the diffusion is slightly faster in the case of water, and the retardation of the fluorescent dye in the gels compared to the pure solutions is almost the same for both solvents, as shown in the inset.

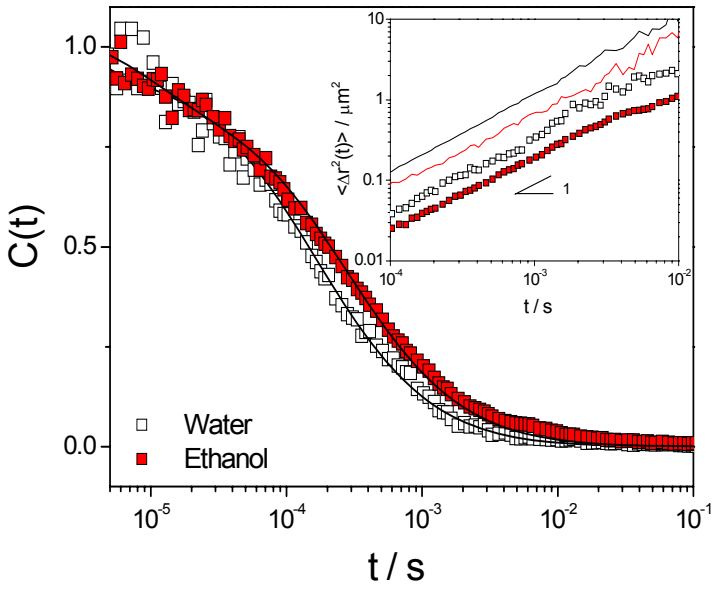

Figure 4.5: Normalized fluorescence intensity autocorrelation functions C(t)= G(t) - 1 corresponding to the diffusion of AlexaFluor647 dye in a gel cross-linked for 60min (corresponding to 6.3 J cm^{-2} energy dose), in ethanol and water. The lines in the inset represent the data for the diffusion in pure solvents (red line for ethanol) from Fig.4.1a.

In Fig.4.6, the normalized diffusion times for AlexaFluor647 dye in the gel swollen in both solvents (water and ethanol) versus the cross-linking energy dose are compared. Within the error range and the reproducibility of the measurements, the slowing down of the dye diffusion in the gels is about the same in both solvents, as stated above, and this is true for all the tested cross-linking densities.

In addition to the possibility to observe the gel in a single plane (xy axis) by moving the stage where the sample in mounted on, the current experimental set-up offers the possibility to translate the objective lens in the z-direction ("Z-scan''). In that way the positioning of the measuring volume can change, scanning the entire volume of the gel, starting from the interface substrate-gel and reaching the solvent above it. The results are presented in the form of fluorescence intensity (count rate in kHz) plotted as a function of the distance from the substrate.

In the inset of Fig.4.6, such a profile of fluorescence intensity is shown, showing a higher swelling ratio of the gel in ethanol (~ 9 μm instead of 6.4 μm in the case of water).

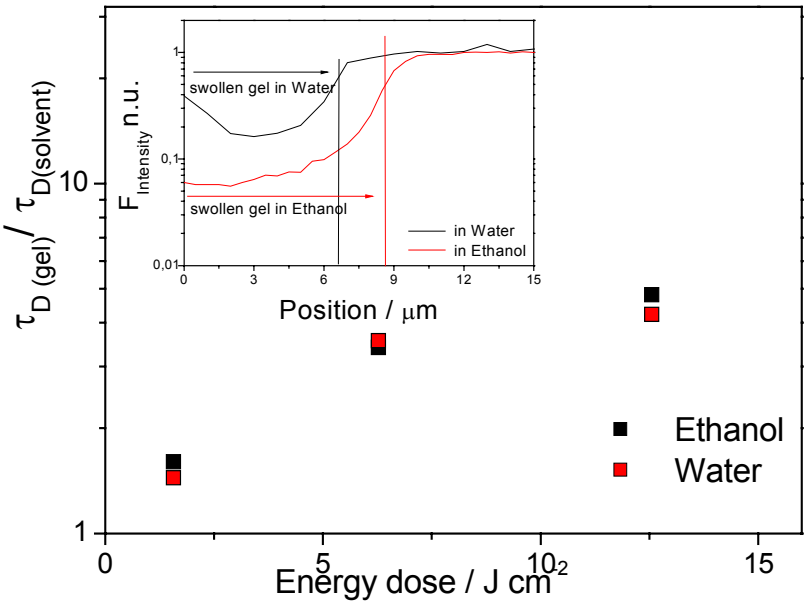

Figure 4.6: Normalized (to the dye in the pure solvents) diffusion time for AlexaFluor647 dye in both solvents (water and ethanol) versus the cross-linking energy dose. The inset shows the fluorescence intensity profile as a function of the distance from the glass substrate (Z-scan). The different swelling ratios of the gel (for 60 min irradiation time corresponding to an irradiation dose of 6.3 J cm^{-2}) in the two solvents are indicated by the two vertical lines (red for ethanol) in the inset.

The partition coefficient of a solute molecule (P) is defined as the equilibrium ratio of concentration in the gel (based on total gel volume) compared to the solution concentration:

$$P = [C]gel \,/\, [C]solvent$$

where C is expressed as solute mass per volume of the designated phase (solution or gel). In the absence of attractive interactions between the solute and gel network, P is less than 1 because the volume occupied by the network excludes the solute based on the solute's size. This excluded-volume effect depends on the volume fraction of the polymer forming the network (φ), the radius of the chains of the polymer, and the size and shape of the solute molecule.

In our case, the partition coefficient of the AlexaFluor647dye in the gel can be estimated from the relative fluorescence intensity in the gel and the free solution.

$P = [C]gel / [C]solvent$, in water P = 0.2, in ethanol P = 0.06

The higher partition coefficient in water implies that AlexaFluor647 preferentially penetrates the gel when the latter is swollen in water instead of ethanol.

Fig. 4.7 shows the normalized fluorescence intensity autocorrelation functions for Rh6G in a gel cross-linked for 60min (corresponding to 6.3 J cm^{-2} energy dose) in ethanol and in water.

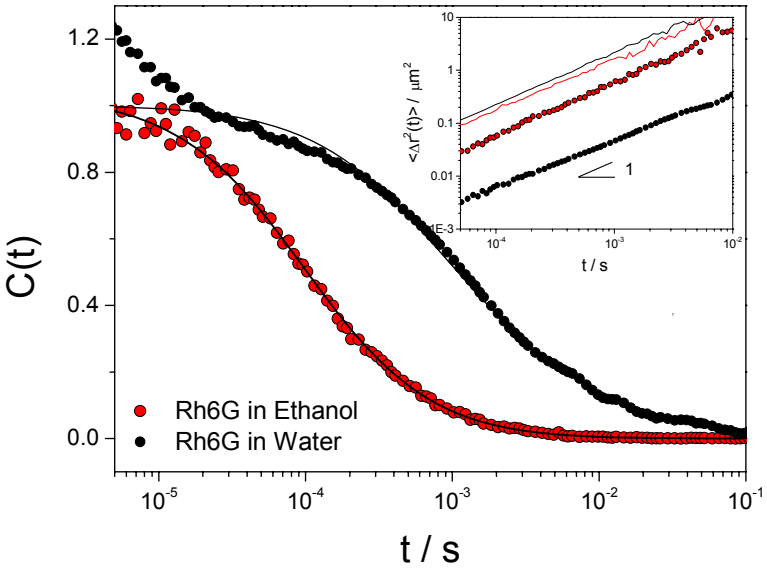

Figure 4.7: Normalized fluorescence intensity autocorrelation functions C(t)= G(t) – 1 corresponding to the diffusion of Rh6G *dye in a gel cross-linked for 60min (corresponding to 6.3 J cm^{-2} energy dose) in ethanol (red symbols) and water (black symbols).*

Compared to the Fig. 4.5, it can be observed that the retardation of the fluorescent dye Rh6G in the gels compared to the pure solutions is not the same for both solvents. In the water swollen gel the diffusion of Rh6G suffers much stronger retardation than in gel swollen in ethanol as also shown in the displacement plot of the inset. In hindered diffusion, the mean-square displacement is often proportional to time to an exponent *x*,

$<\Delta r^2(t)>\sim t^x$ .When $x \neq 1$, the diffusion is called "anomalous", and when $x < 1$ (typical for hindered diffusion), it is called "subdiffusive".

The center of mass displacement of the Rh6G in the gel in water showed weaker time dependence $<\Delta r^2(t)>\sim t^x$ ($x<1$) compared to the gel swollen in ethanol ($<\Delta r^2(t)>\sim t^1$). This behavior was attributed to pronounced attractive electrostatic interactions of the positively charged Rh6G with the negatively charged gel in water, and will be discussed in detail further down in the text.

Fig.4.8 summarizes the normalized diffusion times for the Rh6G dye in gels swollen in both solvents (water and ethanol) versus the cross-linking energy dose. For comparison, the results for AlexaFluor647 have also been included. The diffusion of Rh6G in gels in water (black circles) is distinctly different than in gels swollen in ethanol (red circles). In the gels swollen in ethanol, Rh6G (in red) diffuses faster than AlexaFluor647 (in blue). The steep Rh6G intensity profile in the inset is not understood.

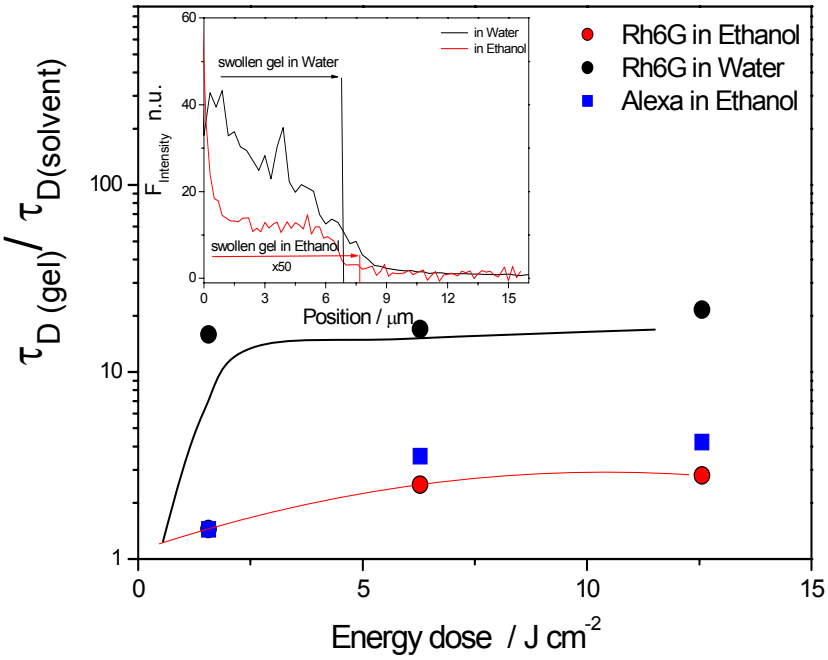

Figure 4.8: Normalized diffusion time in gels swollen with both solvents (water and ethanol) for Rh6G versus the cross-linking energy dose. For comparison, the results for AlexaFluor647 (blue) are also included. The inset shows the fluorescence intensity profile as a function of the distance from the glass substrate.

Size Exclusion

There is an interest in studying the particle size dependence of diffusion, since smaller particles can penetrate into smaller pores in the gel. In this manner the gel structure can be probed at different length scales and an idea about the mesh size of the gel can be obtained. For this reason, measurements were performed with uncharged silica nanoparticles with an estimated R_h in water of about 42 nm and 70 nm, respectively.

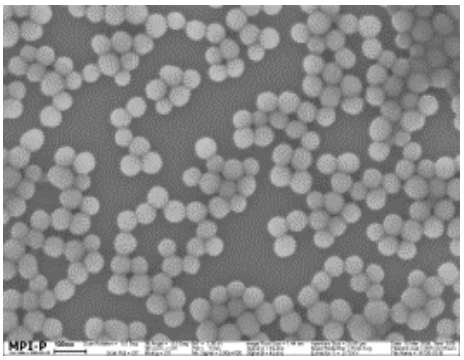

Figure 4.9: Fluorescently labeled silica particles of an estimated R_h ~ 42nm, viewed by SEM.

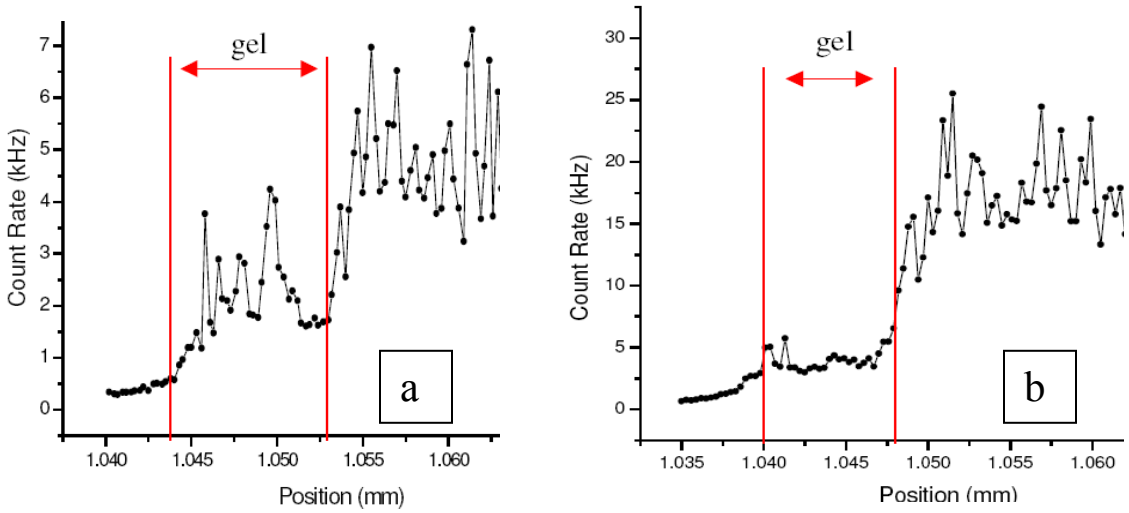

Figure 4.10: Fluorescence intensity plotted as a function of the distance from the substrate-gel interface (Z-scan) for a gel layer cross-linked for 60min (corresponding irradiation dose of 6.3 J cm^{-2}) swollen in ethanol solutions of silica particles (R_h ~ 42nm in water) at two different concentrations, a)5 10^{-9} M and b)2 10^{-8} M.

The measurements were performed initially in ethanol, where the swelling ratio is higher than in water. However, as shown in the Z-scans (Fig. 4.10), the fluorescence intensity (count rate) inside the gel remained constantly low, as before the addition of the probe, while the intensity in the solvent outside the gel increased as expected, leading to the conclusion that the silica particles did not enter the gel and consequently implying that the porosity of the gel layer is smaller than the size of these particles. Experiments not presented here showed that even when the particles were directly introduced to the gel during the preparation process followed by cross-linking, they were still not able to diffuse in the gel, once the latter was swollen, but they remained immobilized between the network chains.

Probe Diffusion in the Presence of Electrostatic Interactions

Studying the Coulombic interactions between the diffusing species and the gel is fundamental in understanding the diffusion mechanisms, however, the presence of such interactions poses a problem when attempting to gain independent information on the gel system under study.

The normalized fluorescence intensity correlation function C(t) for Rh6G in a gel cross-linked for 60min, corresponding to an irradiation dose of 6.3 J cm^{-2}, can be seen in Fig. 4.11. The correlation curve cannot be approximated in a satisfactory way using the one-component model, like in the case of ethanol. Translating the results into mean-square displacement data provides a diffusion exponent of ~0.7, indicating anomalous (non-Fickian) diffusive behavior.

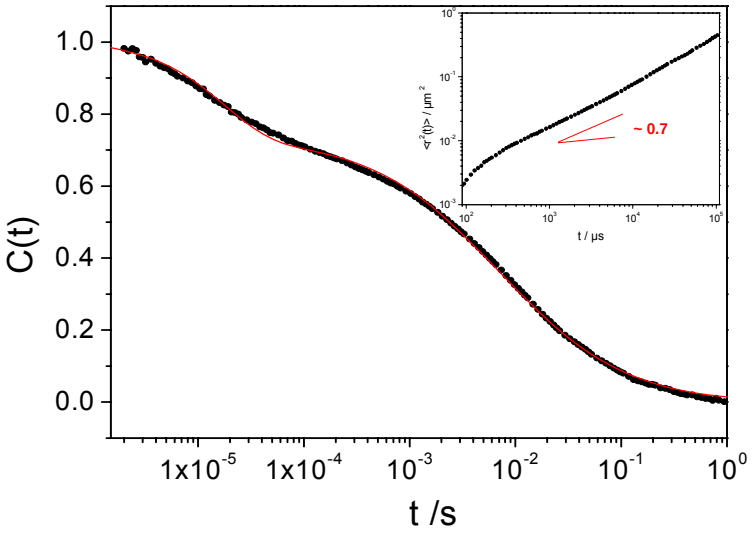

Figure 4.11: Normalized fluorescence intensity correlation function C(t)= G(t) - 1 for Rh6G in a cross-linked pNIPAAm film prepared under 60min UV exposure time (irradiation dose of 6.3 J cm^{-2}) and subsequent swelling in water. The mean square displacement of the single R6Gh dye as a function of time is shown in the double log plot in the inset. The exponent 0.7 indicates anomalous (non-Fickian) diffusive behavior.

This hindered diffusion was attributed to the presence of electrostatic interactions between the negatively charged gels and the positively charged dye (Rh6G).

A final set of measurements was carried out with the dyes being tested simultaneously on the same gel cross-linked for 60min, in ethanol. For the excitation of AlexaFluor647, a HeNe laser emitting at wavelength λ = 633 nm was employed, whereas for Rh6G the HeNe laser at λ = 543 nm was used.

Fig. 4.12 depicts the normalized fluorescence intensity autocorrelation functions corresponding to the diffusion of Rh6G and AlexaFluor647 in a gel cross-linked for 60min and swollen a) in ethanol and b) in water. As one can observe, Rh6G diffuses faster than AlexaFluor647 in the same gel in ethanol, i.e. same swelling ratio, resembling the diffusion trend for the two dyes in pure ethanol (solid lines in the inset).

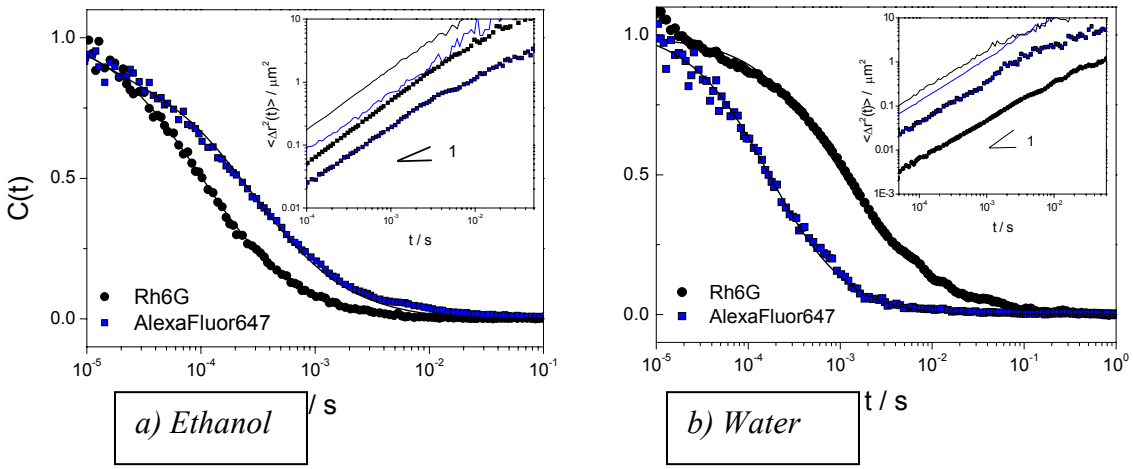

Figure 4.12: Normalized fluorescence intensity autocorrelation functions C(t)= G(t) - 1 corresponding to the diffusion of Rh6G and AlexaFluor647 in a gel cross-linked for 60min (6.3 J cm^{-2} irradiation dose) and swollen in a) ethanol, and b) water. The inset shows the MSD as a function of time, with the straight lines representing the data for the diffusion of the two dyes in pure ethanol.

However, for a gel of the same cross-linking density swollen in water, the situation is different. The inset of Fig. 4.12b shows the strong retardation of the Rh6G diffusion compared to AlexaFluor647, and to the pure solvent.

Experiments were also performed with a series of fluorescent probes (see table 3.1) with different charges and relative sizes.

It was shown that a positively charged perylene dye (structure is given in Fig. 3.3e) exhibited qualitatively the same behaviour in water as Rh6G due to their positive charge. Immediately after the addition of the fluorophore, a significantly high quantity entered the gel whereas only a small amount stayed in the solvent above the films. In Fig. 4.13 the area of the increased count rate, provides the thickness of the gel in the swollen state, in pure water (solid line) and after the addition of the probe solution (dotted line). The increased fluorescence intensity in pure water is most probably due to some type of auto-

fluorescence* of the gel layer, whereas, the further increase of the count rate after the addition of the fluorescent probe indicates its preference to enter and diffuse into the gel.

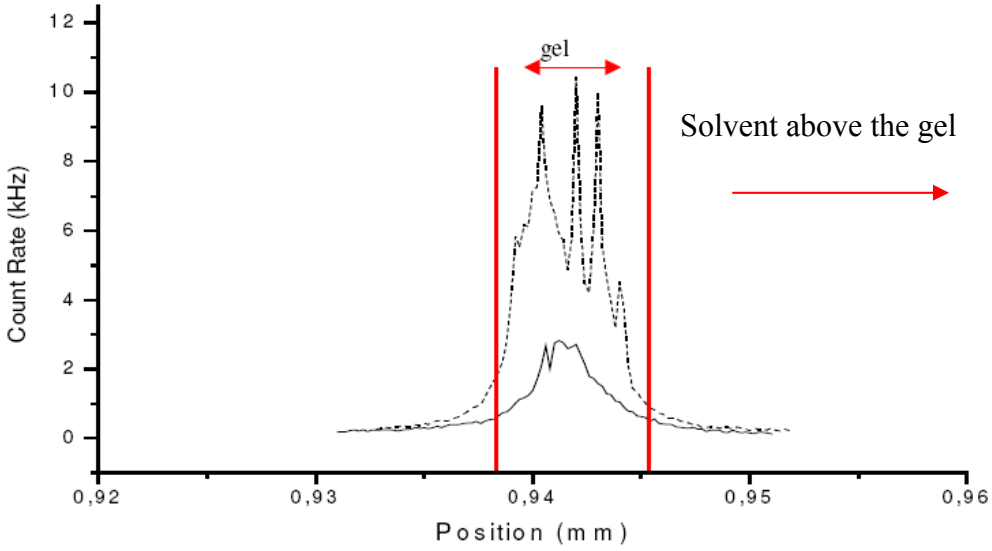

Figure 4.13: Fluorescence intensity plotted as a function of the distance from the substrate-gel interface. The red arrow denotes the thickness of a gel layer cross-linked for 60min (corresponding irradiation dose of 6.3 J cm^{-2}) swollen in pure water (solid line) and in an aqueous solution of positively charged perylene (dotted line).

The situation is reversed in the case of negatively charged tracers. The repulsive electrostatic forces between such probes (e.g. fluorescein and negatively charged perylene) and the negatively charged gels allow only a very small amount of the dye to penetrate into the gel.

The same effect was observed when using fluospheres (PS nanospheres with a negative charge and a diameter of 20 nm) as a tracer (cf Fig. 4.15). However, in this case of fluospheres, steric effects cannot be excluded.

The results for the negatively charged perylene are not presented here but resemble the ones obtained with fluorescein.

* The autofluorescence of the gel was a problem in the initial FCS measurements. We attributed the fact to impurities remaining from the process of synthesis, e.g. stabilizers from solvents. The problem was resolved by rinsing the gels with ethanol in order to remove the non-bound impurities, reducing the autofluorescence by a factor of ~10.

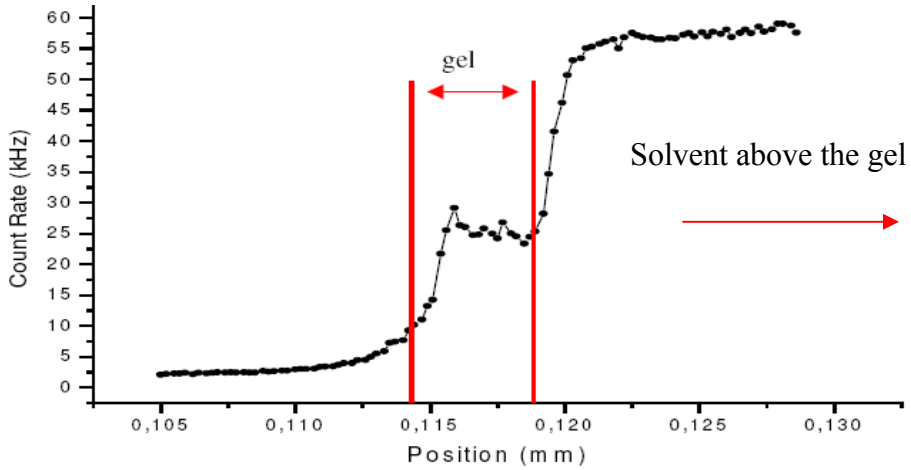

Figure 4.14: Fluorescence intensity plotted as a function of the distance from the substrate-gel interface. The red arrow denotes the thickness of a gel layer cross-linked for 60min (corresponding irradiation dose of 6.3 J cm^{-2}) swollen in an aqueous solution of the negatively charged fluorescein dye. One can observe the higher intensity in the solvent above the gel compared to the fluorescence intensity inside the gel, indicating that the repulsive electrostatic forces acts as a means of hindering the diffusion of the probe inside the gel.

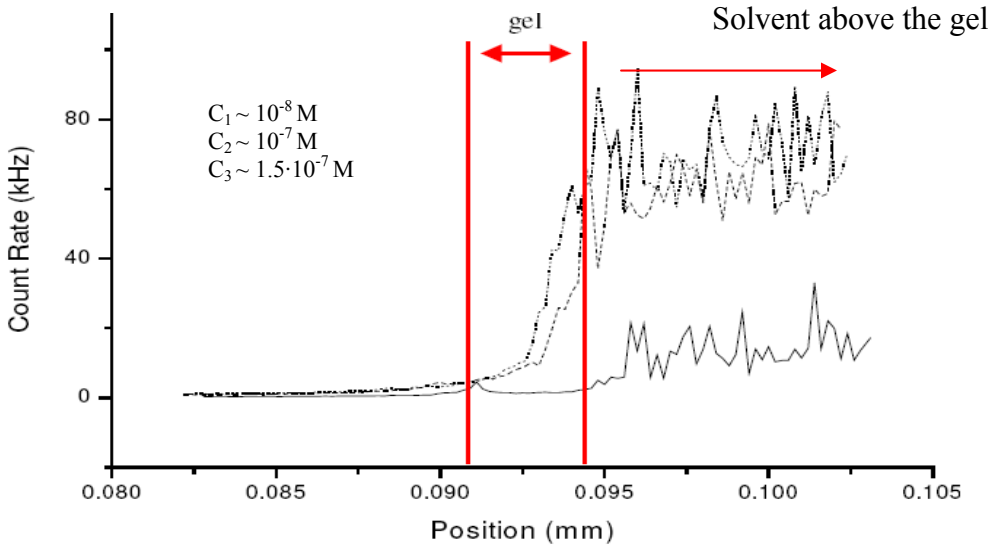

Figure 4.15: Fluorescence intensity plotted as a function of the distance from the substrate-gel interface for a gel layer cross-linked for 60min (corresponding irradiation dose of 6.3 J cm^{-2}) swollen in aqueous suspension of fluospheres (diameter 20 nm) of three different concentrations.

Diffusion of Flexible Macromolecules

An additional goal of this study was to extend the FCS measurements to flexible macromolecules, and try to determine the dependence of the diffusion constant on the concentrations of the gel and the probe polymer. Although there are several theoretical approaches applicable for the diffusion of spherical macromolecules, the diffusion of polymer chains must be addressed using the polymer physics theory.[48,84] The gel is considered as a network of cross-linked chains in which the mesh size is a defining parameter of the system. Thus the chains are treated as fixed obstacles and the diffusion of the flexible macromolecule is defined as the movement of a chain in a tube.

Experimental studies have shown that in agarose gels, despite the same hydrodynamic radius in solution, the diffusion coefficients were greater for flexible macromolecules than for rigid ones, while rigid and/or spherical macromolecules quickly became and remained trapped in pores.[85]

For this reason a polyethyleneglycol (PEG) probe with an average molecular weight of 5.000 gr/mol was employed after labeling with tetramethylrhodamine. Unfortunately, the measurements could not elucidate the diffusion process due to the fact that the strong repulsive electrostatic interactions of the negatively charged PEG dye with the negatively charged gels prevented the diffusion of the flexible probe inside the gel. As shown in Fig. 4.16, after the addition of aqueous solutions of PEG of different concentrations, the fluorescence intensity in the solvent above a gel layer cross-linked for 15min (corresponding irradiation dose of 1.6 J cm^{-2}) was significantly higher than inside the gel where the intensity remained stable.

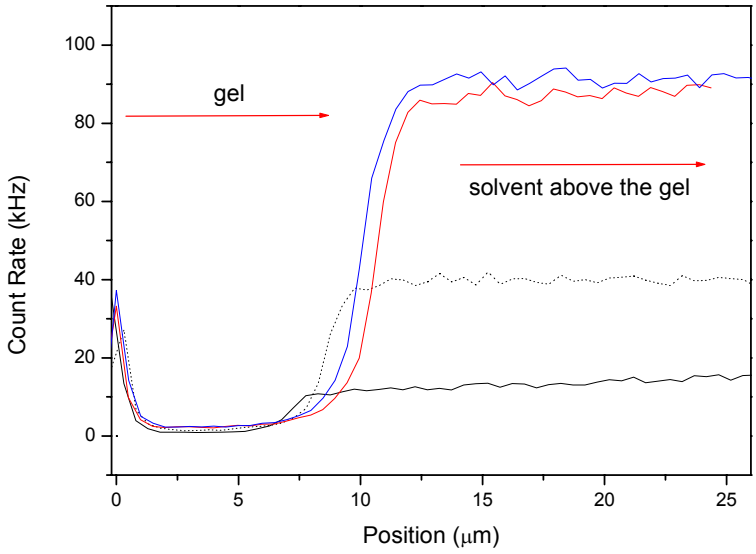

Figure 4.16: Fluorescence intensity plotted as a function of the distance from the substrate-gel interface for a gel cross-linked for 15min (corresponding irradiation dose of 1.6 J cm^{-2}) swollen in aqueous solutions of PEG, with increasing the concentration of PEG from 10^{-8} M (black solid line) up to final concentration of 10^{-7} M (blue line).

Proteins

To design an optimum gel, it is desirable to predict the distribution of solutes between the gel and its surrounding solution. If the hydrogel bears no electric charge, it is often assumed that the protein does not interact with the polymer matrix. However, if the gel is charged (a polyelectrolyte gel, like in our study-case), the distribution of a protein is also affected by electrostatic interactions.

Proteins may interact with the gel matrix through short-range interactions such as hydrogen-bonding and dispersion forces. Short-range interactions between a protein and a polymer are highly dependent on the nature of protein, polymer, and solvent.

Serum albumin is one of the most widely studied proteins and is the most abundant protein in plasma with a typical concentration of 5g/100ml. Albumin is generally regarded to mean serum albumin or plasma albumin. The word albumin is also used to describe a protein or a group of proteins defined by solubility in water.

Two different types of Bovine Serum Albumin (BSA) with a molecular weight of ~66kDa were employed for the following experiments, the so-called native one and a cationized (cBSA). Both of them were labeled with tetramethylrhodamine dye.

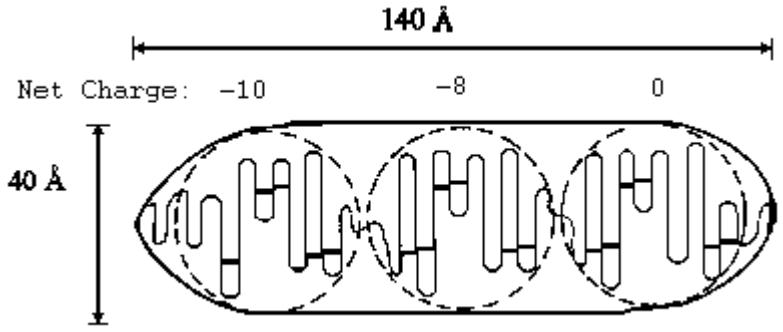

Figure 4.17: Classical perception of the structure of serum albumin (adapted from Peters, T., Jr. (1985). Serum Albumin. Adv. Protein Chem.37; 161-245)

The experimental procedure followed was the same as for the previously mentioned fluorescent probes (described in detail in Chapter 3: Experimental Procedures).
The cBSA was used first and the following effects were observed:

1. Increased fluorescence intensity at the interface between the glass substrate and the gel.
2. Increased fluorescence intensity at the interface between the hydrogel and the solvent above the gel.
3. Increase of the fluorescence intensity inside the hydrogel. No correlation was observed.
4. The diffusion time of 'free' protein in the water above the hydrogel was roughly three times higher than the diffusion time of 'free' protein in pure water.

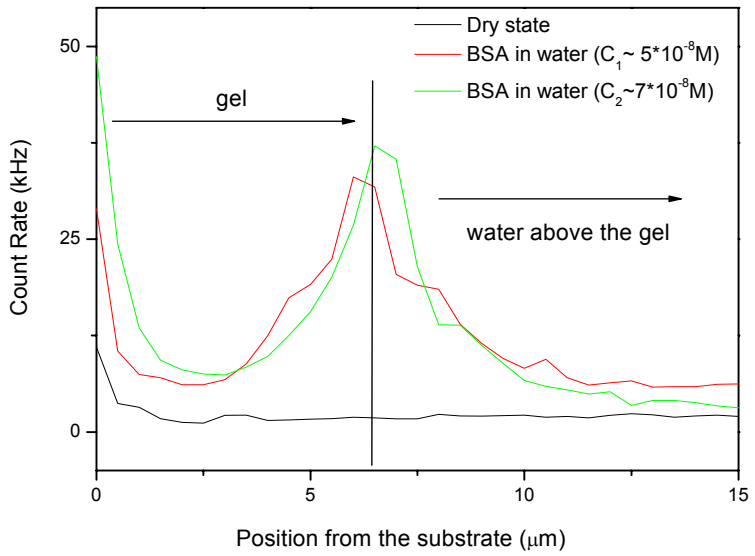

Figure 4.18: Fluorescence intensity plotted as a function of the distance from the substrate-gel interface. The black line represents the data for a gel cross-linked for 60min(corresponding irradiation dose of 6.3 J cm^{-2}) in the dry state, the red line shows the fluorescence intensity after the addition of a aqueous solution of cBSA (5 10^{-8}M) while the green line shows the data after a small increase of the cBSA concentration (7 10^{-8}M)

The data have led to the following conclusions:

1. Proteins did diffuse into and through the HG layer.
2. Possibly, 'free' polymer was released during the swelling process into the water phase.
3. The BSA has multiple positive charges whereas the dissolved polymer is negatively charged. The dissolved polymer probably formed complexes by electrostatic interactions with the particle surface. By this process the effective particle size increased. This could result in the larger diffusion times of the protein in the water above the hydrogel and possibly the larger protein polymer complexes could not enter the hydrogel but were attracted and anchored at the interphase, resulting into the enhanced fluorescence intensity at the water-gel interphase.

4. The increase of the fluorescence intensity was due to the fact that we have a hydrophobic substrate due to the adhesion monomer and BSA tends to absorb to hydrophobic surfaces.

On the other hand, to interpret the results with the native BSA, the charge of the protein should be taken into account. The effective charge of the protein is the one that determines the kinetics of the interactions with other charged molecules or surfaces. In a recent study[86], the effective charge of bovine serum albumin (BSA) in aqueous solution was determined by dynamic NMR as a function of pH. An effective charge of +21.1 ± 1.2 was found at low pH (~ 2.2) while an effective charge of -17.2 ± 0.6 was found at high pH (~ 10.4)

All the measurements presented in here were performed in deionized water with a pH slightly acidic (~5.5) due to the presence of dissolved carbon dioxide (CO2) from the atmosphere.*

At this pH value the effective charge of the protein should be around 0,[86] thus, in a first approximation, the protein is not expected to interact electrostatically with the gel matrix.

---

* Dissolved carbon dioxide reacts slowly with water to give the bicarbonate and hydronium ions.

$CO_2\,(g) + 2H_2O(l) \rightleftarrows HCO_3^- + H_3O^+$

Note that carbonic acid, H_2CO_3, is only formed in strongly acid solutions. Distillation temporarily removes dissolved CO_2 from the water. However, during condensation the water reabsorbs CO_2 again resulting in a pH that is less than 7.0.

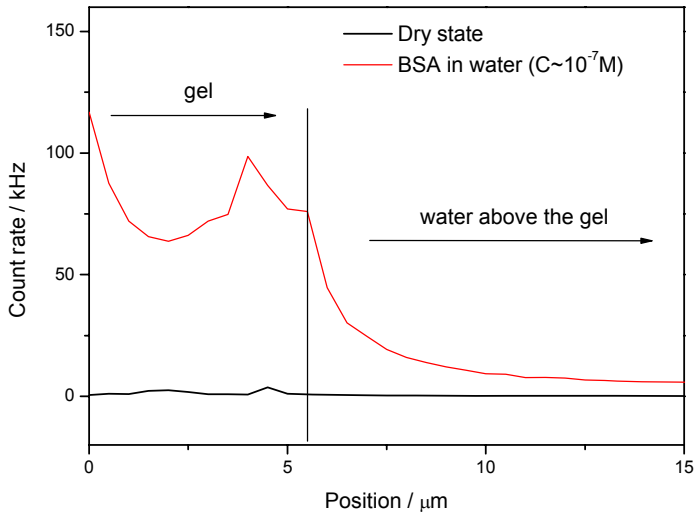

Figure 4.19: Fluorescence intensity plotted as a function of the distance from the substrate-glass interface. The black line represents the data for a gel cross-linked for 60min (corresponding irradiation dose of 6.3 J cm^{-2}) in the dry state, the red line shows the fluorescence intensity after the addition of a aqueous solution of native BSA (10^{-7}M).

Fig. 4.19 reveals that the BSA diffuses into the hydrogel layer, indicated by the increase of the fluorescence intensity inside the gel after the addition of an aqueous solution of BSA. Correlation curves were obtained for the diffusion of the protein in gels of three different cross-linking densities (Fig. 4.20) and an increase of the characteristic diffusion time of the protein with increasing cross-linking density was observed, probably due to steric effects (from 413μs to 1460μs, for 15min and 120min irradiation times, respectively.) The exponent 0.7 of the mean square displacement in the inset indicates hindered (non-Fickian) diffusive behavior.

From the evaluation of the experimental data, two main conclusions can be drawn; a) the native BSA is attracted and diffuses into the gel (indicated by the increase of the fluorescence intensity inside the gel and the very low count rate in the solvent above the gel), and b) its diffusion is hindered by the gel matrix (slope 0.7 of the mean square displacement). The initial assumption that the BSA in neutral at the pH value of the measurements (~ 5.5) is valid as long as the protein is located in the bulk solvent

above the gel. However, this is not necessarily true once the protein has entered the gel, where the local molecular environment (e.g. the presence of the polymer network) could give rise to a different pH and affect the isoelectric point of the protein. Thus, attractive electrostatic interactions of the protein with the gel matrix, that would explain the obtained experimental data, cannot be excluded.

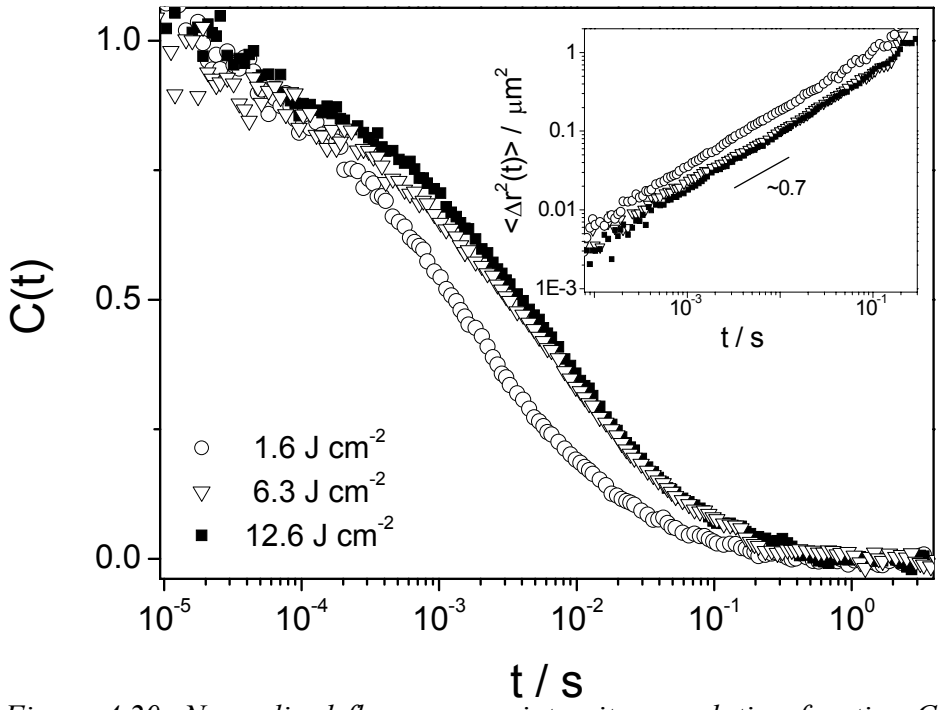

Figure 4.20: Normalized fluorescence intensity correlation function C(t)= G(t) - 1 for native BSA protein in cross-linked pNIPAAm films of three different cross-linking densities, corresponding to 15min, 60min and 120min irradiation time or irradiation doses of 1.6, 6.3 and 12.6 J cm^{-2}, respectively.

The cell cytoplasm and extracellular cellular matrix (ECM) are composite aqueous solution of multiple solutes, proteins, and electrolytes intersected by the three-dimensional structure of negatively charged polyelectrolytes such as actin filaments/microtubule and aggrecan/hyaluronic acid. Protein mobility within this complex environment is therefore suspected to deviate notably from mobility in dilute solutions due to a complicated sum of the intrinsic viscosity of the liquid cell medium, nonspecific binding of probe molecule to macromolecules, and the mechanical barriers as imposed by the network.[87] The effect of charge density of an anionic gel, the shape and

the aspect ratio of the protein, and the surface charge density of proteins on protein diffusion in the polyelectrolyte gel has been investigated.[88] In uncharged agarose gels, diffusion of myoglobin is not effected by the change in pH and ionic strength, indicating no electrostatic interaction between the gel and myoglobin. In contrast, in the negatively charged λ-carrageenan gel, the diffusion of myoglobin is accelerated by electrostatic attraction when the pH < pI (myoglobin) but it is extensively hindered by the electrostatic repulsion when pH > pI.[88] Studying the protein diffusion in polyelectrolyte gels is crucial in the understanding of the biochemical kinetics of the cell or practical applications, such as construction of biomimetic actuator and replacement of biological tissues.

The FCS technique was able to provide us with both qualitative and quantitative results on the diffusion process of a protein inside thin hydrogel layers, taking into account parameters like the charge of the protein, the charge and the cross-linking density of the gel matrix. Based on these interesting experimental findings, there is a series of arising questions that could be addressed in the future, e.g. the effect of temperature or ionic strength on the protein diffusion process in gels.

.

4.3 FCS Results on pNIPAAm Solutions

Small Probe (Rh6G) Diffusion

We investigated the diffusion of Rh6G in two PNIPAAm/ethanol semidilute solutions near and well-above the overlap concentration c^* ~ 0.4 w/v % at 20 °C and the net experimental correlation functions $C(t) = G(t) - 1$ for the are shown in Fig. 4.21.

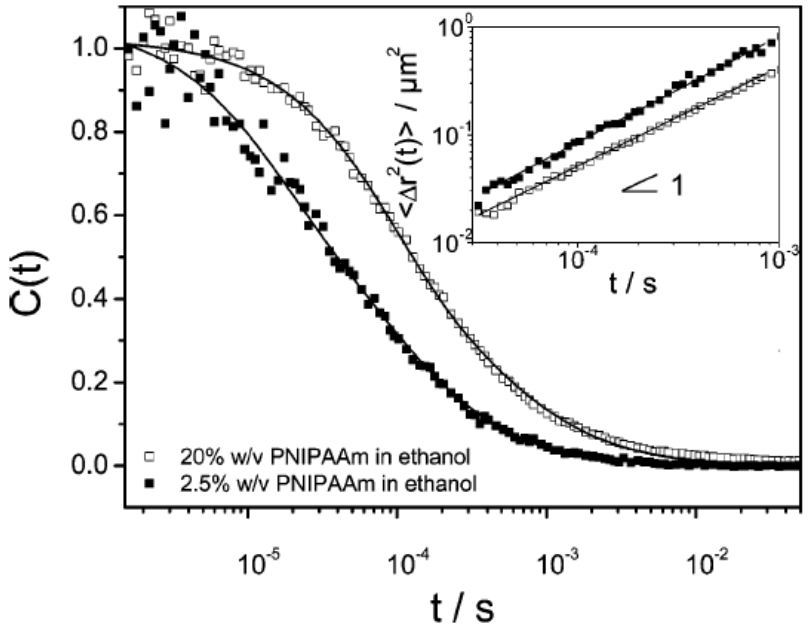

Figure 4.21: Normalized fluorescence intensity correlation function C(t) = G(t) - 1 (symbols) for Rh6G in two pNIPAAm /ethanol solutions in the semidilute regime along with the fit (solid lines) of eq 4.1. The diffusive (slope one) mean square displacement (eq 4.2) of the Rh6G is shown in the double log plot in the inset.

The experimental $C(t)$ are adequately represented by eq 4.1 with $M = 1$, and the diffusion time τ_D in the illuminated volume is expectedly an increasing function of the pNIPAAm concentration. Owing to the very low fluorophore concentration, FCS allows for the computation of the tracer mean square displacement $\left\langle \Delta r^2(t) \right\rangle$ in the observation volume V_{obs} with lateral r_0 and vertical z_0 dimensions.[18]

The inset to Figure 4.21 displays the $\left\langle \Delta r^2(t) \right\rangle$ of the small dye as a function of time t. In order to avoid any photophysical effect (triplet decay) the initial decay times are excluded in the plot of $\left\langle \Delta r^2(t) \right\rangle$ versus t. The slope 1 (in the inset of Figure 4.21), $\left\langle \Delta r^2(t) \right\rangle \sim t$ indicates a purely random Brownian diffusion with some deviations at the highest concentration. From the known value of the self-diffusion coefficient of Rh6G in ethanol, the experimental τ_1 is directly translated to the self-diffusion $D_s(c)$ of the Rh6G in pNIPAAm/ethanol solutions covering the concentration range 1×10^{-4} to 0.2 g/cm^3 at 20°C.

In the absence of specific interactions between probe and polymer segments, the decrease of $D_s(c)$ with the pNIPAAm concentration should reflect that of the viscosity $\eta_b(c)$ that captures the flow around the static particle of diameter b. Since b is smaller than the size of the pNIPAAm chain, its motion should displace chain portions of size of the order of b.[89] Hence, $Ds(c) \sim \eta_b(c)^{-1}$ should be independent of the polymer molecular weight and display weaker c dependence than the macroscopic shear viscosity $\eta(c)$. This was pointed out some time ago in several investigations of particle sedimentation[14] and probe diffusion[81,90,91] in semidilute polymer solutions and gels. For the examined small probes, D_s was expressed as a function of the relevant length scales of the system that is, the mesh size (ξ) of the polymer network and the particle size (b).

Since this characteristic size of a transient polymer network at $c > c^*$ is approximately the correlation length $\xi(c)$ representing the average distance between two adjacent contacts, the same pNIPAAm /ethanol solutions were characterized by PCS (results presented later).

Large Probe (pNIPAAm) Diffusion

The self-diffusion coefficient of polymers has received the most attention in the literature among various dynamic properties of the polymeric systems. It is usually measured by pulse-field gradient NMR[92] optical grating techniques,[81] and, under some specific optical contrast conditions, by photon correlation spectroscopy.[16,93] FCS has been applied to synthetic polymers only recently,[23,22] and hence, there is still limited information. In these techniques, the diffusion coefficient Ds of the labeled (tracer) polymer with molar mass M becomes independent of the matrix molecular weight M_m if M_m exceeds M.[94] Since in the present study $M \approx M_m$, D is close to the self-diffusion and hence is expected to sense the global dynamics of the pNIPAAm nondilute solutions as reflected in the solution viscosity $\eta(c)$. Fig. 4.22 depicts normalized fluorescent intensity autocorrelation functions for the diffusion of the labeled pNIPAAm for two concentrations in the nondilute regime. These functions are clearly much slower than the corresponding decay functions for the small probe in Fig. 4.21 at similar polymer matrix concentrations.

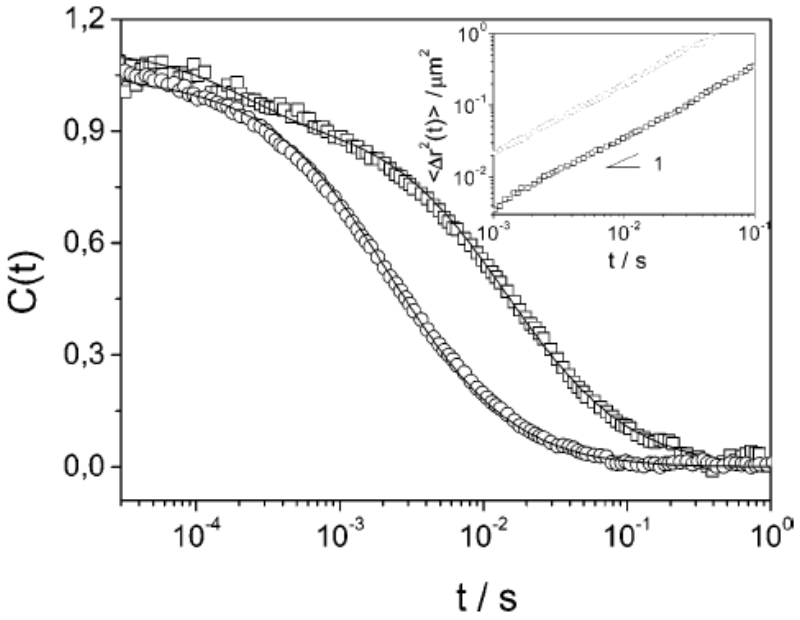

Figure 4.22: Normalized fluorescence intensity correlation function C(t) = G(t) - 1 for labeled pNIPAAm in two pNIPAAm /ethanol solutions with c = 0.02 g/mL (circles) and c = 0.15 g/mL in the semidilute regime. The diffusive (slope one) mean square displacement of the single pNIPAAm chain obtained from the slow decay of G(t) is shown in the double log plot in the inset.

The initial decay of $G(t)$ in Fig. 4.22 (between 0.1 and 0.4 ms) might be due to the presence of a small amount of free dye. Excluding this initial decay, the tracer mean square displacement in the inset to Fig. 4.22 conforms to a random Brownian diffusive motion even at the highest concentration experiments in polystyrene nondilute solutions.[94] The inset to Fig. 4.23 shows the diffusion coefficients D of the small and large probe along with the translational diffusion (open circle) of pNIPAAm measured by PCS, as discussed in detail in Chapter 5; the latter is about 10% faster because of its slightly lower R_h compared with the labeled chain. The vastly different Einstein diffusion coefficient D_0 of the small and large probe in the dilute regime reflects the disparity of their sizes. For a clear presentation of the concentration dependence, Fig. 4.23 displays the normalized diffusion coefficients relative to the corresponding (D_0) values at the lowest pNIPAAm concentration.

The large probe diffusion clearly exhibits stronger concentration dependence than the small probe[81,89,94] and resembles that of the solution viscosity shown in Fig. 4.25 for comparison.

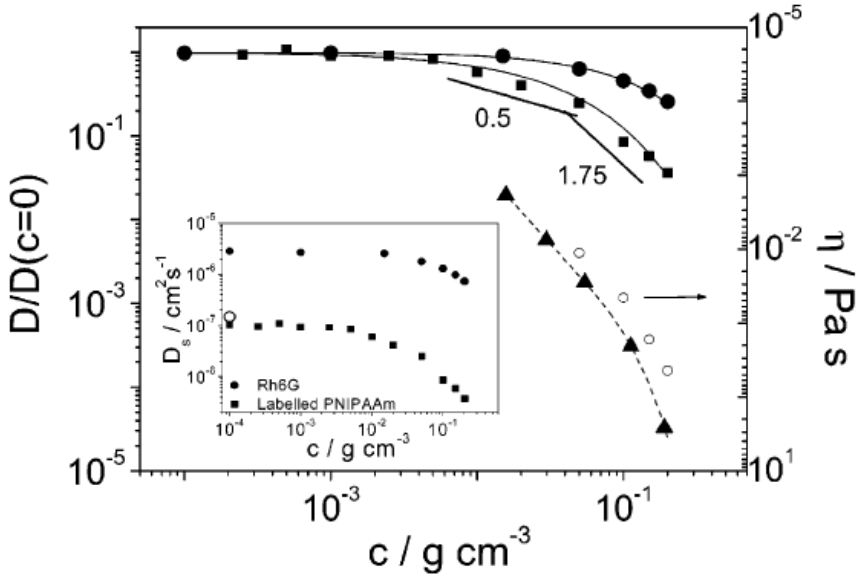

Figure 4.23: Normalized self-diffusion coefficient for the two indicated dyes in pNIPAAm/ethanol solutions over a wide concentration range below and above the overlap concentration c (3 x 10^{-3} g/mL). For comparison, the solution viscosity (open circles) and the cluster diffusion coefficient (solid triangles – PCS data, discussed later) are also shown as a function of concentration. The dashed line through the latter is to guide the eye. Inset: the experimental self-diffusion coefficients of the two dyes (solid symbols) and translation diffusion coefficient (single open circle) of the pNIPAAM from the PCS experiment (described in Chapter 5) are shown as a function of concentration.*

Chapter 5: Photon Correlation Spectroscopy (PCS) - Results and Discussion

5.1 PCS Results on pNIPAAm Solutions

PCS measurements were performed with the same pNIPAAm/ethanol solutions as used in the FCS experiments. Figure 5.1 displays the relaxation function $C(q,t)$ for the concentration fluctuations with wave vector q = 0.031 nm^{-1} in pNIPAAm/ethanol solutions at two concentrations in the dilute and semidilute regime.

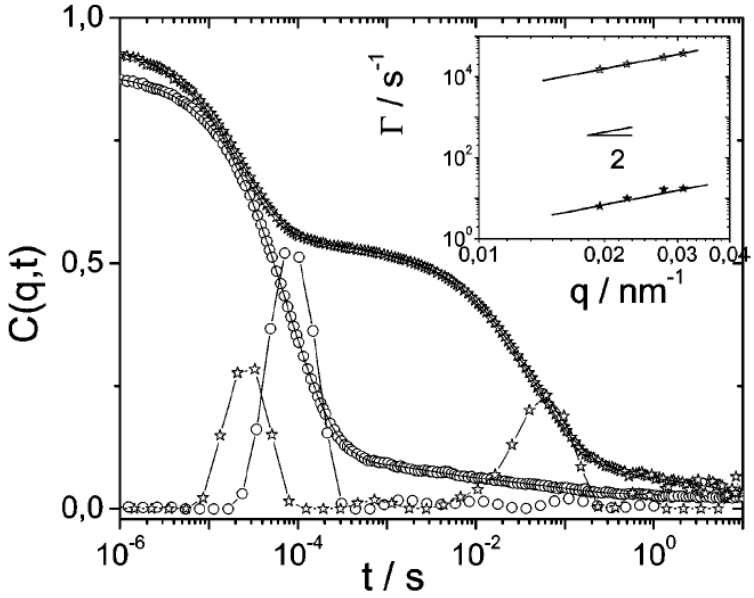

Figure 5.1: Relaxation function C(q,t) for the concentration fluctuations in dilute (c =2.4 x 10^{-3} g/cm^3 open circles) and semidilute (c = 5.4 x 10^{-2} g/cm^3 open stars) pNIPAAm/ethanol solutions at q = 0.031 nm^{-1} along with the corresponding distribution of relaxation times. The two diffusive (slope 2) relaxation rates for the semidilute solution are shown in the inset, where the relaxation rate (Γ) is plotted versus the scattering vector q.

In the case of more than one decay, in order to analyze the relaxation function $C(q,t)$, we proceed through its inverse Laplace transformation, where $L(\ln \tau)$ is the distribution of relaxation times. The relaxation rates $\Gamma = 1/\tau_{max}$ correspond to the peak positions of $L(\ln \tau)$ at τ_{max}, and the area under the peak defines the value of a (eq.3.2) and hence the intensity $aI(q)$ associated with the particular process. For dilute solutions,

$C(q,t)$ displays a single process associated with pNIPAAm translational diffusion $D_0 = \Gamma/q^2$ which becomes the cooperative diffusion D_{coop} in the semidilute regime. In addition, a second slower process appears with also a diffusive (q^2 dependent) rate as shown in the inset of Fig. 5.1. The D_{slow} ($=\Gamma_{slow}/q^2$) which appears to follow the concentration dependence of $\eta(c)^{-1}$ might relate to the self-diffusion of pNIPAAm[93] or most likely to cluster diffusion[95]. The crossover to a semidilute solution at $c \sim c^*$ is marked by an increase of $D(c)$ and concurrent decrease of $I(c)$ with polymer solute concentration c because of the increase of the solution osmotic pressure. This behavior is clearly depicted in Fig. 5.2 with $c^* = 3 \times 10^{-3}$ g/cm^3. In the semidilute regime, $D_{coop}(c) = k_B T/(6\eta\pi)$ defines the mesh size $\xi(c)$ of the transient polymer network; $D_{coop}(c)$ display slightly weaker concentration dependence than the good solvent scaling $c^{0.77}$ prediction (solid line in Fig. 5.2) over the examined semidilute range $1 < c/c^* < 70$. Since for a theta solvent the predicted scaling is even stronger, the observed $D_{coop}(c)$ might be due to the pNIPAAm size polydispersity.

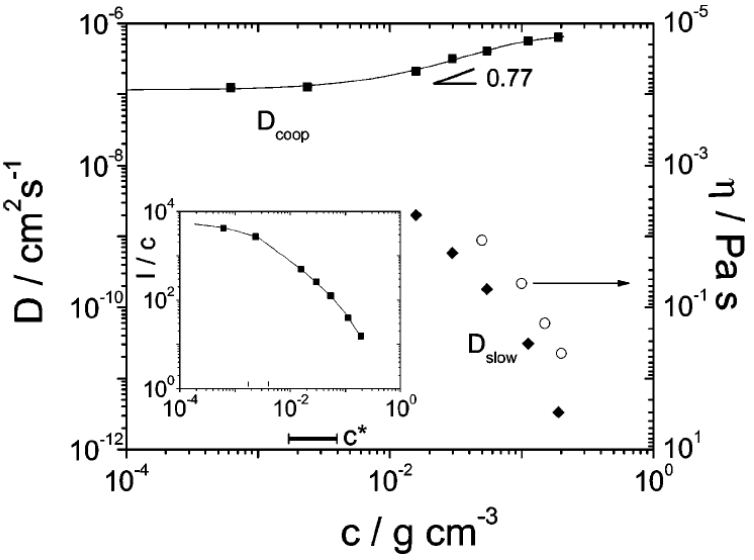

Figure 5.2: Cooperative D_{coop} and D_{slow} diffusion coefficients of pNIPAAm/ethanol solutions over a wide concentration range below and above the overlap concentration c. The solution viscosity is also shown as a function of concentration. The reduced I/c scattering intensity of the fast diffusion process is shown in the inset.*

The compilation of the different diffusion data in Fig. 4.23 (cf Chapter 4) obtained from two complementary experimental techniques, i.e. FCS and PCS, clearly disputes the assignment of the slow diffusion process in the PCS experiment (Figure 5.1) to the self-diffusion.[95] Instead, this process relates to the diffusion of a cluster of pNIPAAm chains closely following the macroscopic solution viscosity. This assignment is further supported by the observation of the slow process in the semidilute solutions $c > c^*$. Fig. 5.2 clearly shows that only FCS and not PCS can safely measure the self-diffusion in semidilute homopolymers, but both techniques can be complementarily employed. In the present case, FCS measures both local dynamics associated with length scales $O(\xi)$ and global dynamics over the size of the used probe in the semidilute entangled regime well above c^*, whereas PCS can safely measure the mesh size $\xi(c)$ and the concentration dependence of $\eta(c)$ via the slow cluster mode. In the very dilute regime ($c << c^*$), both techniques measure the chain translational diffusion with FCS being applicable even at extremely dilute solutions.

PCS measurements were not performed on aqueous solutions of pNIPAAm due to solubility problems at room temperature.

5.2 μ-PCS Results on pNIPAAm Gels

Ethanol

For the laser light scattering measurements on pNIPAAm gels the experimental set-up shown previously in Fig. 3.6 was developed. Hydrogel layers with three different cross-linking densities, obtained by different irradiation doses used in the photo-cross-linking process, were swollen in ethanol. The initial dry thickness of the films was 1μm, and the swelling ratio, which was calculated as the ratio of the swollen film thickness divided by the initial dry film thickness, depended on the cross-linking time. The swelling ratio was estimated by surface plasmon resonance[27] and fluorescence correlation spectroscopy.[96] The dynamics of the gel layers at thermal equilibrium are manifested in the relaxation function $C(q,t)=[G(q,t)-a]/f^*$ which is computed from $G(q,t)$; $f^*<1$ is an instrumental factor and a is the base line of $G(q,t)$ at long times (~1s). To our knowledge this set-up has not been used previously in the present configuration for thin polymer

films The correlation function $G(q,t)$ at short times (< μs) saturates to $b\sim 2\langle I\rangle_E/I_c$ where I_c denotes the elastic contribution from the laser beam and the frozen fluctuations (static heterogeneities) and $\langle I\rangle_E$ is the ensemble average scattering intensity from the gel layer. [74 45]

The relaxation functions of the concentration fluctuations in Fig. 5.3 display two distinct decays and interestingly enough the slow process relaxes within the experimental time window (t<100s). This relaxation pattern is robust (ergodic) as it is insensitive to variations of the probed spots in the films. In addition, there exist much slower fluctuations at decay times beyond 10s which, however, do not affect the characteristics of the two well resolved relaxation processes in $f(q,t)$. A qualitatively similar behavior was observed for the gel films with different cross-linking densities. Due to the well separated time scales of the two processes, $f(q,t)$was represented by the double exponential decay function

$$f(q,t) = a\exp(-\Gamma_f t)+(1-a)\exp(-\Gamma_s t)+ a' \qquad (5.1)$$

using the two relaxation rates Γ_f , Γ_s for the fast and slow process and the amplitude a as adjustable parameters, respectively. To account for misnormalization and small base line fluctuations, we also allowed for a small non-zero value of the parameter a'. This simple expression represents well the experimental $C(q,t)$ as indicated by the solid lines in Fig.5.3.

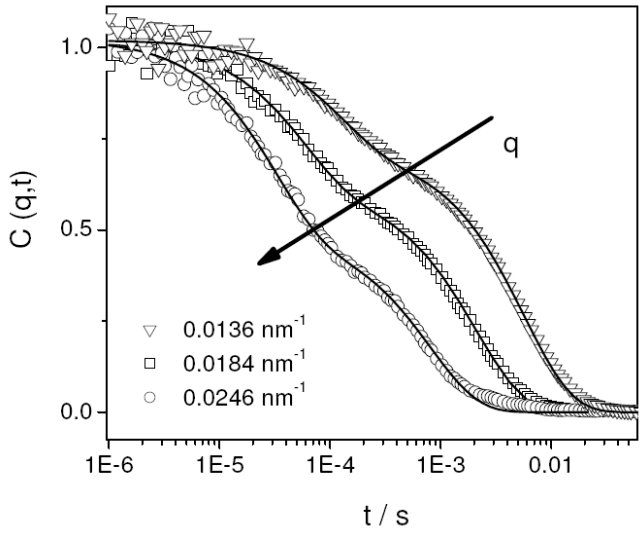

Figure 5.3: Normalized autocorrelation function C(q,t) of the scattered intensity at different scattering wave vectors q, for an ethanol-swollen gel cross-linked for 15min

(corresponding to an irradiation dose of 1.6 J cm^{-2}), acquired under heterodyne conditions.

Both relaxation modes depend on the magnitude of the scattering wave vector q and the observed dependence of the relaxation rates is characteristic of a pure isotropic diffusive ($\Gamma \sim q^2$) behaviour as indicated by the slope 2 in the double logarithmic plot of Fig. 5.4 for the three films with different cross-linking densities. The scattered intensity associated with both dynamic processes in $f(q,t)$ is approximately given by $\langle I(q) \rangle = I_0\, b$ where I_0 is the averaged intensity over the measurement time. While the dynamic intensity $I_f = a\langle I(q) \rangle$ associated with the fast process is insensitive to the variation of q, the dynamic intensity $I_s(q) = (1-a)\ \langle I(q) \rangle$ associated with the slow mode was found to increase with decreasing q. The former suggests a small correlation length as found for the concentration fluctuations in semidilute polymer solutions that exemplify physical (transient) networks. Hence, we attribute the fast process to the cooperative diffusion with $D_{coop} = \Gamma_f(q)/q^2$ driven by the osmotic pressure of the system. The strong increase of $I_s(q)$ of the slow diffusive process at low q's implies long correlation lengths for these slow concentration fluctuations. The typical slow process reported in 3-D gels usually lies outside of the experimental window and therefore exhibits a non-ergodic behaviour depending on the probed spot in the sample. [33,74,83,45]

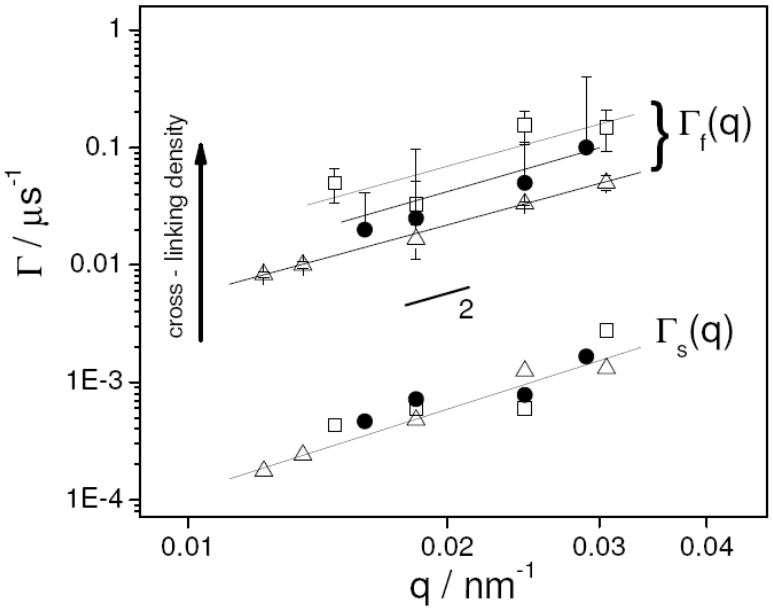

Figure. 5.4: The relaxation rates for the two processes (Fig. 5.3) of pNIPAAm gel films swollen in ethanol versus the scattering vector q in a log-log plot. The fast Γ_f, representing the decay rate of the collective concentration fluctuations, indicates a diffusive behavior with the expected slope of 2. The open triangles, the black circles and the open squares correspond to a gel cross-linked for 15min, 60min and 120min or irradiation doses of 1.6, 6.3 and 12.6 J cm^{-2}, respectively.

Fast Mode Relaxation

The cooperative diffusion coefficient D_{coop} increases with cross-linking density as seen in Fig.5.4. In semidilute polymer solutions,[84] the increase of D_{coop} with polymer concentration (c) is due to the concurrent decrease of the mesh size, ξ(c) and in good solvents, $D_{coop} \sim c^{3/4}$. For pNIPAAm/ethanol solutions,[75] $D_{coop}(c)$ displays a weaker concentration dependence ($D_{coop} \sim c^{0.5}$) than this good solvent scaling. For the anchored chemically cross-linked gels, an effective polymer concentration can be assigned from the swollen gel thickness assuming an uniaxial swelling predominantly in the direction perpendicular to the substrate. Lateral swelling parallel to the substrate is suppressed due to the covalent attachment of the polymer to the solid substrate. The swelling ratio measured by fluorescence correlation spectroscopy is shown in the inset of Fig.5.5 and

the effective polymer volume fraction $\phi=L/L_o$ where L and L_o is the gel layer thickness in the swollen and dry state.

The swelling ratio is governed by the cross-linking density and the solvent quality. The former is expressed by the number of repetition units N_{eff} between crosslinks and the later by the interaction parameter $\chi(\phi,T)$. Using the free energy of a perfect phantom network, the equilibrium swelling state is described by[15]

$$\frac{\mu_S}{kT} = 0 = \ln(1-\phi_e) + \phi_e + \phi_e^2[x_{eff} - (1-\phi)\frac{\partial x_{eff}}{\partial \phi}] + \frac{\phi_0}{N_{eff}}[\frac{\phi_0}{\phi} + \frac{\phi}{2\phi_0}] \qquad (5.2)$$

If $\chi(\phi,T)$ is known, N_{eff} could be deduced from eq (5.2). In fact, this was performed for surface tethered pNIPAAm hydrogels using $\chi(\phi,T)$ obtained from experimental phase diagrams of linear pNIPAAM in aqueous solutions.[97] The apparent similarity between a surface-tethered network and an uncross-linked physical network is based on the good agreement between eq.(5.2) and the experimental swelling data. However, the value of the adjustable parameter N_{eff} is not explicitly known. In order to assign a value for N_{eff} to the gel layers prepared at different irradiation doses, we have followed the same procedure and represented the experimental swelling ratio in water. For the four different UV exposures given in the inset of Fig.5.5, N_{eff} increases from 170 for 1.6 J cm^{-2} irradiation dose to 680 for 12.6 J cm^{-2} energy dose.

Fig. 5.5 displays the increase of D_{coop} with the effective concentration of the pNIPAAm gel films along with the concentration dependence of the cooperative diffusion in semidilute pNIPAAm solutions in ethanol.[96] A comparison of the two data sets reveals a much stronger increase of the D_{coop} with the effective concentration in the chemically cross-linked gels than in the physical network of the semidilute solutions. This feature clearly distinguishes the physical network and the chemically cross-linked network layer of pNIPAAm anchored on the glass substrate, indicating structural differences between the two types of network. At low volume fractions below 0.1, D_{coop} in the anchored gel converges to that of the semidilute polymer solutions. Even lower volume fractions for the gel layers are experimentally not accessible (the crosslinking density becomes lower than one per chain).

With regard to the local dynamics, Fig.5.5 shows the diffusion time τ_D of Rh6G (with R_h=0.8nm) measured by fluorescence correlation spectroscopy as a function of

volume in both systems .Within experimental error, τ_D in the gel layers (open circles) compares very well with the diffusion of the same dye in physical pNIPPAm networks.[96] Since the diffusion time $\tau_D(\phi)$ of small dyes ($R_h < \xi$) depends only on the polymer concentration and not on the polymer molar mass, this finding suggests that the local dynamics are virtually the same in both systems and further supports the estimation of the volume fraction in the gel layers under the condition of uniaxial swelling .

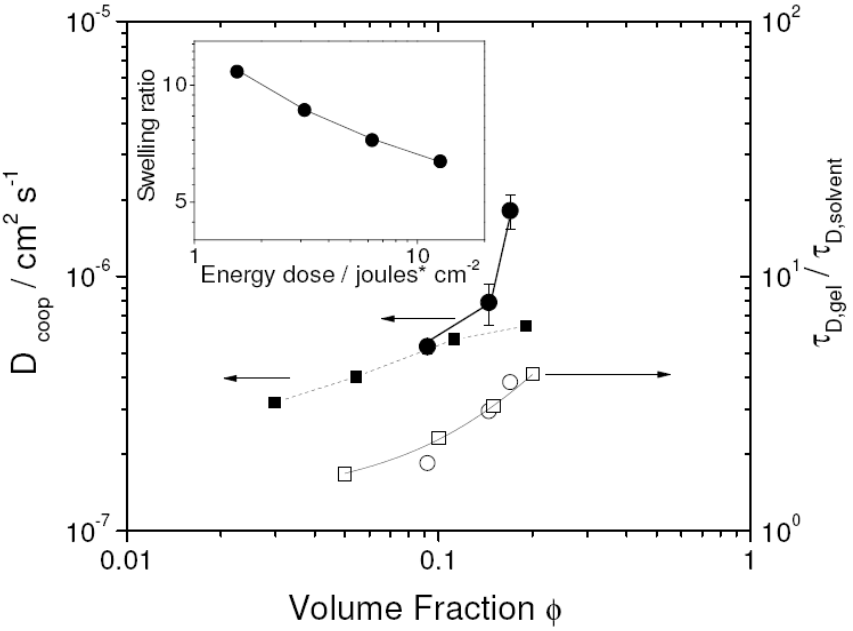

Figure 5.5: Cooperative diffusion coefficient, D_{coop}, plotted as a function of the effective volume fraction ϕ for pNIPAAm gels. The black circles correspond to gels of three different cross-linking densities achieved by different irradiation doses (1.6, 6.3 and 12.6 J cm^{-2}, corresponding to effective volume fractions of 0.092, 0.145, 0.169), swollen in ethanol. The black squares denote data from [96] that correspond to the D_{coop} of semidilute solutions of pNIPAAm in ethanol for different concentrations. The dashed and solid lines are guides to the eye. The normalized (relatively to the neat solvent) dye diffusion time $\tau_{D,gel}/\tau_{D,solvent}$ is shown as a function of pNIPAAm concentration in the crosslinked films (open circles) and in semidilute pNIPAAm/ethanol solutions (open squares). The swelling ratio of the gel films in ethanol as a function of the irradiation dose is shown in the inset.

Thus FCS and PCS of gel layers yield complementary dynamical and structural information as FCS measures the local friction whereas PCS allows the estimation of a

dynamic mesh size ξ. For the gel layers of Fig.5.5, ξ decreases from 3.4 nm for the shortest to 1 nm for the longest cross-linking time. These numbers are rather low as compared to mesh sizes for transient networks suggesting structural differences between the two systems.

Since $D_{coop}(c)$ of transient and permanent networks are, in general, different (see Fig.5.5), the effective mesh size ξ of gels can only be safely obtained from the experiment and not from scaling relationships. Based on the data of Fig.5.5, the cross-linking of the anchored pNIPAAm gel layers reduces their mesh size much stronger than anticipated by the scaling for transient networks in good solvents. This effect could originate from the strong uniaxial swelling only in the direction vertical to the substrate. Interestingly, on the contrary to this dynamic dissimilarity, it was reported very recently[97] that surface-attached pNIPAAM networks exhibit a swelling discontinuity which coincides with the two phase region of uncross-linked pNIPAAm semidilute solutions. This similarity with the demixing temperature of the physical network can imply that confinement by chemical crosslinking does not change the miscibility behaviour of the grafted networks. For uncross-linked polymer brushes, however, evanescent wave dynamic light scattering[98] experiments revealed that confinement by surface grafting modifies the bulk demixing temperature since the brushes can adjust their thickness with solvent quality.

Slow Mode Relaxation

The slow diffusive process in the present anchored gel layers (Fig. 5.3 and 5.4) with diffusion coefficient $D_s = \Gamma_s(q)/q^2$ ($\sim 1.5*10^{-8}$cm^2/s) exhibits two pertinent differences compared to the slow dynamics in the reported polymer systems so far: (i) It is 'faster' and ergodic compared to the very slow, non-ergodic process in a 3D gel, as seen in the well-resolved baseline of the functions of Fig.5.3. (ii) Within the scattering of the experimental data, D_s seems to be virtually insensitive to the variation of the cross-linking density i.e. volume fraction (Fig.5.4), at odd with the slow mode observed in the corresponding semidilute solutions.[96] In this case D_s was found to exhibit a strong decrease with increasing concentration, resembling the concurrent increase of the solution viscosity with concentration and was attributed to the self-diffusion of (polymer)

clusters.[99] However, in the present case of the cross-linked pNIPAAm gel layers, with nominally infinite viscosity, an analog description is hardly conceivable.

Slow mode relaxation processes have been repeatedly observed by dynamic light scattering in binary polymer systems and polymer gels, even in good solvents. In semidilute solutions of linear homopolymers, the origin of the slow mode is still in dispute.[99] It shows a strong slowdown with increasing concentration and significant increase of the light scattering intensity at low wavevectors that suggests large correlation lengths. There is a single report for chemically crosslinked gels,[45] to the best of our knowledge, where the slow mode decays within the experimental time window with a rate ~1s virtually q-independent in contrast to the diffusive fast gel-like mode.

A common feature of the slow diffusive mode in both the semidilute solutions and the chemically crosslinked gels is the large correlation length associated with the measured dynamics. The large correlation length (in the sub-micrometer range) can be phenomenologically assigned to long wavelength concentration fluctuations in the grafted gels. The dynamics associated with these concentration inhomogeneities are frozen in the case of the 3D gels but could be the origin of the observed slow mode in the anchored gel layers, arising from a shorter correlation length. Nevertheless, one may speculate that this slow ergodic process senses the connectivity of the network and the elasticity of the network probably acts as a restoring force. The moieties associated with this mode are part of the rigid network and hence a relation to the fast process should not be excluded. Since the origin of the slow process remains elusive, it would be helpful to examine the dynamics in different solvents and other types of gels e.g. formed by microgel particles.[100] The relation between this ergodic slow mode in the anchored gel films and the non-ergodic much slower process in the conventional 3D gels remains to be clarified.

Water – Salt Effect

Since potential applications of these responsive materials in biological environments will involve water as the major medium and buffer solutions with salts, and because a strong osmotic and electrostatic effect of salt solutions on polyelectrolytes is

known, the response of grafted pNIPAAm layers to the addition of sodium chloride was investigated in the water-swollen state.

Intensity correlations functions were recorded at different scattering angles between 55 and 115^0, for 5 different concentrations of salt (0.02, 0.1, 0.5, 1 and 3 mol / L) and at different positions of the sample to check the homogeneity in the length scale of the measurement. Before the addition of the lowest concentration of salt (0.02 mol / L), measurements in pure water and in ethanol were performed in order to verify that the gel displays the same dynamic behavior as previous gels tested with PCS. After the end of the measurements at each concentration and before adding the higher one, the sample was rinsed with water and new measurements of the gel were performed in the pure solvent to verify that there is no persistent alteration of the gel structure due to the salt exposure. The parameter, which could indicate gel alterations, was the cooperative diffusion coefficient D_{coop}, which was calculated in gels cross-linked for 15 min (corresponding irradiation dose of 1.6 J cm^{-2}) swollen in pure water around the value of 3.5 x 10^{-7} cm^2/s. The results are presented in the Fig. 5.5 below, and as can be seen, within the experimental error range, the gel returns to its initial state, up to a certain salt concentration. At 3 mol / L NaCl concentration the gel is found already in the collapse state and after this point it cannot recover.

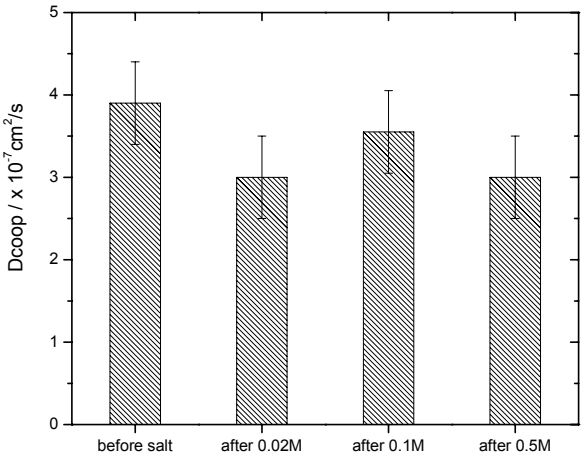

Figure 5.6: Variations of the diffusion coefficient D_{coop} plotted as a function of the rinsing steps, for a gel cross-linked for 15min (corresponding irradiation dose of 1.6 J cm^{-2}), swollen in water. Within the experimental error range, the data reveal no permanent alteration of the gel sample up to 0.5 mol / L salt concentration.

Fig. 5.7 shows normalized intensity autocorrelation functions at 3 different salt concentrations, for a gel cross-linked for 15min (corresponding to an irradiation dose of 1.6 J cm^{-2}), at a scattering vector of 0.18 nm^{-1}. Like in the case of gels swollen in ethanol, two contributions are resolved, a fast one that is attributed to the D_{coop} and a slow one.

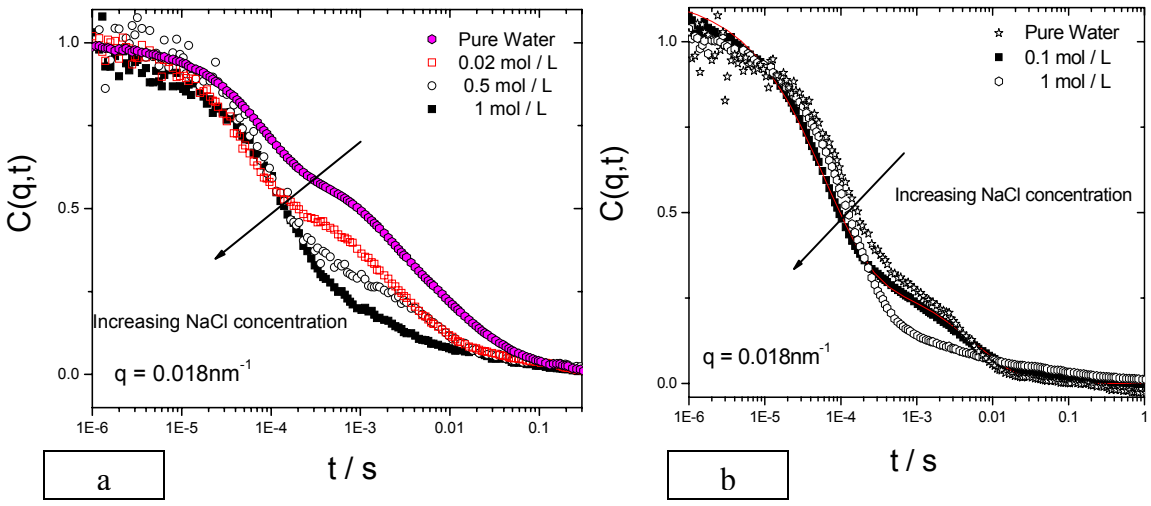

Figure 5.7: Normalized intensity autocorrelation functions for a) a gel cross-linked for 15min swollen in pure water and aqueous solutions of NaCl 0.02, 0.5 and 1 mol / L, and for b) a gel cross-linked for 2h swollen in pure water and aqueous solutions of NaCl 0.1 and 1 mol / L. All the measurements were performed at a scattering angle of 70^0, corresponding to a scattering vector of 0.018 nm^{-1}.

Interesting is the fact that this slow process disappears while increasing the ionic strength as can be seen in the graph below. Due to the well separated time scales of the two processes, *f(q,t)* was represented by the double exponential decay function (5.1).
Fig. 5.8 shows the ratio of the amplitudes of the two processes as a function of the NaCl concentration and depicts better the above evolvement of the slower process, which is suppressed with the increase of the salt concentration (increase of the ratio). Qualitatively the behavior is similar for the gel films of the two different cross-linking densities.

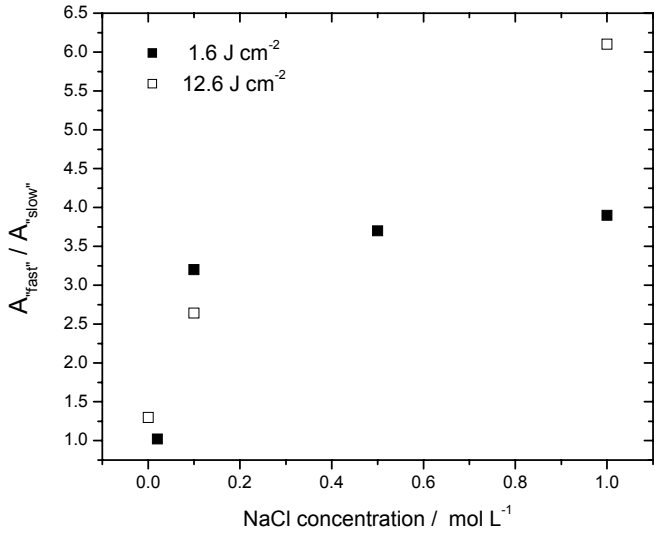

Figure 5.8: Ratio of the amplitudes of the fast with respect to the slow process (A_{fast} / A_{slow}) as a function of the salt concentration, for two different cross-linking densities achieved by different irradiation doses, for a scattering vector of 0.018nm^{-1}.

Figure 5.9 shows the normalized averaged cooperative diffusion coefficient D_{coop}, in the concentration range between 0.02 and 1 mol / L. As shown, the addition of the 0.02 mol / L NaCl, increases the diffusion coefficient D_{coop} from 3.5 x 10^{-7} cm^2/s (in pure water) to the value of 6.3 x 10^{-7} cm^2/s. Further addition of salt up to 1 mol / L NaCl causes a gradual decrease of the diffusion coefficient, thus a slow down of the dynamic mode, indicating probably a phase transition upon increased salt concentration. A very high ionic strength value (3 mol / L) completely erases the dynamic behavior of the gel.

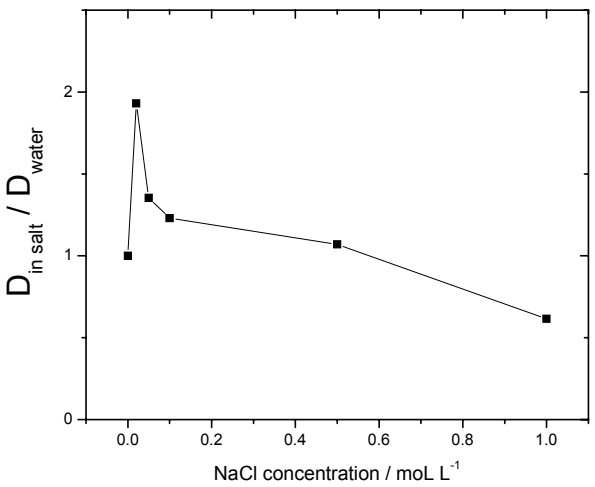

Figure 5.9: Normalized diffusion coefficient D_{coop} as a function of the added NaCl concentration. For each concentration the D_{coop} was calculated at 3 different spots of the sample.

In order to verify the development of the D_{coop} within the value range 0.01 - 0.1 mol / L NaCl, the ion capacity of the hydrogel layer in moles of carboxylic acid (-COOH) functions was estimated. The calculated value was about 10^{-7} -COOH groups in the polymer layer. The concentration of ions in the sample cuvette (volume capacity ~ 40 mL) for 10^{-5} mol / L NaCl was estimated around 4 x 10^{-7}, thus the starting value for the salt experiments was of the same range as the ion capacity of the hydrogel. The results are presented below in Fig.5.10.

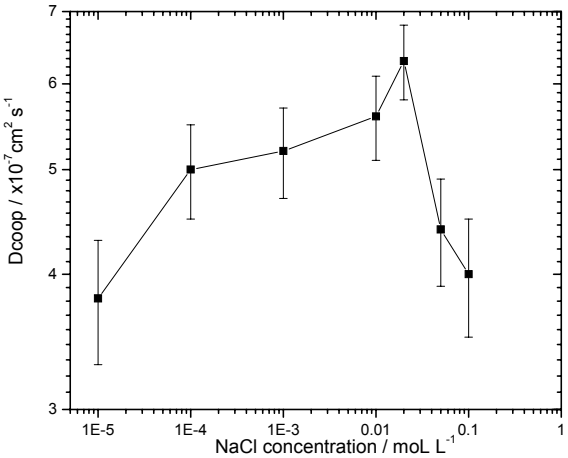

Figure 5.10: Variation of the D_{coop} as a function of the NaCl concentration in the range 10^{-5} – 0.1 mol / L NaCl.

In a related study, Motonaga et al.[31] investigated the pH and temperature dependence of the dynamics in 3 D poly(N-isopropylacrylamide-*co*-sodium acrylate) gels. They suggest that the variation of D_{coop} as a function of the pH is quite similar to that of the swelling ratio versus pH; initially it increases rapidly with $4 \leq pH \leq 6$, due to the ionization of the AAc. A highly swollen state lasts until pH ~ 10 and then the swelling ratio decreases as a result of increase of the screening effect of electrostatic interactions. Their results indicate that D scales with ϕ^1, where ϕ is the polymer volume fraction in the gel, rather than the theoretical prediction $\phi^{3/4}$ for semidilute polymer solutions in a good solvent. They argue that the variation of the collective diffusion coefficient D_{coop} is strongly correlated with that of the swelling ratio, implying that D_{coop} is mainly governed by the polymer concentration in the gel.

This could be also a possible explanation for the present pNIPAAm layers, since in the case of higher salt concentration (> 10^{-2} mol / L NaCl) the development of D_{coop} follows the same trend as the swelling ratio, the latter being measured by SPR/OWS technique.[27] However, in the range between 10^{-5} – 2 x 10^{-2} mol / L of added NaCl there are no experimental data on how the swelling ratio develops.

A hypothesis is that in the low salt region (10^{-5} – 2 x 10^{-2} mol / L), the initial small increase of the ionic strength results to the electrostatic screening of the anionic carboxylate groups in the polymer gel, decreasing the effective distance of their mutually repulsive interactions. This decrease of the D_{coop} that follows the initial increase can be rationalized in terms of chain salting-out properties resulting from removal of hydrating water molecules from the polymer chains to solvate excessive salt present at high ionic strength.

Again, it should be stressed that the explanation for the appearance of these two regions is hypothetical and the underlying mechanism still needs to be elucidated.

Water - Temperature Effect

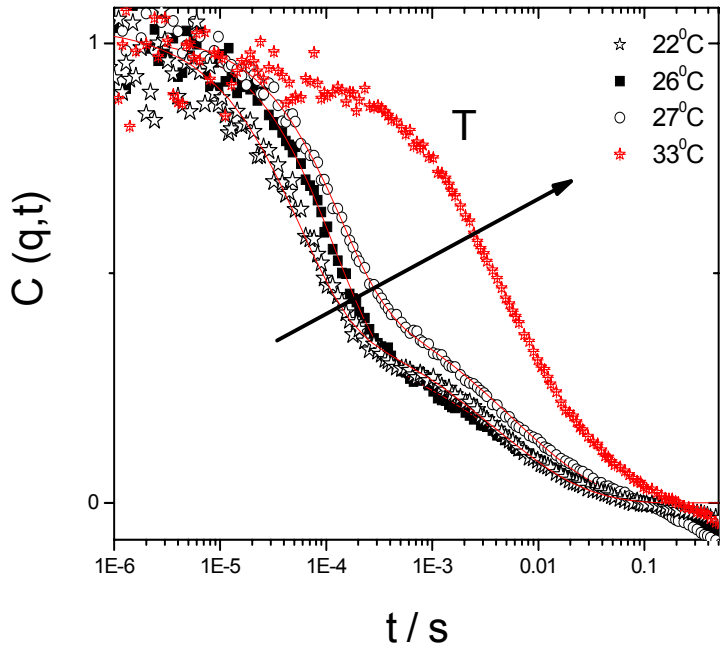

Figure 5.11: Normalized intensity autocorrelation functions for a gel cross-linked for 1h (corresponding to an irradiation dose of 6.3 J cm^{-2}) at different temperatures, acquired at the same scattering wave vector q ~ 0.018nm^{-1}.

Fig. 5.11 shows the effect of the increase of the temperature to the obtained intensity autocorrelation function. As we approach the critical temperature LCST, the time corresponding to the fast relaxation process increases slightly (shift of the curves to the right) while the second slow process does not seem to vary, within the experimental error range. At a temperature above the LCST (i.e. 33^{0}C) the shape of the correlation curve changes from a two-process relaxation function to a one slow process, giving rise to a dramatic decrease of D_{coop}. A hypothetical reason could be the return of the gel towards its initial preparation dry state due to the collapse, and the decrease of the inhomogeneities due to the reduction of the swelling ratio.

Fig. 5.12 shows the temperature dependence of the cooperative diffusion coefficient, D_{coop}, for gels with different cross-linking densities. The common feature for the 2 cross-linking densities is that D_{coop} drops steadily with increasing temperature T. A critical slow down of the cooperative diffusion takes place on approaching the critical

temperature. Similar phenomenon was observed by Motonaga et al. for NIPAAm / Aac gels.[31]

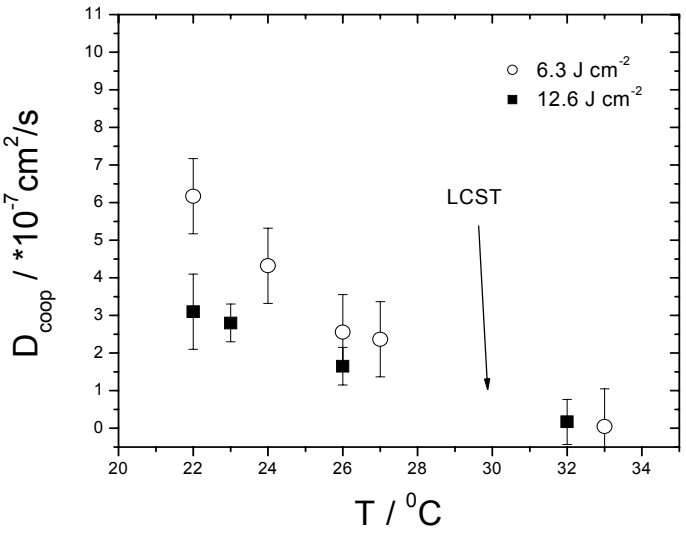

Figure 5.12: Normalized diffusion coefficient D_{coop} as a function of temperature, for 1h and 2h cross-linked gel (corresponding irradiation dose of 6.3 and 12.6 J cm^{-2}, respectively).

Another interesting feature while studying the temperature effect on the dynamics of the pNIPAAm layers was the appearance of a scattering peak (pattern) on the swollen gel already at room temperature, resembling the "butterfly patterns'' that appeared in uniaxially deformed gels as studied by Bastide;[101] by means of light scattering, they investigated gels prepared by statistical cross-linking of semidilute solutions. Such gels should show large-scale inhomogeneities related to the random distribution of tie points. They argue that, under uniaxial stretching, the concentration fluctuations spectra should exhibit an unusual anisotropy, which should be revealed by scattering experiments. Even a very small uniaxial stretching should lead to an unusual scattering spectrum characterized by an increase of intensity in the direction parallel to the stretching and to isointensity curves of very unusual shape, known as "butterfly patterns''.

In the case of the present tethered pNIPAAm layers, a simple scattering geometry, presented in Fig. 5.13, was used in order to investigate the effect of temperature on the scattering pattern. The laser beam from the Nd:YAG laser at a wavelength of λ = 532 nm impinges on the round sample cuvette carrying the sample swollen in water and the

scattering light creates the pattern which is projected onto a white sheet of paper and recorded by a charge-coupled device (CCD) camera.

The temperature of the gel was increased with a step of 1 ^{0}C from room temperature to 42 ^{0}C and then a cooling circle followed until the gel returned to its initial temperature.

The geometrical calculation* of the feature dimensions that are responsible for the appearance of these patterns gave an average value of ~ 3 μm.

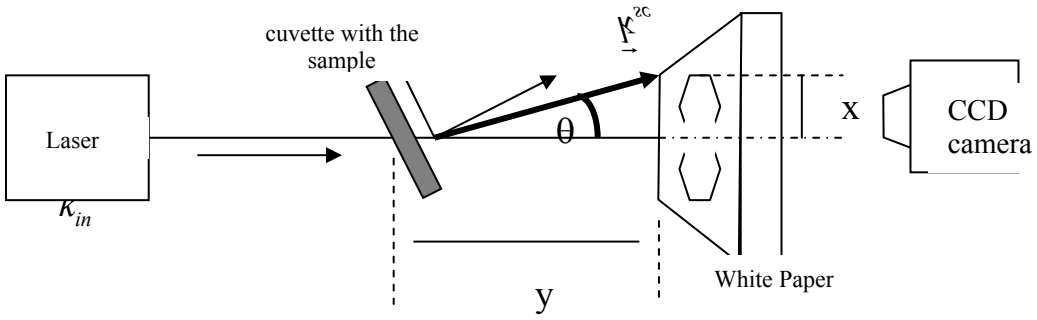

Figure 5.13: Schematic depiction of the light scattering geometry used for monitoring the evolution of the scattering pattern as a function of the temperature. The distance α of the sample from the projection of the scattering peak on the paper y was 12.5 cm and the distance of the center of the pattern to its outer ring x ~2.7cm.

For a gel cross-linked for 15min the development of the scattering pattern upon heating is shown in Fig.5.14. The initial "butterfly" pattern at room temperature becomes an isotropic ring when reaching the LCST (~ 31^{0}C) and disappears almost completely well above the LCST (40^{0}C). The process is completely reversible and upon cooling to the initial temperature the pattern recovers its original shape.

---

* From the experimental set-up geometry, the scattering angle θ is calculated from the relation $\tan\theta = \frac{x}{y}$.

The scattering vector is calculated from the equation $q = (4\pi n/\lambda)\sin(\theta/2)$, where n the refractive index of the solution, and λ the wavelength of the laser beam.

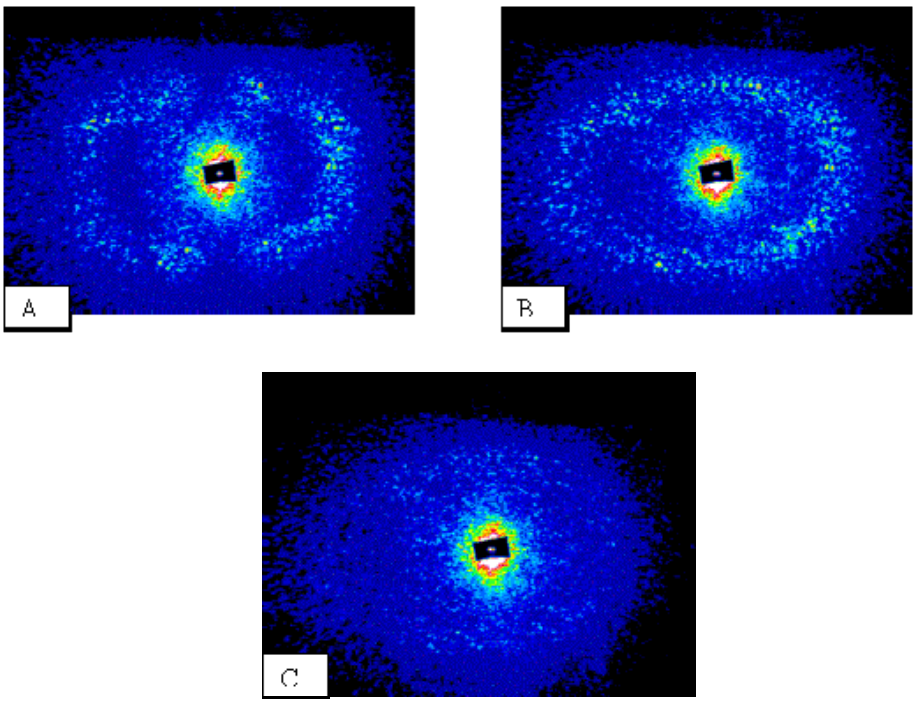

Figure 5.14: CCD photos of the scattering peak for a gel cross-linked for 15 min (corresponding irradiation dose of 1.6 J cm^{-2}) at A) room temperature (22 ^{0}C), B) 32 ^{0}C, and C) 40 ^{0}C.

A possible explanation of the peak could be a surface buckling of the gel due to stress-release caused by the one-dimensional swelling imposed by the chemical confinement of the layer to the substrate. The scattering pattern was also observed in a gel swollen in ethanol, after treatment with water and salt. This hypothesis is maybe supported by optical microscopy photos of a dry gel, after treating it with salt and ethanol, showing the features of Fig. 5.15.

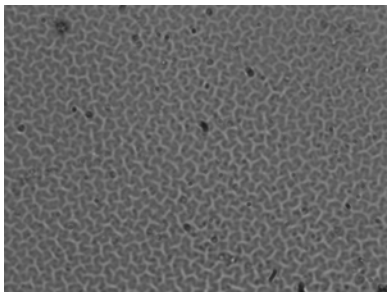

Figure 5.15: Microscopy photo of a dry gel sample after treated with salt solution and ethanol.

However, this is a mere hypothesis, further investigations to this direction should be performed, e.g. the case of ethanol should be checked again, but without any previous treatment of the gel with water or salt.

Chapter 6: Conclusions and Outlook

6.1 Conclusions

This dissertation elaborates on the structure and dynamics investigation of supported pNIPAAm gel films and the corresponding polymers in solutions, inferred by optical techniques. The applicability of Fluorescence Correlation Spectroscopy (FCS) to study the tracer diffusion in, and Photon Correlation Spectroscopy (PCS) to investigate the collective dynamics of these materials, was exploited.

FCS results:

In the gel films, methacrylic acid (MAA) as comonomer provides a polyelectrolyte character; therefore, it was found that the behavior of the fluorescent probe inside the gel depends strongly on its chemical nature, leading to electrostatic or other interactions of the fluophore with the matrix. Experiments performed with a variety of differently charged probes have shown in the case of negatively charged tracers repulsive electrostatic forces between such probes (e.g. fluorescein and a negatively charged perylene derivative) and the negatively charged gels even preventing the diffusion into the gels. The situation is reversed in the case of positively charged tracers, which are strongly attracted into the gel and undergo a hindered diffusion due to attractive electrostatic interactions.

The effect of solvent on the diffusion process was resolved by simultaneous excitation of two different dyes, Rh6G and AlexaFluor647, of similar size (R_h~1 nm, in water) at different wavelengths followed by a concurrent detection of the dyes in the same gel sample. Rh6G diffuses faster than AlexaFluor647 in ethanol, but for a gel of the same cross-linking density swollen in water, the retardation of the Rh6G diffusion was much stronger compared to AlexaFluor647 or to the free dye in pure water. This fact is attributed to the dissociation of the ion pairs (in the dye and the polymer, respectively) in water, resulting in strong attractive electrostatic interactions of Rh6G with the gel. This ion dissociation is mostly absent in ethanol, so no electrostatic interactions are observed.

In addition, the FCS technique was able to provide both qualitative and quantitative results on the diffusion process of a protein inside thin hydrogel layers, taking into account parameters like the charge of the protein, and the charge and the cross-linking density of the gel matrix. A positively charged protein (cBSA) was strongly attracted to, but did not demonstrate any mobility inside the hydrogel layer, whereas native BSA, non-charged at the working pH (~5.5), diffuses inside the hydrogel layer.

The major conclusion drawn from the above mentioned FCS data is that the effect of charge density of a polyelectrolyte gel and its crosslinking density, as well as the shape and the surface charge density of the diffusants are highly significant parameters that should be taken into account when employing these materials in analyte biosensing applications.

Further on, FCS measurements on nondilute pNIPAAm solutions (near and well-above the overlap concentration c* ~ 0.4 w/v %) of the same polymer as used for the gels indicate that a small probe diffusant (Rh6G) appears to sense local dynamics on the length scale of the mesh size obtained from photon correlation spectroscopy, whereas a polymer probe (fluorescently labelled pNIPAAm), comparable to the pNIPAAm polymer size in solution, reveals global chain motions.

PCS results:

Probing the dynamics of surface anchored pNIPAAm crosslinked layers of different crosslinking densities in ethanol by means of PCS allowed the estimation of a dynamic mesh size ξ. The numbers obtained were rather low as compared to mesh sizes for transient networks in polymer solutions suggesting structural differences between the two systems. The relaxation function obtained exhibited two decays: a) a fast one, which increased with the cross-linking density and was assigned to the cooperative diffusion and b) a slower contribution. The latter was found to display some interesting features, i.e. it was ergodic and insensitive to the variation of the cross-linking density. It is these features that differentiate this ergodic slow process from the non-ergodic slow process in the conventional 3D gels; however, its origin still remains to be clarified.

Based on the PCS and FCS data, the cross-linking of the anchored pNIPAAm gel layers reduces their mesh size much stronger than anticipated by the scaling for transient

networks in good solvents. This effect could originate from the strong uniaxial swelling only in the direction vertical to the substrate, implying that the effect of constraint imposed on the gel layers by the presence of a fixed substrate is an important parameter to be considered.

6.2 Outlook

The results of this PhD work generated new questions and suggest future efforts in: (i) FCS investigation in thin anchored hydrogel layers, and (ii) dynamics investigation and characterization of these materials by PCS.

1. The technique of FCS could be a powerful tool in elucidating the parameters that control the diffusion process and could address a lot of significant questions.
    - Investigation of flexible macromolecules would be important, since diffusion of such molecules through porous media involves their conformational reorganization and is important in many fields of the biological sciences, which deal with biomacromolecules, like proteins, DNA and RNA, etc. Comparison of the diffusion data for linear and globular configurations of macromolecules will provide information on diffusion phenomena essentially linked to the conformational nature of the diffusing macromolecule (rigid or flexible).
    - Utilizing neutral fluorescent probes of various sizes could probe the mesh (pore) size of the gels at different length scales by purely steric interactions and allow the estimation of a molecular weight cut-off limit of the gel for the diffusant.
    - Temperature-dependent FCS measurements would be of great interest due to the temperature-dependent swelling behavior of these materials.

2. Concerning the dynamics characterization of these thin films, many more possibilities lay ahead.

- A preparation of a three dimensional photo-crosslinked macroscopic non-achored gel and its comparison with our surface anchored gels in the same solvent would be helpful in elucidating some of the features observed in the present study (e.g. existence of slow mode, scattering peak etc.), which may be related to the 2D confinement by surface anchoring.
- The effect of the ionic strength, pH, and temperature dependence of the dynamics and spatial heterogeneities of the gel layers needs to be further explored.
- The incorporation of particles of similar or bigger size than the pore size in the hydrogel layers could allow for a mechanical properties characterization of these networks by microrheological measurements.

REFERENCES

1. Peppas, N. A.; Khare, A. R., Preparation and diffusion behavior of hydrogels in controlled release. *Advanced Drug Delivery Reviews* **1993,** 11, 1-35.
2. Martin, B. D.; Gaber, B. P.; Patterson, C. H.; Turner, D. C., Direct protein microarray fabrication using a hydrogel "stamper". *Langmuir* **1998,** 14, (15), 3971-3975.
3. Revzin, A.; Russell, R. J.; Yadavalli, V. K.; Koh, W. G.; Deister, C.; Hile, D. D.; Mellott, M. B.; Pishko, M. V., Fabrication of poly(ethylene glycol) hydrogel microstructures using photolithography. *Langmuir* **2001,** 17, (18), 5440-5447.
4. Koh, W. G.; Revzin, A.; Pishko, M. V., Poly(ethylene glycol) hydrogel microstructures encapsulating living cells. *Langmuir* **2002,** 18, (7), 2459-2462.
5. Kiyonaka, S.; Sada, K.; Yoshimura, I.; Shinkai, S.; Kato, N.; Hamachi, I., Semi-wet peptide/protein array using supramolecular hydrogel. *Nature Materials* **2004,** 3, (1), 58-64.
6. Zhang, S. G., Hydrogels - Wet or let die. *Nature Materials* **2004,** 3, (1), 7-8.
7. Ratner, B. D.; Hoffman, A. S.; Schoen, F. J.; Lemons, J. E., *Biomaterials Science; An introduction to materials in medicine*. Elsevier / Academic Press: London UK, 2004.
8. Mart, R. J.; Osborne, R. D.; Stevens, M. M.; Ulijn, R. V., Peptide-based stimuli-responsive biomaterials. *Soft Matter* **2006,** 2, (10), 822-835.
9. Frey, W.; Meyer, D. E.; Chilkoti, A., Dynamic addressing of a surface pattern by a stimuli-responsive fusion protein. *Advanced Materials* **2003,** 15, (3), 248-+.
10. Miyata, T.; Uragami, T.; Nakamae, K., Biomolecule-sensitive hydrogels. *Advanced Drug Delivery Reviews* **2002,** 54, (1), 79-98.
11. Tanaka, T., Phase-Transitions in Gels and a Single Polymer. *Polymer* **1979,** 20, (11), 1404-1412.
12. Onuki, A., Theory of Phase-Transition in Polymer Gels. *Advances in Polymer Science* **1993,** 109, 63-121.
13. Lewis, G.; Coughlan, D. C.; Lane, M. E.; Corrigan, O. I. J., Preparation and release of model drugs from thermally sensitive poly(N-isopropylacrylamide) based macrospheres. *Microencapsulation* **2006,** 23, (9), 677-685.
14. Tong, P.; Ye, X.; Ackerson, B. J.; Fetters, L. J., Sedimentation of colloidal particles through a polymer solution. *Physical Review Letters* **1997,** 79, (12), 2363-2366.
15. Phillies, G. D. J., The Hydrodynamic Scaling Model for Polymer Self-Diffusion. *Journal of Physical Chemistry* **1989,** 93, (13), 5029-5039.
16. Lodge, T. P.; Rotstein, N. A.; Prager, S., Dynamics of Entangled Polymer Liquids - Do Linear-Chains Reptate. *Advances in Chemical Physics* **1990,** 79, 1-132.
17. Rigler, R.; Elson, E. L., *Fluorescence Correlation Spectroscopy*. Springer-Verlag: New York, 2001.
18. Lumma, D.; Keller, S.; Vilgis, T.; Raedler, J. O., Dynamics of large semiflexible chains probed by fluorescence correlation spectroscopy. *Physical Review Letters* **2003,** 90, (21).
19. Zettl, H.; Haefner, W.; Boeker, A.; Schmalz, H.; Lanzendoerfer, M.; Mueller, A.; Krausch, G., Fluorescence correlation spectroscopy of single dye-labeled polymers in organic solvents. *Macromolecules* **2004,** 37, (5), 1917-1920.

20. Best, A.; Pakula, T.; Fytas, G., Segmental dynamics of bulk polymers studied by fluorescence correlation spectroscopy. *Macromolecules* **2005,** 38, (10), 4539-4541.
21. Sukhishvili, S. A.; Chen, Y.; Mueller, J. D.; Gratton, E.; Schweizer, K. S.; Granick, S., Surface diffusion of poly(ethylene glycol). *Macromolecules* **2002,** 35, (5), 1776-1784.
22. Michelman-Ribeiro, A.; Boukari, H.; Nossal, R.; Horkay, F., Structural changes in polymer gels probed by fluorescence correlation spectroscopy. *Macromolecules* **2004,** 37, (26), 10212-10214.
23. Matejicek, P.; Podhajecka, K.; Humpolickova, J.; Uhlik, J.; Jelinek, K.; Limpouchova, Z.; Prochazka, K.; Spirkova, M., Polyelectrolyte Behavior of Polystyrene-block-poly(methacrylic acid) Micelles in Aqueous Solutions at Low Ionic Strength. *Macromolecules* **2004,** 37, (26), 10141-10154.
24. Walldal, C.; Wall, S., Coil-to-globule-type transition of poly(N-isopropylacrylamide) adsorbed on colloidal silica particles. *Colloid and Polymer Science* **2000,** 278, (10), 936-945.
25. Zhu, P. W.; Napper, D. H., The longer time collapse kinetics of interfacial poly(N-isopropylacrylamide) in water. *Journal of Chemical Physics* **1997,** 106, (15), 6492-6498.
26. Balamurugan, S.; Mendez, S.; Balamurugan, S. S.; O'Brien, M. J.; Lopez, G. P., Thermal response of poly(N-isopropylacrylamide) brushes probed by surface plasmon resonance. *Langmuir* **2003,** 19, (7), 2545-2549.
27. Beines, P. W.; Klosterkamp, I.; Menges, B.; Jonas, U.; Knoll, W., Responsive thin hydrogel layers from photo-cross-linkable poly(N-isopropylacrylamide) terpolymers. *Langmuir* **2007,** 23, (4), 2231-2238.
28. Yim, H.; Kent, M. S.; Satija, S.; Mendez, S.; Balamurugan, S. S.; Balamurugan, S.; Lopez, G. P., Evidence for vertical phase separation in densely grafted, high-molecular-weight poly(N-isopropylacrylamide) brushes in water. *Physical Review E* **2005,** 72, (5), -.
29. Yim, H.; Kent, M. S.; Mendez, S.; Lopez, G. P.; Satija, S.; Seo, Y., Effects of grafting density and molecular weight on the temperature-dependent conformational change of poly(N-isopropylacrylamide) grafted chains in water. *Macromolecules* **2006,** 39, (9), 3420-3426.
30. Ishida, N.; Biggs, S., Direct observation of the phase transition for a Poly(N-isopropylacryamide) layer grafted onto a solid surface by AFM and QCM-D. *Langmuir* **2007,** 23, (22), 11083-11088.
31. Motonaga, T.; Shibayama, M., Studies on pH and temperature dependence of the dynamics and heterogeneities in poly(N-isopropylacrylamide-co-sodium acrylate) gels. *Polymer* **2001,** 42, (21), 8925-8934.
32. Fillipidi, E.; Michailidou, V. N.; Loppinet, B.; Ruehe, J.; Fytas, G., Brownian diffusion close to a polymer brush. *Langmuir* **2007,** 23, (9), 5139-5142.
33. Furukawa, H.; Horie, K.; Nozaki, R.; Okada, M., Swelling-induced modulation of static and dynamic fluctuations in polyacrylamide gels observed by scanning microscopic light scattering. *Physical Review E* **2003,** 68, (3).
34. Wang, W.; Zhang, C.; Wang, S.; Zhao, J., Diffusion of Single Polyelectrolytes on the Surface of Poly(N-isopropylacrylamide) Brushes. *Macromolecules* **2007,** 40, (26), 9564-9569.

35. Cahill, D. J., Protein and antibody arrays and their medical applications. *Journal of Immunological Methods* **2001,** 250, (1-2), 81-91.
36. Templin, M. F.; Stoll, D.; Schrenk, M.; Traub, P. C.; Vohringer, C. F.; Joos, T. O., Protein microarray technology. *Drug Discovery Today* **2002,** 7, (15), 815-822.
37. Tanaka, T.; Hocker, L. O.; Benedek, G. B., Spectrum of Light Scattered from a Viscoelastic Gel. *Journal of Chemical Physics* **1973,** 59, (9), 5151-5159.
38. Shibayama, M.; Tanaka, T., Volume Phase-Transition and Related Phenomena of Polymer Gels. *Advances in Polymer Science* **1993,** 109, 1-62.
39. Dusek, K.; Patterson, D., A transition in swollen polymer networks induced by intramolecular condensation. *J. Polym. Sci.* **1968,** Pt. A-2, 6, 1209.
40. Dusek, K., *Responsive Gels: Volume Transitions I*. Springer-Verlag: Berlin, 1993; Vol. 109.
41. Dusek, K., *Responsive Gels : Volume Transitions II*. Springer-Verlag: Berlin, 1993; Vol. 110.
42. Annaka, M.; Tanaka, T., Multiple Phases of Polymer Gels. *Nature* **1992,** 355, (6359), 430-432.
43. Pusey, P. N.; Vanmegen, W., Dynamic Light-Scattering by Non-Ergodic Media. *Physica A* **1989,** 157, (2), 705-741.
44. Vanmegen, W.; Underwood, S. M.; Pusey, P. N., Nonergodicity Parameters of Colloidal Glasses. *Physical Review Letters* **1991,** 67, (12), 1586-1589.
45. Xue, J. Z.; Pine, D. J.; Milner, S. T.; Wu, X. L.; Chaikin, P. M., Nonergodicity and Light-Scattering from Polymer Gels. *Physical Review A* **1992,** 46, (10), 6550-6563.
46. Tanaka, T.; Fillmore, D. J., Kinetics of Swelling of Gels. *Journal of Chemical Physics* **1979,** 70, (3), 1214-1218.
47. Tanaka, T., *Dynamic Light Scattering*. Pecora, R. ed.; Plenum Publishing: New York, 1985; p 347-362.
48. de Gennes, P. G., *Scaling Concepts in Polymer Physics*. Cornell University: Ithaca, 1979.
49. Bae, Y. H.; Okano, T.; Ebert, C.; Heiber, S.; Dave, S.; Kim, S. W., Heterogeneous Interpenetrating Polymer Networks for Drug Delivery. *Journal of Controlled Release* **1991,** 16, (1-2), 189-196.
50. Mandel, M., The Physical-Chemistry of Poly-Electrolyte Solutions. *Angewandte Makromolekulare Chemie* **1984,** 123, (Aug), 63-83.
51. Schild, H. G., Poly (N-Isopropylacrylamide) - Experiment, Theory and Application. *Progress in Polymer Science* **1992,** 17, (2), 163-249.
52. Heskins, M.; Guillet, J. E., Solution properties of poly(N-isopropylacrylamide). *J. Macromol. Sci. Chem.* **1986,** A2, (8), 1441-1455.
53. Fujishige, S.; Kubota, K.; Ando, I., Phase-Transition of Aqueous-Solutions of Poly(N-Isopropylacrylamide) and Poly(N-Isopropylmethacrylamide). *Journal of Physical Chemistry* **1989,** 93, (8), 3311-3313.
54. Sun, P.; Li, B.; Wang, Y.; Ma, J.; Ding, D.; He, B., 1H NMR studies of poly(N-isopropylacrylamide) gels near the phase transition. *European Polymer Journal* **2003,** 39, (5), 1045-1050.
55. Wu, C.; Zhou, S. Q., Laser-Light Scattering Study of the Phase-Transition of Poly(N-Isopropylacrylamide) in Water .1. Single-Chain. *Macromolecules* **1995,** 28, (24), 8381-8387.

56. Chen, G.; Hoffman, A. S., A new temperature- and pH-responsive copolymer for possible use in protein conjugation. *Macromolecular Chemical Physics* **1995,** 196, (4), 1251-1259.
57. Yamazaki, Y.; Tada, T.; Kunugi, S., Effects of acrylic acid incorporation on the pressure-temperature behavior and the calorimetric properties of poly(N-isopropylacrylamide) in aqueous solutions. *Colloid and Polymer Science* **2000,** 278, (1), 80-83.
58. Priest, J. H.; Murray, S. L.; Nelson, R. J.; Hoffman, A. S.; , LCST of Aqueous Copolymer of NIsopropylacrylamide
and Other N-Substituted
Acrylamides. In *Reversible Polymer Gels and Related*
Systems, Rosso, F., Ed.; ACS Press: Washington DC, 1987; pp 255–264.
59. Bae, Y. H.; Okano, T.; Hsu, R.; Kim, S. W., Thermosensitive Polymers as On–Off Switches for Drug Release. *Makromol. Chem. Rapid Commun.* **1987,** 8, 481–485.
60. Tanaka, H.; Matsumura, M.; Veliky, I. A., Diffusion Characteristics of Substrates in Ca-Alginate Gel Beads. *Biotechnology and Bioengineering* **1984,** 26, (1), 53-58.
61. Magde, D.; Webb, W. W.; Elson, E., Thermodynamic Fluctuations in a Reacting System - Measurement by Fluorescence Correlation Spectroscopy. *Physical Review Letters* **1972,** 29, (11), 705-&.
62. Rigler, R.; Widengren, J., Ultrasensitive detection of single molecules by fluorescence correlation spectroscopy. *Bioscience* **1990,** 3, 180-183.
63. Rigler, R.; Widengren, J.; Mets, Ü., *Interactions and Kinetics of Single Molecules as Observed by Fluorescence Correlation Spectroscopy, Fluorescence Spectroscopy - New Methods and Applications*. Springer Verlag: 1992.
64. Rigler, R.; Mets, U.; Widengren, J.; Kask, P., Fluorescence Correlation Spectroscopy with High Count Rate and Low-Background - Analysis of Translational Diffusion. *European Biophysics Journal with Biophysics Letters* **1993,** 22, (3), 169-175.
65. Eigen, M.; Rigler, R. In *Sorting single molecules: Application to diagnostics and evolutionary biotechnology*, Proc. Natl. Acad. Sci. , USA, 1994; USA, 1994; pp 5740-5747.
66. Elson, E. L.; Magde, D., Fluorescence Correlation Spectroscopy .1. Conceptual Basis and Theory. *Biopolymers* **1974,** 13, (1), 1-27.
67. Magde, D.; Elson, E. L.; Webb, W. W., Fluorescence Correlation Spectroscopy .2. Experimental Realization. *Biopolymers* **1974,** 13, (1), 29-61.
68. Magde, D.; Webb, W. W.; Elson, E. L., Fluorescence Correlation Spectroscopy .3. Uniform Translation and Laminar-Flow. *Biopolymers* **1978,** 17, (2), 361-376.
69. Ehrenber, M.; Rigler, R., Rotational Brownian-Motion and Fluorescence Intensity Fluctuations. *Chemical Physics* **1974,** 4, (3), 390-401.
70. Krichevsky, O.; Bonnet, G., Fluorescence correlation spectroscopy: the technique and its applications. *Reports on Progress in Physics* **2002,** 65, (2), 251-297.
71. Muller, J. D.; Chen, Y.; Gratton, E., Fluorescence correlation spectroscopy. *Biophotonics, Pt B* **2003,** 361, 69-92.
72. Berne, B. J.; Pecora, R., *Dynamic Light Scattering with Applications to Chemistry, Biology and Physics*
Dover: New York, 2000.

73. Pecora, R., *Dynamic Light Scattering: Applications of Photon Correlation Spectroscopy*
Plenum: New York, 1985.
74. Joosten, J. G. H.; Gelade, E. T. F.; Pusey, P. N., Dynamic Light-Scattering by Nonergodic Media - Brownian Particles Trapped in Polyacrylamide Gels. *Physical Review A* **1990,** 42, (4), 2161-2173.
75. Toomey, R.; Freidank, D.; Ruhe, J., Swelling behavior of thin, surface-attached polymer networks. *Macromolecules* **2004,** 37, (3), 882-887.
76. Marciniec, B., *ComprehensiVe Handbook of Hydrosilylation;*. Pergamon Press: : Oxford, 1992.
77. Boksanyi, L.; Liardon, O.; Kovats, E. S., Chemically Modified Silicon Dioxide Surfaces Reaction of N-Alkyldimethylsilanols and N-Oxaalkyl-Dimethylsilanols with Hydrated Surface of Silicon Dioxide-Question of Limiting Surface Concentration. *Advances in Colloid and Interface Science* **1976,** 6, (2), 95-137.
78. Prucker, O.; Naumann, C. A.; Ruhe, J.; Knoll, W.; Frank, C. W., Photochemical attachment of polymer films to solid surfaces via monolayers of benzophenone derivatives. *Journal of the American Chemical Society* **1999,** 121, (38), 8766-8770.
79. Gianneli, M.; Roskamp, R. F.; Jonas, U.; Loppinet, B.; Fytas, G.; Knoll, W., Dynamics of swollen gel layers anchored to solid surfaces. *Soft Matter* **2008,** 4, 1443 - 1447.
80. Kroeger, A.; Belack, J.; Larsen, A.; Fytas, G.; Wegner, G., Supramolecular structures in aqueous solutions of rigid polyelectrolytes with monovalent and divalent counterions. *Macromolecules* **2006,** 39, (20), 7098-7106.
81. Cheng, Y.; Prud'homme, K. R., Diffusion of Mesoscopic Probes in Aqueous Polymer Solutions Measured by Fluorescence Recovery after Photobleaching. *Macromolecules* **2002,** 35, 8111-8121.
82. Horkay, F.; Hecht, A. M.; Geissler, E., Small-Angle Neutron-Scattering in Poly(Vinyl Alcohol) Hydrogels. *Macromolecules* **1994,** 27, (7), 1795-1798.
83. Ikkai, F.; Shibayama, M., Inhomogeneity control in polymer gels. *Journal of Polymer Science Part B-Polymer Physics* **2005,** 43, (6), 617-628.
84. Doi, M.; Edwards, S. F., *The theory of Polymer Dynamics*. Clarendon Press: Oxford U.K., 1986.
85. Pluen, A.; Netti, P. A.; Jain, R. K.; Berk, D. A., Diffusion of macromolecules in agarose gels: Comparison of linear and globular configurations. *Biophysical Journal* **1999,** 77, 542-552.
86. Bohme, U.; Scheler, U., Effective charge of bovine serum albumin determined by electrophoresis NMR. *Chemical Physics Letters* **2007,** 435, (4-6), 342-345.
87. Verkman, A. S., Solute and macromolecule diffusion in cellular aqueous compartments. *Trends Bioch. Science* **2002,** 27, 27-33.
88. Hirota, N.; Kumaki, Y.; Narita, T.; Gong, J. P.; Osada, Y., Effect of charge on protein diffusion in hydrogels. *J. Phys. Chem. B* **2000,** 104, (9904-08).
89. Brochard Wyart, F.; P.G. de Gennes, P. G., Viscosity at small scales in polymer melts. **2000,** 1, (1), 93-97.
90. Petit, J. M.; Zhu, X. X.; Macdonald, P. M., Solute probe diffusion in aqueous solutions of poly(vinyl alcohol) as studied by pulsed-gradient spin-echo NMR spectroscopy. *Macromolecules* **1996,** 29, (1), 70-76.

91. Desmedt, S. C.; Lauwers, A.; Demeester, J.; Engelborghs, Y.; Demey, G.; Du, M., Structural Information on Hyaluronic-Acid Solutions as Studied by Probe Diffusion Experiments. *Macromolecules* **1994,** 27, (1), 141-146.
92. Fleischer, G.; Appel, M., Chain-Length and Temperature-Dependence of the Self-Diffusion of Polyisoprene and Polybutadiene in the Melt. *Macromolecules* **1995,** 28, (21), 7281-7283.
93. Jian, T.; Anastasiadis, S. H.; Semenov, A. N.; Fytas, G.; Adachi, K.; Kotaka, T., Dynamics of Composition Fluctuations in Diblock Copolymer Solutions Far from and near to the Ordering Transition. *Macromolecules* **1994,** 27, (17), 4762-4773.
94. Kim, H. D.; Chang, T. Y.; Yohanan, J. M.; Wang, L.; Yu, H., Polymer Diffusion in Linear Matrices - Polystyrene in Toluene. *Macromolecules* **1986,** 19, (11), 2737-2744.
95. Yuan, G. C.; Wang, X. H.; Han, C. C.; Wu, C., Reexamination of slow dynamics in semidilute solutions: Temperature and salt effects on semidilute poly(N-isopropylacrylamide) aqueous solutions. *Macromolecules* **2006,** 39, (18), 6207-6209.
96. Giannelli, A.; Beines, P. W.; Roskamp, R. F.; Koynov, K.; Fytas, G.; Knoll, W., Local and global dynamics of transient polymer networks and swollen gels anchored on solid surfaces. *Journal of Physical Chemistry C* **2007,** 111, (35), 13205-13211.
97. Vidyasagar, A.; Majewski, J.; Toomey, R., Temperature induced volume-phase transitions in surface-tethered Poly(N-isopropylacrylamide) networks. *Macromolecules* **2008,** 41, (3), 919-924.
98. Yakubov, G. E.; Loppinet, B.; Zhang, H.; Ruhe, J.; Sigel, R.; Fytas, G., Collective dynamics of an end-grafted polymer brush in solvents of varying quality. *Physical Review Letters* **2004,** 92, (11), -.
99. Li, J. F.; Li, W.; Huo, H.; Luo, S. Z.; Wu, C., Reexamination of the slow mode in semidilute polymer solutions: The effect of solvent quality. *Macromolecules* **2008,** 41, (3), 901-911.
100. Cho, E. C.; Kim, J. W.; Fernandez-Nieves, A.; Weitz, D. A., Highly responsive hydrogel scaffolds formed by three-dimensional organization of microgel nanoparticles. *Nano Letters* **2008,** 8, (1), 168-172.
101. Bastide, J.; Leibler, L.; Prost, J., Scattering by Deformed Swollen Gels - Butterfly Isointensity Patterns. *Macromolecules* **1990,** 23, (6), 1821-1825.

ACKNOWLEDGMENTS

First and foremost, I like to offer my sincere gratitude to my direct supervisor Prof. George Fytas who has supported me throughout my thesis with his patience and knowledge.

I would also like to express my deep thanks to the co-supervisor Prof. Wolfgang Knoll for offering me this wonderful chance to work in his group. His friendly attitude and ever encouraging remarks has been a source of motivation for this work.

I simply could not wish for better or friendlier supervisors.

I would like to give my great thanks to Dr U. Jonas at Max Planck Institute for Polymer Research in Mainz (MPIP) and later in the Institute of Electronic Laser and Structure (IESL), who provided me great assistance in all chemistry related topics and not only. He was also so kind to proofread my thesis and contribute significantly to the final outcome.

My unlimited appreciation also extends to Andreas Best and Dr. Kaloian Koynov from MPIP and Dr. Benoit Loppinet from IESL, for their valuable scientific support, friendship and many hours of conversation, including many ideas presented here.

I gratefully acknowledge the scientific contribution of Robert F. Roskamp and Dr. Patrick Beines for performing the synthesis and kindly provided the polymer and the adhesion promoters used in this work.

I am grateful to many people in the Knoll Group at MPIP as well as in the Polymer Group, IESL, in Heraklion, for their help, guidance and friendship.

Finally, I would like to express my deepest gratitude and love to my parents and brother for their wisdom, guidance and support, both psychological and financial, during all these long years of my studies. Thank you so much!

ΔΟΜΗ ΚΑΙ ΔΥΝΑΜΙΚΗ ΛΕΠΤΩΝ ΥΜΕΝΙΩΝ HYDROGEL ΜΕ ΤΙΣ ΜΕΘΟΔΟΥΣ ΦΑΣΜΑΤΟΣΚΟΠΙΑΣ ΣΥΣΧΕΤΙΣΧΗΣ ΦΘΟΡΙΣΜΟΥ ΚΑΙ ΦΑΣΜΑΤΟΣΚΟΠΙΑΣ ΣΥΣΧΕΤΙΣΗΣ ΦΩΤΟΝΙΩΝ

ΜΑΡΙΑ ΓΙΑΝΝΕΛΗ

ΠΑΝΕΠΙΣΤΗΜΙΟ ΚΡΗΤΗΣ
ΤΜΗΜΑ ΕΠΙΣΤΗΜΗΣ ΚΑΙ ΤΕΧΝΟΛΟΓΙΑΣ ΥΛΙΚΩΝ

ΗΡΑΚΛΕΙΟ, ΙΟΥΛΙΟΣ 2008

ΠΕΡΙΛΗΨΗ

Αυτή η διατριβή αφορά στην δομή και τη δυναμική hydrogel φιλμς. Photocross-linked λεπτά φιλμ θερμο-αποκρινόμενου πολυμερούς σταθεροποιημένα σε στερεά υποστρώματα προετοιμάστηκαν από συμπολυμερή του N-isopropylacrylamide (NIPAAm, 94%), μεθακρυλικό οξύ (MAA, 5%) και 4-methacryloyloxy-βενζοφαινόνη (MaBP, 1%).

FCS μετρήσεις πραγματοποιήθηκαν στα συγκεκριμένα φιλμς διογκωμένα σε δύο διαφορετικούς διαλύτες, αιθανόλη και νερό, και διαφορετικοί ανιχνευτές φθορισμού διαφόρων μεγεθών και φορτίων χρησιμοποιήθηκαν.

Στο νερό, θετικά φορτισμένοι ανιχνευτές (π.χ. Rh6G, καθώς και ένα θετικά φορτισμένο παράγωγο του περυλενίου) ήταν έντονα προσελκυμένοι στο εσωτερικό των gels και υπέστη παρεμποδισμένη (μη-ελεύθερη) διάχυση λόγω της ύπαρξης ελκτικών ηλεκτροστατικών αλληλεπιδράσεων με το αρνητικά φορτισμένο πολυμερές. Το αντίθετο φαινόμενο παρατηρήθηκε με αρνητικά φορτισμένους ανιχνευτές φθορισμού.

Μετρήσεις σχετικές με την διαδικασία διάχυσης των πρωτεϊνών έδειξαν ότι θετικά φορτισμένες πρωτεΐνες (cBSA) ακινητοποιήθηκαν μέσα στο hydrogel στρώμα, ενώ εκτιμάται ότι μια ουδέτερη (native BSA) διαχέεται στο στρώμα.

Η δυναμική των επιφανειακών pNIPAAm-MAA-MaBP στρωμάτων με διαφορετικές πυκνότητες crosslinking διογκωμένα στο καλό διαλύτη αιθανόλη μελετήθηκαν από την νέα τεχνική που αναπτύχθηκε στο εργαστήριο, τη μικρο-φασματοσκοπία συσχετισμού φωτονίων, για χρόνους μεταξύ 1 x 10-6 s to 1 s.

Τέλος, διερευνήθηκε η επίδραση άλατος και μεταβολής της θερμοκρασίας στη δυναμική των pNIPAAm φιλμς διογκωμένα σε νερό. Μια πρώτη μικρή αύξηση της ιονικής ισχύος (προσθήκη NaCl έως 0,02 mol / L) οδήγησε σε αύξηση του συντελεστή συνεργατικής διάχυσης Dcoop. Περαιτέρω αύξηση της ιονικής δύναμης οδήγησε σε μείωση του Dcoop με αυξανόμενη συγκέντρωση NaCl, το οποίο μπορεί να σχετίζεται με salting-out επίδραση εξαιτίας της μείωσης της ποιότητας του διαλύτη. Πολύ υψηλές συγκεντρώσεις άλατος (> 1M) απαλείφουν πλήρως τη δυναμική συμπεριφορά λόγω κατάρρευσης του gel.

Εν κατακλείδι, FCS και PCS αποδείχθηκαν συμπληρωματικές και ισχυρές οπτικές τεχνικές για να ερευνήσουν τη δομή και τη δυναμική των λεπτών υμενίων hydrogel σταθεροποιημένων σε στερεά υποστρώματα.

Λέξεις-κλειδιά:
hydrogels, θερμο-αποκρινόμενα τζελ, δυναμική πολυμερών, συνεργατική διάχυση, φασματοσκοπία συσχέτισης φθορισμού, φασματοσκοπία συσχετισμού φωτονίων